

**NONLINEAR FINITE ELEMENT ANALYSES ON THE  
BOLT BENDING DEFORMATION**

**CIVATA EĞİLME DEFORMASYONU ÜZERİNE  
DOĞRUSAL OLMAYAN SONLU ELEMANLAR  
ANALİZLERİ**

**AHKER GÜNEŞ DİLBER**

**ASST. PROF. MEHMET OKAN GÖRTAN**

**Supervisor**

Submitted to

Graduate School of Science and Engineering of Hacettepe University

as a Partial Fulfilment to the Requirements

for the Award of the Degree of Master of Science

in Mechanical Engineering.

# **ABSTRACT**

## **NONLINEAR FINITE ELEMENT ANALYSES ON THE BOLT BENDING DEFORMATION**

**Ahker Güneş DİLBER**

**Master of Science, Department of Mechanical Engineering**

**Supervisor: Asst. Prof. Mehmet Okan GÖRTAN**

**June 2023, 135 pages**

Joining and assembly processes in mechanical design are performed by using permanent or non-permanent methods. Among the non-permanent techniques, threaded fasteners are commonly used mechanical components providing disassembly of the connections. The connections consisted of bolt and nut, which are externally and internally threaded members, are widely used in many engineering products because of the replaceable feature. Although the bolted joints are particularly designed to carry axial forces, they can be subjected to not only concentric loads but also eccentric loadings. Some of the eccentric loadings may lead to prying action which raises the axial force carried by the bolt due to the contact occurring between the connected members. In addition to the bending moment developed due to the eccentric loading, the prying action affects the bolt by increasing excessively the axial force carried by the bolt. The strength of the bolt in the joint decreases with regards to the level of the eccentricity under the prying action with a combination of the two facts which are bending moment and excessive tensile force. This additional tensile load is considered in the studies investigating the bolted joints under the prying action, however, the bending moment

that occurred due to the eccentricity of the joint is not always an interested phenomenon. Outcomes about the bolt bending moment occurred under prying action in the literature are usually limited by only comments, and there are still unaddressed points about the bolt bending deformation such as the location of the maximum bending moment and effects of the preloading on the bending-tension interaction of the bolt. In this thesis, the bending deformation mechanism of a bolted joint under prying action was studied comprehensively by performing static structural finite element analysis considering the material, geometric and contact nonlinearities. After introducing a brief background about the bolted joints under the eccentric loadings and prying action, a comprehensive literature survey was presented. The studies in the literature about the three-dimensional finite element modelling techniques of the bolted joints, bolt bending, and prying action were explained in detail. The experimental and numerical study programs were planned in accordance with the objectives. Experimental studies were performed prior to finite element analyses to provide required inputs such as material properties and displacement boundary conditions. Before presenting the analysis results, the construction of the finite element analysis models was represented in detail. The results obtained from the finite element analyses were presented in four different sections. The force-displacement behaviour, strain-force variations throughout the loading, and results of the mechanical parameters for all configurations and modelling techniques were compared with the experimental results. After comparing the experimental and numerical results, the modelling techniques were analysed in terms of the bending deformation capability, and this feature was evaluated by using the bolt bending moment results throughout the clamped region and bending-tension interaction curves. The bolted joint configurations were also analysed by using three different pre-tightening force levels. In conclusion, the structural response of a bolted joint involving a partially threaded fastener under prying action was comprehensively evaluated by considering the bending deformation capacity. For the flexural features of the studied bolted joint type under prying action, finite element analysis modelling issues and design considerations were presented.

**Keywords:** Finite Element Analysis, Bolted Joints, Prying Action, Bolt Bending, T-Stub

## ÖZET

# CIVATA EĞİLME DEFORMASYONU ÜZERİNE DOĞRUSAL OLMAYAN SONLU ELEMANLAR ANALİZLERİ

**Ahker Güneş DİLBER**

**Yüksek Lisans, Makine Mühendisliği Bölümü**

**Tez Danışmanı: Dr. Öğr. Üyesi Mehmet Okan GÖRTAN**

**Haziran 2023, 135 sayfa**

Mekanik tasarımda birleştirme ve montaj işlemleri kalıcı veya kalıcı olmayan metotlar kullanılarak gerçekleştirilir. Bağlantıların sökülmesini sağlayan mekanik parçalar olan vidalı bağlantı elemanları kalıcı olmayan teknikler arasında çoğunlukla kullanılmaktadır. Dıştan ve içten vidalı bağlantı elemanları olan civata ve somundan oluşan bağlantılar mühendislik ürünlerinin çoğunda değiştirilebilir özelliklerinden ötürü yaygın olarak kullanılmaktadır. Civatalı bağlantılar özellikle aksel yüklerin taşınması için tasarlanmış olsalar da sadece aksel değil ayrıca eksenden kaçık yüklemelere de maruz kalabilirler. Eksenden kaçık yüklemelerin bazıları bağlanan parçalar arasındaki temastan kaynaklanarak civata tarafından taşınan aksel kuvveti artıran kanırtma etkisine neden olabilirler. Eksenden kaçık yüklemelerden oluşan eğilme momentine ek olarak, kanırtma etkisi, civata tarafından taşınan aksel kuvveti yoğun bir şekilde artırarak civatayı etkiler. Aksel kaçıklığın seviyesine bağlı olarak civatanın dayanımı, eğilme momenti ve fazladan çekme kuvvetinin kombinasyonu ile kanırtma etkisi altında azalır. Fazladan çekme kuvvetine, kanırtma etkisi altındaki civatalı bağlantı çalışmalarında dikkate alınmaktadır, ancak, bağlantının aksel

kaçıklığından ötürü oluşan eğilme momenti her zaman ilgilenilen bir fenomen değildir. Literatürdeki kanırtma etkisi altındayken oluşan cıvata eğilme momenti çıktıları genellikle sadece yorumlarla sınırlı kalmaktadır ve maksimum eğilme momentinin konumu ile önyüklemenin cıvata eğilme-çekme etkileşimine olan etkisi gibi cıvatanın eğilme deformasyonu hakkında açıklanmamış noktalar bulunmaktadır. Bu tezde malzeme, geometrik ve temas doğrusalsızlıklarının ele alındığı statik yapısal sonlu elemanlar analizleri gerçekleştirilerek kanırtma etkisi altındaki bir cıvatalı bağlantının eğilme deformasyonu mekanizması kapsamlı bir biçimde çalışılmıştır. Eksenel kaçık yükleme ve kanırtma etkisi altındaki cıvatalı bağlantılar için kısa bir temel bilgi aktarıldıktan sonra geniş kapsamlı bir literatür araştırması sunulmuştur. Cıvatalı bağlantıların üç boyutlu olarak sonlu elemanlar modelleme teknikleri, cıvata eğilmesi ve kanırtma etkisi hakkında olan literatürdeki çalışmalar detaylıca açıklanmıştır. Deneysel ve nümerik çalışma programları hedefler doğrultusunda planlanmıştır. Malzeme özellikleri ve deplasman sınır koşulları gibi gerekli girdilerin sağlanması için sonlu elemanlar analizleri öncesinde deneysel çalışmalar gerçekleştirilmiştir. Sonlu elemanlar analizi modellerinin yapısı, analiz sonuçlarının sunulmasından önce detaylıca açıklanmıştır. Sonlu elemanlar analizlerinden elde edilen sonuçlar dört farklı bölümde sunulmuştur. Kuvvet-deplasman davranışı, yükleme boyunca gerinim-kuvvet değişimi ve bütün konfigürasyonlar ile modelleme teknikleri için mekanik parametrelerin sonuçları deneysel sonuçlar ile karşılaştırılmıştır. Modelleme teknikleri, eğilme deformasyonu kapasitesi kapsamında deneysel ve nümerik sonuçların karşılaştırılmasından sonra analiz edilmiştir ve bu olgu, gerilmeye maruz kalan bölge boyunca olan cıvata eğilme momenti sonucu ile eğilme-çekme etkileşim eğrisi kullanılarak değerlendirilmiştir. Cıvatalı bağlantı konfigürasyonları ayrıca üç farklı önyüklemeye kuvvet seviyesi kullanılarak analiz edilmiştir. Sonuç olarak, yarım pasolu bir bağlantı elemanı içeren bir cıvatalı bağlantının kanırtma etkisi altındaki yapısal tepkisi, eğilme deformasyonu kapasitesi dikkate alınarak kapsamlı bir biçimde değerlendirilmiştir. Çalışılan cıvatalı bağlantı tipinin kanırtma etkisi altındaki eğilmeye ilişkin olguları için sonlu elemanlar analizi modelleme hususları ve tasarım değerlendirmeleri sunulmuştur.

**Anahtar Kelimeler:** Sonlu Elemanlar Analizi, Cıvatalı Bağlantı, Kanırtma Etkisi, Cıvata Eğilmesi, T-Stub.

## **ACKNOWLEDGMENT**

First of all, I would like to thank Ali YETGİN for helping me to discover the subject of this thesis. All the time we worked together, his guidance and recommendations let me understand the engineering point of view and became me more confident in my work life and this thesis study.

I would like to express my sincere gratitude to my supervisor Asst. Prof. Mehmet Okan GÖRTAN for guidance and recommendations throughout the thesis study.

All staff of Physical Test Department at Roketsan Inc. deserve to be acknowledged for their support while performing the tensile tests in many configurations.

And very special thanks to my family for their efforts to make easier my life complicated by academic stuff.



# TABLE OF CONTENTS

ABSTRACT .....	i
ÖZET .....	iii
ACKNOWLEDGMENT .....	v
TABLE OF CONTENTS .....	vii
LIST OF FIGURES .....	xi
LIST OF TABLES .....	xvii
1. INTRODUCTION .....	1
1.1. Background .....	1
1.2. Objectives.....	3
1.3. Limitations .....	3
1.4. Structure of the Thesis.....	4
2. LITERATURE REVIEW .....	5
2.1. Introduction .....	5
2.2. Three-Dimensional Finite Element Modelling Techniques of the Bolted Joints	6
2.3. Bolt Bending .....	12
2.4. Prying Action .....	20
2.5. Methods for Bolt Strength Evaluation .....	24
2.6. Conclusion.....	25
3. EXPERIMENTAL STUDY .....	27
3.1. Bolt Tensile Tests.....	27
3.1.1. Test Configuration.....	27
3.1.2. Results .....	28
3.2. Material Characterization Tests .....	29
3.2.1. Test Configuration.....	30



3.2.2.	Results .....	31
3.3.	Monotonic T-Stub Tests.....	32
3.3.1.	Test Configuration.....	33
3.3.2.	Strain Gauge Instrumentation.....	37
3.3.3.	Results .....	40
3.3.3.1.	Response of the T-Stub Samples.....	40
3.3.3.2.	Strain Gauge Results .....	41
3.4.	Conclusion.....	42
4.	FINITE ELEMENT ANALYSIS MODELS .....	45
4.1.	Finite Element Analysis Parameters .....	45
4.1.1.	Material Models.....	45
4.1.2.	Assembly .....	46
4.1.3.	Steps .....	47
4.1.4.	Interactions .....	48
4.1.5.	Loads and Boundary Conditions .....	49
4.1.6.	Mesh .....	50
4.2.	Bolted Joint Models .....	51
4.2.1.	Three-Dimensional Models without Threads .....	52
4.2.2.	Three-Dimensional Models with Threads .....	53
4.2.3.	Proposed Model.....	54
5.	RESULTS .....	57
5.1.	Non-Preloaded Bolted Joint Models .....	57
5.1.1.	Comparison with Experimental Results .....	57
5.1.2.	Modelling Technique Comparison .....	69
5.2.	Overview of the Modelling Techniques.....	76
5.3.	Preloaded Bolted Joint Results.....	77
6.	CONCLUSION.....	85

REFERENCES .....	91
APPENDICES .....	99
APPENDIX 1 - The technical drawing of the dogbone specimens .....	99
APPENDIX 2 - The technical drawing of the setup parts.....	100



## LIST OF FIGURES

Figure 1.1. Outline for the bolted joint types [3].....	1
Figure 2.1. (a) The bolted joint with emphasizing the pressure cone lines, (b) The representation of the joint modelling by completely disregarding the bolts (Interface of the members are bonded to each other along the pressure cone area). .....	7
Figure 2.2. (a) The bolted joint, (b) The representation of the bolted joint modelling by using a connector (The connector end points are linked with the contact area of the bolt head and the nut, or washers if included). ....	8
Figure 2.3. Schematic view of the construction of the equivalent beam element modelling of the bolted joint by considering axial and bending stiffness including geometric properties (subscript ‘s’ represents the shank region of the bolt, subscript ‘t’ represents the threaded region of the bolt, and subscript ‘eq’ represents the new equivalent beam element). ....	10
Figure 2.4. (a) The bolted joint. The most common finite element modelling techniques of the bolts at the clamped region of the joint by using (b) only minor diameter, (c) only major diameter and (d) both the minor and major diameter to separate the shank and threaded region. ....	11
Figure 2.5. Application of the tightening torque by using shear stress on the outer surfaces of the nut indirectly.....	13
Figure 2.6. The representation of the “turn-of-nut method” method which is a way to apply the tightening force by rotating the nut with respect to corresponding angular displacement for the required force is a way [36]. ....	13
Figure 2.7. Two-piece washer for minimizing bolt bending (a) undeformed, (b) deformed configuration [45]. ....	15
Figure 2.8. Moment relief barrel washer (a) undeformed, (b) deformed configuration [46]. .....	16
Figure 2.9. Surface inclination [48].....	16
Figure 2.10. (a) Deformed situation of a bolted joint under prying action, (b) a schematic representation of the stress distribution of the bolt by mentioning the internal bending moment and axial force, (c) free-body diagram of the bolt and upper side member.....	21

Figure 3.1. The views of the test configuration of the bolt tensile test, (a) assembly at the tensile test machine, (b) section view of the test setup. ....	28
Figure 3.2. The force-displacement graph for both bolt strength grades including the representative views of the destructed test samples. ....	29
Figure 3.3. The demonstration of the manufacturing process applied for cutting the tensile specimens from an I-shaped beam. ....	30
Figure 3.4. The stress-strain graph for each tensile specimen category including the representative views of the destructed test samples. ....	32
Figure 3.5. The end-plate connection and its equivalent T-Stub model [92]. ....	33
Figure 3.6. The representative view of the initial cutting process of the beam [93]. ....	34
Figure 3.7. The whole process for obtaining the T-Stub components from an I-profile beam, (a) the raw shape of the beam, (b) the final shape of the T-Stub part with lower eccentricity, (c) the final shape of the T-Stub part with higher eccentricity. ...	34
Figure 3.8. (a) The view of the final assemblies of the T-Stub samples, (b) assembly at the tensile test machine of the T-Stub model with lower eccentricity, (c) assembly at the tensile test machine of the T-Stub model with higher eccentricity. ....	35
Figure 3.9. Dimensions of the T-Stub assemblies for (a) lower eccentricity, (b) higher eccentricity. ....	36
Figure 3.10. (a) The front view of the strain gauge bonded to the bolt, (b) the side view of the strain gauges, (c) the alignment of the strain gages by using the black marks on the bolt head, (d) the sensor denomination of the bolt strain gauges. ....	38
Figure 3.11. Schematically representation of the groove. ....	39
Figure 3.12. The location of the rosette strain gauges. ....	39
Figure 3.13. (a) The close view of the strain gauge bonded at the left side of the T-section, (b) the close view of the strain gauge bonded at the right side of the T-section, (c) the longitudinal direction of the strain gage, (d) the transverse direction of the strain gage. ....	40
Figure 3.14. The force-displacement graph for each test configuration including the representative views of the destructed test samples. ....	41
Figure 3.15. Strain-force graph for the strain gauge sensors from the web side of the bolt. ....	42
Figure 3.16. Strain-force graph for the strain gauge sensors from the end side of the bolt. ....	42
Figure 3.17. Strain-force graph in the longitudinal direction for the strain gauge sensors from the setup part. ....	43

Figure 3.18. Strain-force graph in the transverse direction for the strain gauge sensors from the setup part.....	43
Figure 4.1. The demonstration of the T-Stub assembly components.....	46
Figure 4.2. The reduction from the whole model into the quarter model.....	47
Figure 4.3. The common contact pairs between (a) the bolt head and upper T-section, (b) the nut and lower T-section, (c) the upper and lower T-section.....	49
Figure 4.4. The surfaces where the symmetry boundary conditions were applied. ....	51
Figure 4.5. The mesh structure of the T-section parts for (a) lower eccentricity, (b) higher eccentricity.....	52
Figure 4.6. The representation and mesh structure of the bolted joints model of (a) V1, (b) V2, (c) V3.....	53
Figure 4.7. The threaded bolted joint modelling method with representing the mesh structure of the threads.....	54
Figure 4.8. Load distribution at the mating threads of a bolted joint [98].....	55
Figure 4.9. The stiffness arrangement by removing the threads. ....	55
Figure 4.10. The representation and mesh structure of the proposed bolted joints modelling technique.....	55
Figure 5.1. Representation of the mechanical parameters of the force-displacement behaviour. ....	58
Figure 5.2. The force-displacement graphs of the configuration of (a) 8.8 – E1, (b) 8.8 – E2. ....	59
Figure 5.3. The force-displacement graphs of the configuration of (a) 12.9 – E1, (b) 12.9 – E2.....	60
Figure 5.4. The strain-force curves created from the web side strain gauge location of the bolts for the configuration of (a) 8.8 – E1, (b) 8.8 – E2. ....	61
Figure 5.5. The strain-force curves created from the end side strain gauge location of the bolts for the configuration of (a) 8.8 – E1, (b) 8.8 – E2. ....	61
Figure 5.6. The strain-force curves created from the web side strain gauge location of the bolts for the configuration of (a) 12.9 – E1, (b) 12.9 – E2. ....	62
Figure 5.7. The strain-force curves created from the end side strain gauge location of the bolts for the configuration of (a) 12.9 – E1, (b) 12.9 – E2. ....	62
Figure 5.8. The strain-force curves created from the strain gauge location of the T-sections for the longitudinal direction of the configuration of (a) 8.8 – E1, (b) 8.8 – E2. ....	63

Figure 5.9. The strain-force curves created from the strain gauge location of the T-sections for the transverse direction of the configuration of (a) 8.8 – E1, (b) 8.8 – E2.	63
Figure 5.10. The strain-force curves created from strain gauge location of the T-sections for the longitudinal direction of the configuration of (a) 12.9 – E1, (b) 12.9 – E2.	64
Figure 5.11. The strain-force curves created from the strain gauge location of the T-sections for the transverse direction of the configuration of (a) 12.9 – E1, (b) 12.9 – E2.	64
Figure 5.12. The bolt bending moment diagram at the elastic limit of the T-Stub connection for the clamped region of the configuration of (a) 8.8 – E1, (b) 8.8 – E2.	70
Figure 5.13. The bolt bending moment diagram at the elastic limit of the T-Stub connection for the clamped region of the configuration of (a) 12.9 – E1, (b) 12.9 – E2.	71
Figure 5.14. The bolt bending moment diagram at the ultimate strength of the T-Stub connection for the clamped region of the configuration of (a) 8.8 – E1, (b) 8.8 – E2.	72
Figure 5.15. The bolt bending moment diagram at the ultimate strength of the T-Stub connection for the clamped region of the configuration of (a) 12.9 – E1, (b) 12.9 – E2.	73
Figure 5.16. The bending-tension interaction curves of the bolt at the configuration of (a) 8.8 – E1, (b) 8.8 – E2.	74
Figure 5.17. The bending-tension interaction curves of the bolt at the configuration of (a) 12.9 – E1, (b) 12.9 – E2.	75
Figure 5.18. The preloaded bolt bending moment diagram at the elastic limit of the T-Stub connection for the clamped region of the configuration of (a) 8.8 – E1, (b) 8.8 – E2.	80
Figure 5.19. The preloaded bolt bending moment diagram at the elastic limit of the T-Stub connection for the clamped region of the configuration of (a) 12.9 – E1, (b) 12.9 – E2.	81
Figure 5.20. The preloaded bolt bending moment diagram at the ultimate strength of the T-Stub connection for the clamped region of the configuration of (a) 8.8 – E1, (b) 8.8 – E2.	82
Figure 5.21. The preloaded bolt bending moment diagram at the ultimate strength of the T-Stub connection for the clamped region of the configuration of (a) 12.9 – E1, (b) 12.9 – E2.	83

Figure 5.22. The bending-tension interaction curves of the preloaded bolt at the configuration of (a) 8.8 – E1, (b) 8.8 – E2, (c) 12.9 – E1, (d) 12.9 – E2. ....	84
Figure A.1. The technical drawing of the dogbone specimens of (a) 0-W, (b) 45-W, (c) 90-W, (d) 0-F. ....	99
Figure A.2. The technical drawing of the setup part with higher eccentricity. ....	100
Figure A.3. The technical drawing of the setup part with lower eccentricity. ....	101





## LIST OF TABLES

Table 2.1. The effects of increasing the parameter values on the different evaluation items. .....	23
Table 3.1. The mechanical properties of bolt grades with average values including standard deviation. ....	29
Table 3.2. The test matrix for the dogbone tensile specimens. ....	31
Table 3.3. The mechanical properties of tensile dogbone test specimens with average values including standard deviation.....	32
Table 3.4. The test matrix for the T-Stub prying tests.....	36
Table 3.5. The results of the mechanical parameters of each T-Stub prying test specimen. .....	41
Table 4.1. The mechanical properties used in this study.....	46
Table 4.2. Displacement boundary condition values.....	50
Table 4.3. The total number of elements and nodes of the T-section parts.....	52
Table 4.4. The total number of elements and nodes of the bolts of the three-dimensional models without threads. ....	53
Table 4.5. The total number of elements and nodes of the parts of the three-dimensional model with threads.....	54
Table 5.1. Comparison at the 8.8 – E1 configuration for the initial stiffness between numerical and experimental results. ....	65
Table 5.2. Comparison at the 8.8 – E2 configuration for the initial stiffness between numerical and experimental results. ....	65
Table 5.3. Comparison at the 12.9 – E1 configuration for the initial stiffness between numerical and experimental results. ....	65
Table 5.4. Comparison at the 12.9 – E2 configuration for the initial stiffness between numerical and experimental results. ....	66
Table 5.5. Comparison at the 8.8 – E1 configuration for the maximum force between numerical and experimental results. ....	66
Table 5.6. Comparison at the 8.8 – E2 configuration for the maximum force between numerical and experimental results. ....	66

Table 5.7. Comparison at the 12.9 – E1 configuration for the maximum force between numerical and experimental results. ....	67
Table 5.8. Comparison at the 12.9 – E2 configuration for the maximum force between numerical and experimental results. ....	67
Table 5.9. Comparison at the 8.8 – E1 configuration for the displacement at the ultimate force between numerical and experimental results.....	67
Table 5.10. Comparison at the 8.8 – E2 configuration for the displacement at the ultimate force between numerical and experimental results.....	68
Table 5.11. Comparison at the 12.9 – E1 configuration for the displacement at the ultimate force between numerical and experimental results.....	68
Table 5.12. Comparison at the 12.9 – E2 configuration for the displacement at the ultimate force between numerical and experimental results.....	68
Table 5.13. The computation effort comparison of the modelling techniques for 8.8 – E1 configuration.....	76
Table 5.14. The computation effort comparison of the modelling techniques for 8.8 – E2 configuration.....	77
Table 5.15. The computation effort comparison of the modelling techniques for 12.9 – E1 configuration.....	77
Table 5.16. The computation effort comparison of the modelling techniques for 12.9 – E2 configuration.....	77
Table 5.17. Preload values for the bolted joint analyses. ....	78

# 1. INTRODUCTION

## 1.1. Background

A bolt is a term which is used for representing a threaded fastener designed for the use in conjunction with a nut to clamp together two or more parts in an assembly [1], while the term of the screw is generally used to describe a threaded fastener used in the joint which one of the members in the connection has internal threads. The assembly consisted of bolt and nut, which are externally and internally threaded members, is extensively used in engineering products by the reason of replacement feature and simple installation [2]. An outline for the bolted joint types can be given in Figure 1.1 as mentioned in VDI 2230 [3].

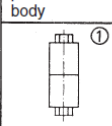
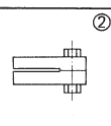
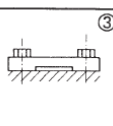
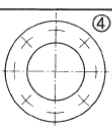
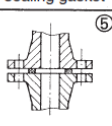
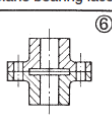
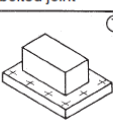
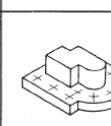
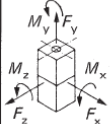
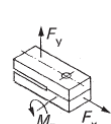
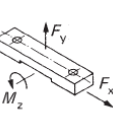
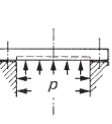
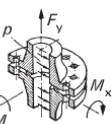
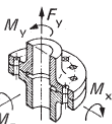
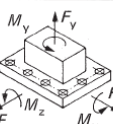
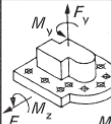
Single-bolted joints		Multi-bolted joints						Bolted joints
concentric or eccentric		in a plane	axial symmetry			symmetrical	asymmetrical	bolt axes
Cylinder or prismatic body	Beam	Beam	Circular plate	Flange with sealing gasket	Flange with plane bearing face	Rectangular multi-bolted joint	Multi-bolted joint	
								Joint geometry
								Relevant loads
Axial force $F_A$ Transverse force $F_Q$ Working moment $M_B$	Axial force $F_A$ Transverse force $F_Q$ Moment in the plane of the beam $M_Z$	Axial force $F_A$ Transverse force $F_Q$ Moment in the plane of the beam $M_Z$	Internal pressure $p$	Axial force $F_A$ (Pipe force) Working moment $M_B$ Internal pressure $p$	Axial force $F_A$ Torsional moment $M_T$ Working moment $M_B$	Axial force $F_A$ Transverse force $F_Q$ Torsional moment $M_T$ Working moment $M_B$	Axial force $F_A$ Transverse force $F_Q$ Torsional moment $M_T$ Working moment $M_B$	Forces and moments
VDI 2230		limited treatment by VDI 2230		DIN 2505 AD Note B7 VDI 2230 (limited treatment)	limited treatment by VDI 2230			
Bending beam theory with additional conditions			Plate theory	limited treatment using simplified models				Calculation procedure
Finite Element Method (FEM)								

Figure 1.1. Outline for the bolted joint types [3].

Bolted joints are generally subjected to not concentric loads although they are specially designed for carrying axial loading. The eccentric loadings may cause the bolt to not only carrying axial load but also exposed additional axial load and bending moment. As shown in Figure 1, nearly all the load cases can induce such eccentric loads on the bolts. Some of the eccentric loadings lead to prying action which increases the axial load on the bolt due to

contact nonlinearity. Prying is the noun form of the verb “pry” which is defined as using the force to separate something from something else according to the Oxford Advanced American Dictionary [4]. This effect occurs when the external load applied on the bolted joint is not concentric with the bolt center axis. The prying action affects the bolt by increasing the axial load on the bolt due to contact nonlinearity [4].

The strength of the bolt in the joint decreases with regards to the level of the eccentricity under the prying action with a combination of the two facts which are bending moment and excessive tensile force. This additional force is generally considered at the studies investigating the bolted joints under the prying action, however, the bending moment occurred due to the eccentricity of the joint is not always the interested phenomena. Outcomes about the bolt bending moment under prying action in the literature are usually limited by only comments, and there are still unaddressed points about the bolt bending deformation at the literature.

In addition to lack of attention on the bolt bending deformation under the prying action, it is important to evaluate the bending-tension interaction of the bolt under the prying action by using engineering approaches. Numerical and experimental studies can generally give more accurate results than analytical methods due to the nonexistence of a comprehensive analytical formulation. On the other hand, numerical approaches are more popular than the experimental works among the literature because of the high financial and time costs. In brief, the finite element method which is one of the widely used numerical methods for the structural analysis can be appropriate for investigating the bending-tension interaction of the bolt under the prying action.

The bending deformation behaviour of a fastener at a bolted joint under the prying action was studied comprehensively in this thesis by using static structural finite element analysis. Different finite element modelling techniques of the bolted joints were examined. A novel modelling technique was also proposed for evaluating the bending deformation response of the bolted joint. The results of the finite element analyses were compared with several experimental studies. The bending-tension interaction of the bolted joint studied in this thesis

was evaluated with respect to such parameters as the eccentricity of the load, strength grade of the bolt and bolt preload level.

## **1.2. Objectives**

Performing a detailed study on the bending deformation characteristics of the fastener at a bolted joint under the prying action was aimed in this thesis by using finite element analysis. Global force-displacement response of the bolted connection, bending moment change along the longitudinal axis of the fastener, axial force and bending moment carrying ratios throughout both the elastic and plastic loading phases will be investigated by comparing different finite element modelling techniques of the non-preloaded bolted joints. A novel modelling method will be introduced while performing comparisons, and the outcomes will be supported by the experimental results.

After selecting the proper modelling method, bending moment change along the longitudinal axis of the fastener and axial force and bending moment carrying ratios throughout both the elastic and plastic loading phases will be studied for the preloaded bolted joints with respect to different preload levels.

Because the flexural capacity of the finite element modelling technique may affect the bending deformation behaviour of the bolted joint, the outcomes obtained from comparison of the modelling techniques can be used by engineers and academicians who desire to consider the bending deformation response of the bolted joint under the prying action. Aspects of the effects of such parameters as the eccentricity of the load, strength grade of the bolt, and bolt preload level on the bending deformation characteristics of a fastener can also be used by professionals.

## **1.3. Limitations**

Numerical and experimental studies within the context of this thesis were carried out by applying monotonic loading under static conditions. Static structural finite element analyses were performed for the numerical studies by the implicit solver. Thermal and dynamic effects were not included in studies, and they were neglected.

There are some disregarded features of geometric and material properties for the finite element modelling technique of the bolted joint. The helix angle was neglected while modelling the threads of the bolt. The damage properties of the materials used in the studies were also neglected. The post-necking behaviour of the materials was represented by extrapolating the strain-hardening behaviour.

#### **1.4. Structure of the Thesis**

A brief background about the topic of the thesis was expressed by mentioning objectives and limitations in the introduction part. At the literature survey part, the studies for the three-dimensional finite element analyses for the bolted joints, bolt bending phenomenon, and prying action were shared. Because of the widespread usage of bolted joints, not only the mechanical engineering field but also civil and aerospace engineering studies were also searched. The configurations and results of the conducted tests were given at the experimental study part. Finite element modelling parameters and bolted joint modelling techniques were highlighted at the part of the finite element models. After expressing the features of the finite element models, the results were shared, where the bolted joint models were evaluated in terms of force-displacement response, bolt force, and bolt bending moment by comparing the experimental and numerical results. Computational efforts were also compared in terms of CPU time. Some consideration items which cannot be included in the experimental program such as bolt preload were also studied, and their results were shared at the part of the results. In the final section of this part, the modelling techniques were overviewed. Lastly, the results were discussed, and future studies were emphasized.

## 2. LITERATURE REVIEW

### 2.1. Introduction

The studies related to the demand on the three-dimensional finite element analysis of the bolted joints with different modelling techniques of the fasteners, the bolt bending deformation, and prying action are presented in this section of the thesis.

There can be several reasons to construct a finite element model consisting of a bolted joint in terms of the aim of the studies. Yılmaz investigated the effect of the main contact parameters which are contact stiffness factor, penetration tolerance factor, and contact algorithm on the accuracy and solution time of the finite element analysis of a bolted flange joint [5]. Yıldırım used a bolted flange connection to develop a methodology for utilizing artificial neural network approximation of finite element analysis database [6]. Kumar et al. studied the bolted flange joint of a pressure vessel under internal pressurization by considering plasticity and contact effects by using a three-dimensional finite element model [7].

A remarkable number of engineering problems in the field of structural mechanics may not be solved by using two-dimensional assumptions, such as plane strain or axisymmetric modelling, due to geometry, loads, and boundary conditions. In addition, a bolted joint can be given as an example that prevents it to be applied in two-dimensional finite element modelling techniques. Constructing a two-dimensional finite element model neglecting the geometry of the bolted joint can cause discrepancies in the results. Mistakidis et al. proposed a two-dimensional plane stress T-Stub finite element model including a bolted joint, however, the force-displacement curve of the two-dimensional model is not quite accurate with experimental results [8]. Some discrepancies were also observed in the load-deformation response between numerical and experimental results of a T-Stem connection with bolted joint in [9]. A simplified two-dimensional finite element model was proposed based on component approach with 1-node and 2-node elements to represent the actual T-Stub behaviour in [10]. Although the proposed two-dimensional finite element model is easily applied and occasionally accurate with experimental results, it was shown that the proposed model was not robust in terms of the results shared in this study [10]. In



consequence, constructing the finite element model of a bolted joint three-dimensionally can be obligatory with respect to the engineering problem.

One of the reasons for the finite element modelling of the bolted joint with the three-dimensional approach is the bending deformation of the bodies under eccentric loadings. Because the bolts can be subjected to eccentric loadings such as prying action throughout their life cycle, bolt bending can be regarded as a possible deformation mode at the bolted joint under prying action. Although there is a significant number of studies that investigate the response of the bolted joints under the prying action in the literature, the bolt bending phenomenon under this type of loading was not evaluated as much as the global deformation behaviour of the bolted joint. The bolt bending deformation was not included in the study of simulating the prying action on the T-Stub with bolted joints by a finite element model in [11]. A mechanical model was developed to investigate the effect of the contact forces between members in the bolted joint assemblies on the behaviour of bolted T-Stub and L-Stub connections in tension by Couchaux et al., but the flexural rigidity of the bolt, bending deformation of the bolt in other words, was neglected and not included in this mechanical model [12]. Yilmaz did not mention the bolt bending deformation although the prying action was considered in the finite element analysis of the bolted flanges [5]. Some studies did not examine the bolt bending even the eccentric loading or prying action is present in the investigated finite element models of these studies with different model configurations such as bolted flange, end-plate, and welded T-Stub connections [13 - 17]. The detailed information for the bolt bending deformation from the literature will be given in Section 2.3.

## **2.2. Three-Dimensional Finite Element Modelling Techniques of the Bolted Joints**

In the case of representing the static structural response of a bolted joint under monotonic loading, the finite element modelling techniques of the bolts vary with respect to the objectives of the corresponding analysis. These methods can be varied with respect to their modelling efforts for the engineering problem, providing outputs, and contribution to the load path and global stiffness of the structure. For this reason, the variety of the modelling technique of the bolts in the three-dimensional finite element analysis may be in the most primitive version as well as the most realistic form.

The general modelling methods of the bolted joints in the three-dimensional finite element analysis are demonstrated from the most primitive version to the most realistic form as follows. The most primitive modelling technique of the bolted joint can be seen in Figure 2.1 [4]. In this type of method, the fasteners in the joint are completely disregarded and the interface of the members are bonded to each other to maintain the load path. The stiffnesses in terms of the geometric and material characteristics of the fasteners and contact nonlinearity caused from the contact between the fasteners and members in the joint cannot be included in the analysis in this type of method.

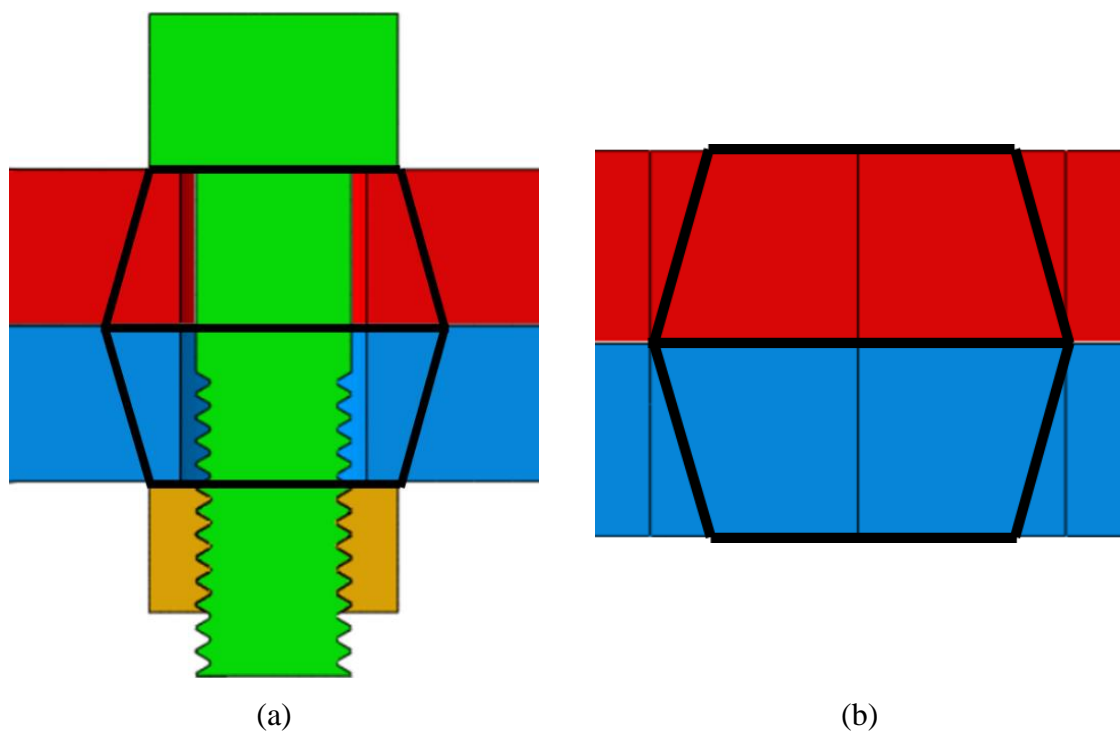


Figure 2.1. (a) The bolted joint with emphasizing the pressure cone lines, (b) The representation of the joint modelling by completely disregarding the bolts (Interface of the members are bonded to each other along the pressure cone area).

To include the geometric and material stiffness of the fasteners, the joint can be modelled by using a finite element connector which is a one-dimensional member generally used in the finite element analysis to model mechanical relationships between structural components in an assembly [18]. It is important to mention that the connectors can be chosen also as rigid which makes the connection stiffer than the elastic one. A representation of a bolted joint by

using a connector is given in Figure 2.2, the detailed information for the attachment of the connector onto the members in the joint can be found in the Finite Element Models Section.

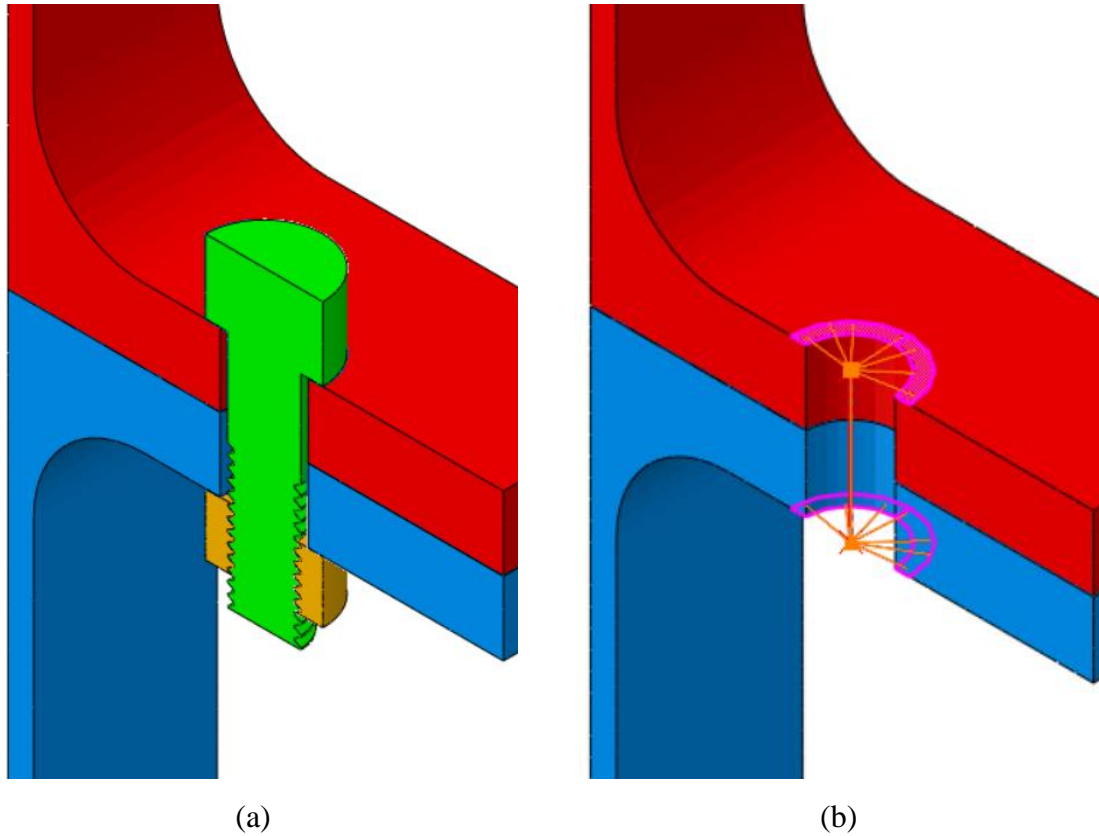


Figure 2.2. (a) The bolted joint, (b) The representation of the bolted joint modelling by using a connector (The connector end points are linked with the contact area of the bolt head and the nut, or washers if included).

There are several improvement studies for the finite element connector to include different nonlinearities and deformation modes such as bolt bending. A nonlinear finite element connector was proposed by Verwaerde et al. to reflect the tangential behaviour in the normal plane of the connector axis for providing frictional contact between the members in the joint by considering axial and bending stiffness of the bolt. However well agreement between the three-dimensional reference model and the connector model and a significant computational effort reduction was obtained, the proposed connector can be used in linear elastic range and under small-perturbations assumption [19]. The axial, bending, shear, and bearing characteristics of the bolt was represented by using different finite element connectors in the model proposed by Askri et al. Reduction for calculation times while providing a good

estimate for the mechanical response of the bolted joint assembly was obtained in this study, but any information was not shared for the bending deformation mode performance of the proposed method [20]. It is not always necessary to reflect the geometric stiffness by defining a finite element connector as the study by Razavi et al. The required degree of freedom adjustments for bolt axial and bending stiffness to maintain connector behaviour were arranged by background code implementation. The proposed algorithm was verified by using an experimental investigation from the literature, but no results were given for the bending deformation characteristics of the proposed method [21]. As shown by using examples from the literature, finite element connectors can provide to represent the stiffness of the bolt in terms of geometry. Stress output cannot be obtained from the finite element connector, and nonlinearities such as material and contact are not included in this technique. It should be also mentioned that using finite element connector may not provide satisfactory results to represent the bolt bending behaviour based on the studies referred above.

The usage of the elastic beam element for representing the bolts is similar to the finite element connectors. There are several similarities with respect to modelling opportunities such as arranging the bolt stiffness and being a one-dimensional element. However, stress and strain outputs can be obtained from the beam elements while the finite element connectors cannot provide them. The usage of the elastic beam element took part in the finite element modelling technique for the bolted joints in the literature. Blachowski and Gutowski used the beam elements to represent the bolts in a circular bolted flange connection at the telecommunication tower [22]. Kim et al. include the modelling technique with beam element to their study which is about comparing the modelling techniques of the bolted joints [23]. When the bolt is not fully threaded and has a shank region with a threaded region inside the grip length, the bolts can be modelled with different sections or equivalent sections by arranging the geometric and material stiffness as schematically represented in the study for the development of a calculation macro-model for the sizing of aircraft wheel fasteners as shown in Figure 2.3 [24]. Besides the easy implementation and relatively low computational effort, some three-dimensional effects such as stress distribution in the cross-sections and contact nonlinearities cannot be included in the three-dimensional finite element analysis for the bolted joints by the usage of the beam elements.

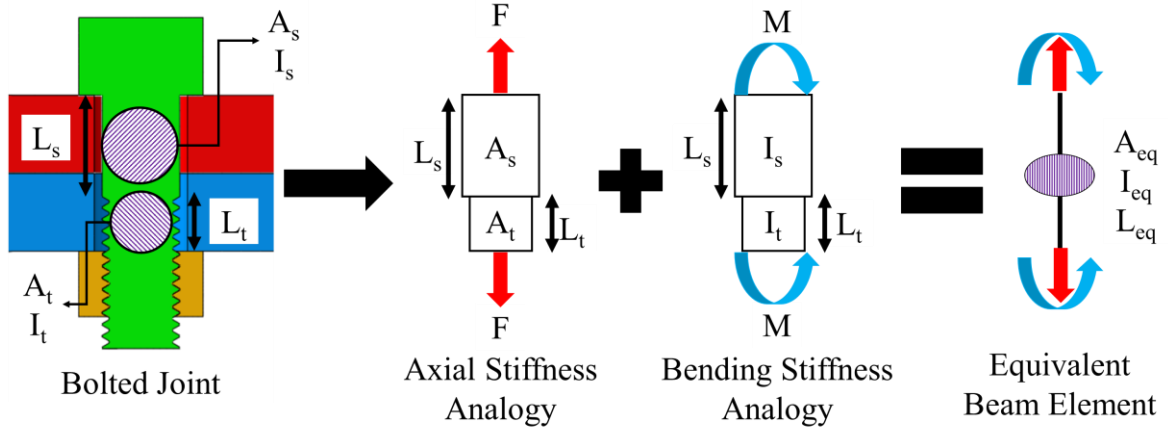


Figure 2.3. Schematic view of the construction of the equivalent beam element modelling of the bolted joint by considering axial and bending stiffness including geometric properties (subscript ‘s’ represents the shank region of the bolt, subscript ‘t’ represents the threaded region of the bolt, and subscript ‘eq’ represents the new equivalent beam element).

To include the three-dimensional effects, the bolts can be modelled by using solid elements which are three-dimensional elements by facing up to increase in the computational effort. The three-dimensional modelling techniques have also different versions from primitive to realistic forms. Wu et al. showed the simplified bolt models commonly used in the literature as given in Figure 2.4 (a). In these types of methods, the threaded regions and contacts are not included in the model, instead, this threaded region is replaced by a cylinder with respect to chosen approach. As shown in Figure 2.4, the clamped region can be modelled with a uniform cross-section or stepped regions with different cross-sections and lengths. In this study, it was mentioned that bolted joint modelling techniques with uniform cross-sections generally overestimate the amount of the deformation at the failure because of neglecting the plastic deformation mechanism on the threaded part. Wu et al. obtained that the proposed model overestimates the bolt stiffness between 9 and 20%, and load-carrying capacity of the bolt and ductility results are consistent with the refined finite element model which was constructed by using the most realistic form of the bolted joint model. Not including the contact between the external and internal threads on the bolt and the nut affected the computation effort positively by not requiring longer running time. [25]. These primitive forms of the three-dimensional modelling method of the bolts can be found in different configurations as shared in [2, 4, 11, 26-29].

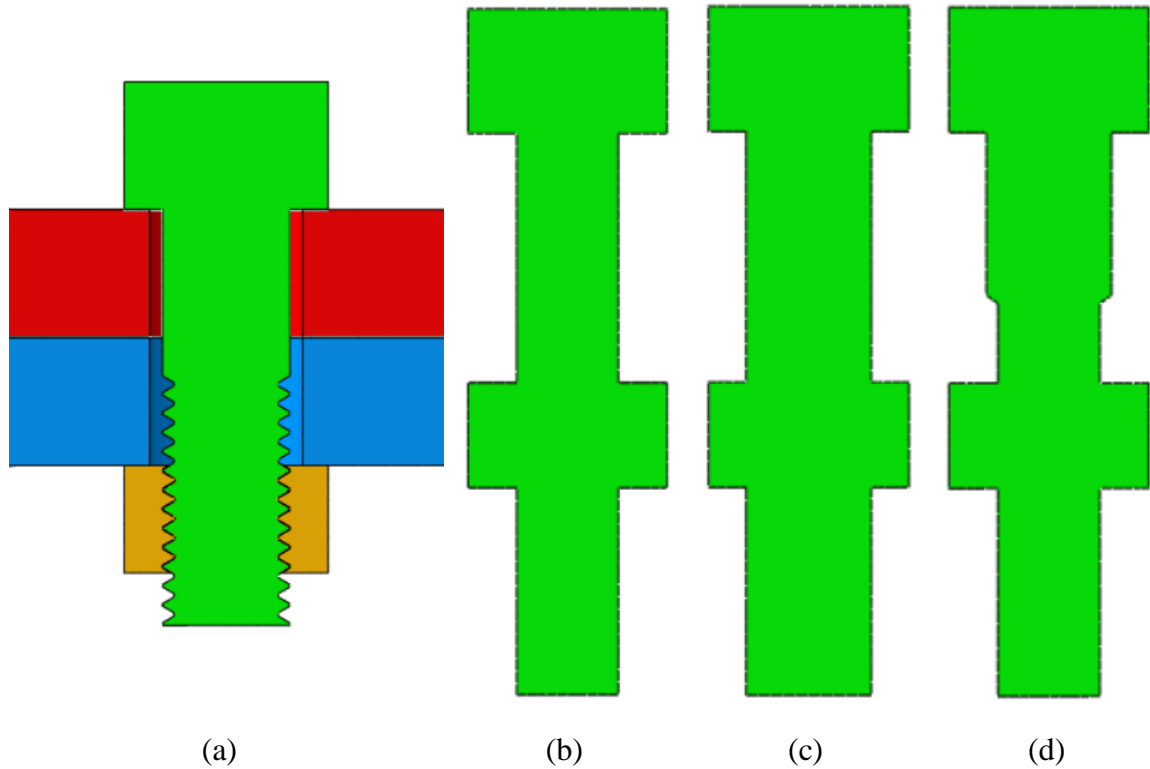


Figure 2.4. (a) The bolted joint. The most common finite element modelling techniques of the bolts at the clamped region of the joint by using (b) only minor diameter, (c) only major diameter and (d) both the minor and major diameter to separate the shank and threaded region.

The extent of the finite element model of a bolted joint can be enhanced further by including the contact phenomenon between the internal and external threads on the nut and bolt. However, this method may cause an increase in computation effort and convergence problems. A finite element analysis tool helps to overcome these problems by not including the threads physically but making the computations by considering the contact between the mating threads. Söderlund demonstrated the advantages and disadvantages of this modelling technique and compared the computational effort of this method with other techniques [29]. Although this method has remarkable features among the other modelling techniques in terms of representing the contact between the threads, there is a considerable time consumption with respect to methods without threads.

There are several studies that the threads are included for the finite element modelling of the bolted joint by physically modelling the internal and external threads on the nut and bolt.

The threads can be modelled with helix angle or not. Molnár et al. constructed finite element models for investigating the sufficiency of the numerical analysis of the bolted joints. In this study, threaded contact and bonded contact between the bolt and nut were compared with ignoring the helix angle of the threads. It was obtained that bonded contact modelling between the nut and the bolt increases the rigidity of the joint by approximately 10% compared to threaded contact, but this result was not proved to any experimental work in this study [30]. Finite element models of the bolted joints including helix angle are not rare in the literature although they generally cause high computational and modelling effort including convergence problems. The inappropriate transition for the run-out region for helical threaded geometry can cause also geometric faults. Bommisetty and Narayanan used helical thread geometry in their study for the three-dimensional finite element analysis of the bolted joint of a flange connection [31]. Hu et al. included the helical threaded geometry while investigating the mechanical performance of the high-strength 8.8 grade bolts subjected to tensile loading [32]. The geometric fault for the run-out region and the sudden transition can be seen clearly in [32, 33].

When the threaded bolts are modelled with helix angle, the pretension cannot be done directly with an embedded finite element tool which is generally known as bolt load and becomes a concern for the modelling procedure. Different configurations take place in the literature for applying the bolt preload for this situation. Firstly, the bolt pretension can be maintained by the tightening torque applied to the bolt head or nut directly [34, 35]. This tightening torque can be also applied by shear stress on the outer surfaces of the nut indirectly as given in Figure 2.5 [33]. Secondly, rotating the nut with respect to corresponding angular displacement for the required force is a way to apply the tightening force. The method is shown in Figure 2.6, and it is known as the “turn-of-nut method” [36, 37].

### **2.3. Bolt Bending**

Depending on the loading type and conditions, bending deformation can be occurred on the bolts throughout their life, and this bolt bending deformation may be investigated for the evaluation of static strength, fatigue limit, or stress concentration of an individual bolt or different bolted joint types. A flange connection of the pressure vessel under the internal pressurization is one of the main joint types including the bolt bending deformation. Kumar

et al. studied the static response of a bolted flange joint of a pressure vessel under the internal pressurization, and they mentioned that this loading bent the bolt by causing approximately 40% bending distribution throughout the bolt cross-section [7]. Abid observed the bolt bending deformation at the gasketed flange joints under internal pressure loading [38]. Abid and Nash highlighted bolt bending as one of the main factors affecting the fatigue performance of both gasketed and non-gasketed flange joints [39].

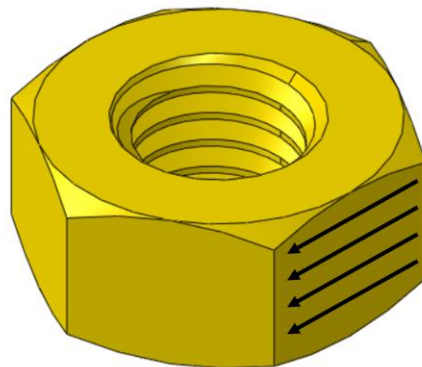


Figure 2.5. Application of the tightening torque by using shear stress on the outer surfaces of the nut indirectly.

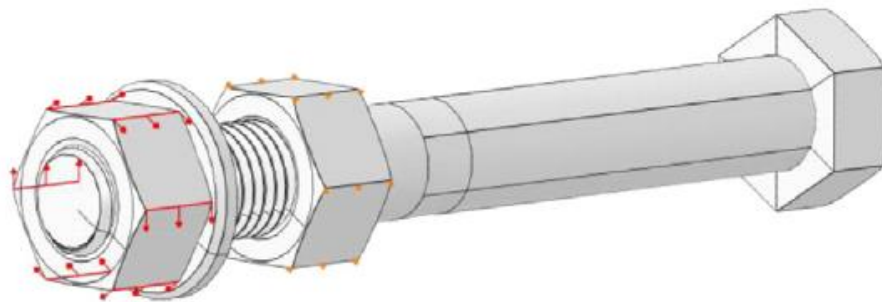


Figure 2.6. The representation of the “turn-of-nut method” method which is a way to apply the tightening force by rotating the nut with respect to corresponding angular displacement for the required force is a way [36].

Structural shapes such as buildings and towers built by using constructional steel also contain connections including fasteners exposed to bolt bending. Before introducing the bolt bending phenomenon among the structural shapes, the following explanations can be useful for the reader. Differently from the pressure vessels, these shapes may have also flange connections.



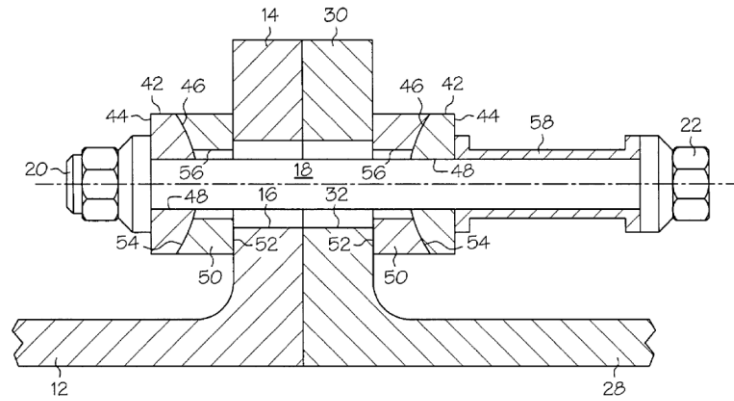
They contain several structural bolted joint types, and the beam-to-column, column-to-column, clip-angle and end-plate connections are some types of those joints.

Under the axial force in the beams, Dinu et al. observed strength reduction between 15% to 30% on the bolts at the beam-to-column connection due to the bending moment developed in the bolts [40]. Liu et al. experienced that the shank of the bolts of a flange joint at the column-column connection of a prefabricated multi-high-rise steel structure can be subjected to both tensile force and additional bending moment under a combination of bending moment and shear force [41]. Bending deformation of the bolt in a clip-angle connection which is a similar configuration with beam-to-column connection was also seen under the axial force in the beams and occurred in the underneath of the bolt head [42]. Bai et al. mentioned that the bolts in the end-plate connection which is also a similar configuration with beam-to-column connection are not only under tension, but they can be also subjected to bending moment, and this situation was pointed out as a remarkable influence on the strength of the bolts [43]. The bolt bending deformation was observed from different configurations of the structural shapes in the studies, however, this fact was not evaluated adequately by many of the studies while the importance of the bolted connections increases against the welded connections in the structural shapes for its ductile performance due to catastrophic failures caused by the structural weakness and brittle fracture of the welded connections at the major earthquakes [42-44].

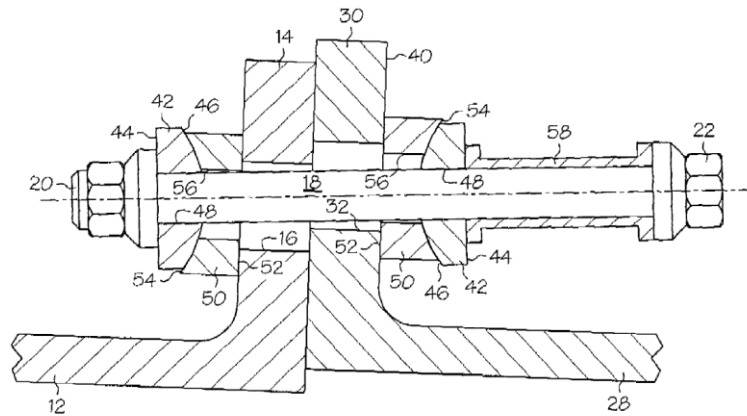
Because the bolt bending phenomenon is an undesired situation for the life-cycle of the bolts due to strength reduction, some preventative methods secured by patents were developed to eliminate the occurrence of the bending moment on the bolts. Two of them are given in Figure 2.7 and Figure 2.8. as examples, and components and detailed information can be found in [45, 46]. These methods may eliminate the bolt bending deformation; however, they are not standard products, can produce some geometric limitations in the design, and their preload maintenance is not clearly defined. These factors may limit the widespread usage of these patents.

After representing the mechanical systems that the bolt bending occurs and preventing methods, the formation of the bolt bending can be expressed from this point. This

deformation behaviour generally occurs under two different configurations which are bolted joints under eccentric loading or deviation on the contacting surfaces.



(a)



(b)

Figure 2.7. Two-piece washer for minimizing bolt bending (a) undeformed, (b) deformed configuration [45].

The surface flatness of the joint members is not the subject for the bolt bending phenomenon of this study, nevertheless, some of the literature studies about this configuration will be given. Non-parallel contact between the fasteners and the surface of the joint affects the tension response while the preloading sequence and may significantly reduce the reliability of the bolted joint due to the high stress concentration in the small initial contact region, which may cause plastic deformation and damage the joint area [47]. In other words, the non-parallel contacting surfaces cause bending moment in bolted joint due to the inclination on one or both of the surfaces, resulting in the surplus of the integral of thread contact force,

which leads to the extra contact and lateral pressing in mating threads [29, 35]. The imperfect joint face angularity of this non-parallel contact can be seen in Figure 2.9.

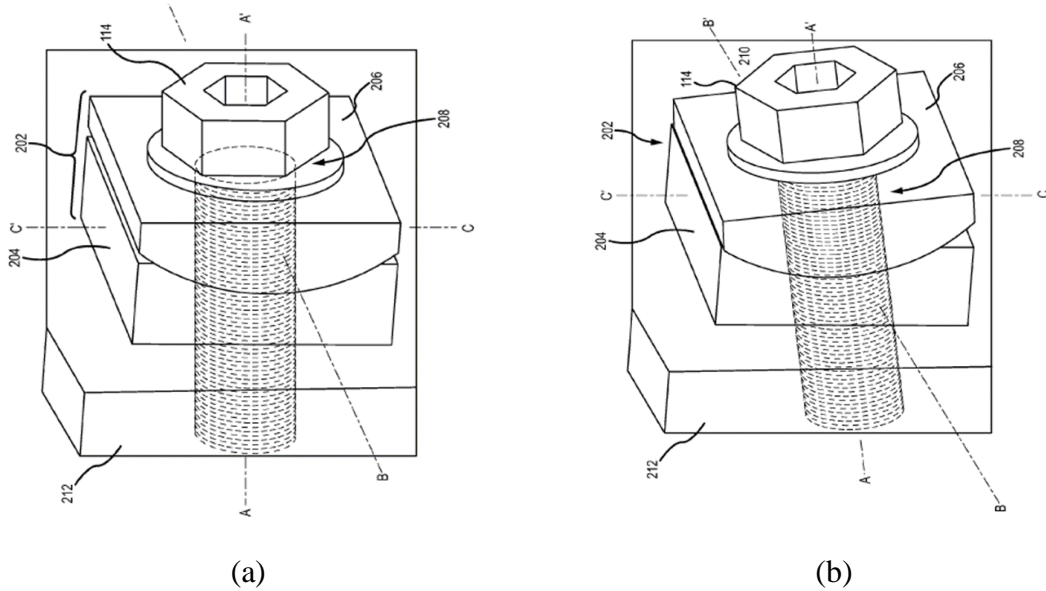


Figure 2.8. Moment relief barrel washer (a) undeformed, (b) deformed configuration [46].

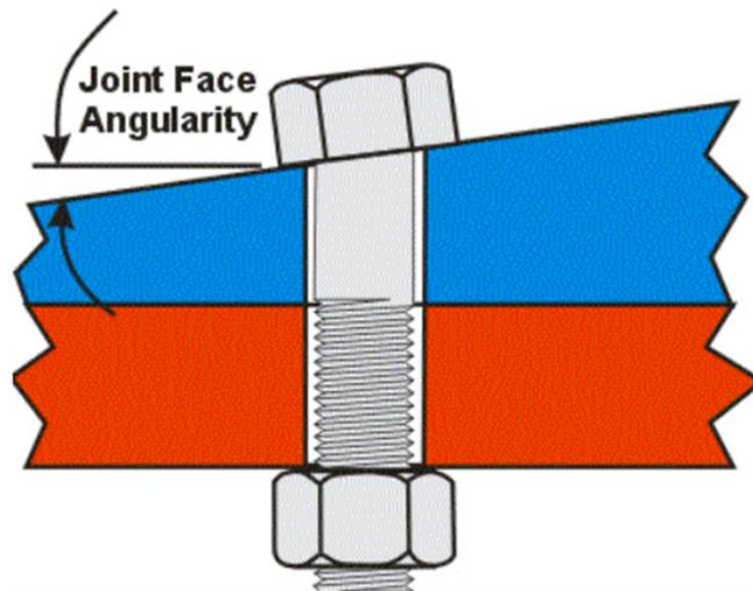


Figure 2.9. Surface inclination [48].

Yang and Nassar considered the bolt bending deformation while proposing an analytical model for the effect of wedge contact on the loosening performance of a bolted joint under the transverse cyclic loading. They concluded that a large bending moment raised from the

eccentrically concentrated load can be occurred when the wedge angle is large enough [49]. Similar results were observed also in the study of which the effect of the non-parallel contact of the members in a bolted joint on the fasteners while the preloading sequence was investigated [34]. As the inclination angle of the bolted joint increases, the bending moment, the additional torque and the preload deviation increase nearly proportionally during the preloading phase, and consequently, the deviating surfaces induce high stresses and especially create a larger stress amplitude which will lower the fatigue strength limit [29, 35].

After a piece of brief information for the bolt bending caused by the surface deviation, the literature content of the bolt bending caused by eccentric loading can be highlighted. The interest for the bolt bending deformation under eccentric loading is not a trending topic among the bolted joint literature, moreover, a remarkable number of studies have been done throughout the years. The compliance of the connected parts was pointed as the main factor affecting the bending stresses in the bolt at one of the earliest studies, and it was mentioned in this study also that the additional bending deformation on the bolt may influence the strength and reliability of a bolted assembly under the eccentric loading [50]. In the earliest studies, it is worth mentioning that there are methodologies that were proposed by using the theory of elasticity approach for the bending moment occurred in the bolts at the T-flanges and pipe flanges under the external loads [51-54]. Besides the analytical formulations, the studies for the mechanical models are also found from the literature for the bolted joints under the eccentric loading in the 20th century. At two of these studies, mechanical models consisted of linear springs and beams for the bolted joints were proposed by considering the bending moment occurred in the bolt due to eccentric loading, however, they could be only validated with the experimental or numerical studies including small eccentric loading [55, 56]. The importance of the consideration for the additional bending stress occurred in the bolt under the eccentric loading was procured from the analytical calculations and mechanical models given in some of the earliest studies [51-56].

The significance of the bolt bending phenomenon is also stressed in many of the studies including different bolted joint configurations such as flanges and structural connections. By the development of the computational tools, the usage of the finite element method for the

structural analysis of the bolt bending deformation behaviour under the eccentric loading has been involved in the literature. The finite element analysis was used to demonstrate the strength reduction in the T-Stub connections due to the bending of the bolts in [57], however, this bending deformation was only related to the flange deformability, and not evaluated comprehensively in this study [57]. The deterioration of the ultimate strength was observed in the clip-angle connection which is another structural joint due to bending deformation of the bolt by finite element analysis in [42], but it was not observed an evaluation for the bolt bending in this study also [42]. There are more examples which barely mention the bolt bending at the bolted structural connections by the usage of finite element analysis. Blachowski and Gutowski observed the presence of the bending moment in the bolts at the circular flange connection under the eccentric loading, however, they only pointed this deformation out by comments merely [22]. Although the bending moment in the bolts may highly influence the maximum stress, which is a critical design parameter, Pedersen slightly referred to the importance of the bending moment occurred in the bolt at the L-flanged connection [58]. The observation by Couchaux et al. stressed that failure of the bolts at the circular flange connection can be concluded by combined tension and bending under the eccentric loading, but this outcome was not evaluated clearly at their finite element analyses in this study [59].

Eccentric loading can be seen also in the leakage studies which are done for the bolted flanges under the internal pressurization. The resultant force created by the internal pressurization is carried eccentrically by the bolts at the flange joints because of the geometry of the connection. Abid mentioned the bolt bending deformation at the flange joint under the internal pressurization, but this phenomenon was not evaluated comprehensively in this leakage study [38]. Khan et al. performed a three-dimensional finite element analysis study to investigate the effect of the different bolt preload sequences on the sealing performance of the flange joint under the internal pressurization and axial loading, and they observed that the bolts bent more at ASME preload strategy than the industrial one at the end of the total loadings. Although this is an important outcome for the bolt bending phenomenon, the results for this deformation were limited by sharing only the stress distribution of the bolts [60].

Despite the studies given above for bolt bending, some bolted joint studies in the literature comprehensively evaluated the bolt bending phenomenon. Abidelah et al. have modified a conventional mechanical model for the eccentric bolted joint by adding a rotational spring for the stiffness analogy to simulate bolt bending which is neglected in the conventional model. The comparisons between the finite element analysis and mechanical model show that the modified model represents well the response of the T-Stub connection while considering the bolt bending. Furthermore, the results of the bending ratios up to 55% at the bolts under the eccentric loading pointed the necessity of including the bolt bending effect out. Besides the high bending ratios, the stress distribution at the shank region of the bolts is nearly full of tensile stress while the bending moment occurred in this region less than 20% of its bending moment that causes yielding. They also mentioned that the increase in the member thickness at the joint leads to a decrease in the bolt bending moment [61]. Bao et al. observed from 13% to 45% bending ratios at the bolts in their study of both experiments and finite element analyses when the bolts yielded under monotonic loading in the T-Stub connection. According to their results, increasing the eccentricity rises the bolt bending moment while this moment decreases by increasing the member thickness. They also showed that increasing the bolt diameter rises the bending moment but decreases the bending stress in the bolts [62]. The results observed in [62] indicate that there is a difference between the bending moment and bending stress in terms of the bolt bending ratio such that higher bending moment is not related to a higher bolt bending ratio. Tartaglia et al. investigated the stiffness and ductility of the T-Stub connection experimentally and numerically. They observed bending deformation at the bolts, and also shear deformation at the large displacements. Some of the fractured bolts have deformed in the shank region without necking due to bolt bending. The influence of the bending moment on the global response of the T-Stub connection was argued in this study. [63]. Although they are remarkable studies considering the bolt bending deformation, evaluation on the critical cross-section which the maximum bending moment occurs at the bolt was not performed, and effects of the bolt preload on the bending-tension interaction of the fastener were not investigated.

As mentioned at the beginning of this section, the bolt bending deformation is investigated in the literature not only for static strength but also for the evaluation of fatigue limit and stress concentration at bolted joints. These phenomena are not mentioned here because of

the scope of the thesis, but there are remarkable studies about the effect of the bolt bending on the fatigue limit and stress concentration [64-67].

#### **2.4. Prying Action**

Bending of the bolt is not the only excessive deformation phenomenon of the bolt under the eccentric loading, prying also occurs in some circumstances. As mentioned in the introduction part, prying action increases the axial load on the bolt due to contact nonlinearity, and this additional force on the bolt can be defined as the prying load. Therefore, eccentric loading on the joint not only bends the bolt by the moment arm but also increases the axial load due to prying action. Consequently, the stress distribution at the bolt is combined with bending and tensile stresses, and the free-body diagram and the detailed view of stress distribution are shown in Figure 2.10. Prying action occurs on the different types of bolted joints under the eccentric loading, however, bolt bending which is one of the most expectable deformation types under the eccentric loading was neglected at many studies which investigated the prying action. As mentioned previously, Simon and Hengehold did not consider the bolt bending deformation at the T-Stub connection under eccentric loading while investigating the prying action by finite element analysis [11]. Abidelah et al. experimentally studied different structural bolted connections to investigate the effect of the stiffeners on the connection behaviour. They observed that including the rib stiffeners to connection structure decreases the prying force on the bolt, however, they did not mention the influence on the bolt bending of this addition [14]. Couchaux et al. theoretically and numerically proved that decline in the ratio between member stiffness and bolt stiffness increases the prying action, but they did not include the flexural rigidity of the bolt in this study, therefore the effect of the bolt bending capacity on the prying action could not be evaluated [12]. It was shown in [68] that increasing the member thickness deduces the prying force on the bolt, but the bending moment occurred on the bolt was not evaluated although the bending stiffness of the member changed. Hua et al. did not consider the bolt bending while they stressed the bending flexibility of the members in the connection for the presence of the prying action causing the excessive tensile force [16]. Atasoy investigated the prying action comprehensively by mentioning that the prying load on the bolt cannot be determined directly with analytical methods but can be assigned by using empirical modifications. It was shown in this study that prying load increases when the bolts are preloaded. The ratio of the prying load over the external force decreases when the ratio of

the member thickness over the bolt diameter increases. The reason for this change can be the increased dominance of the member bending stiffness to bolt bending stiffness, however, there was not any comment about this fact in the study because of the negligence of the flexural rigidity of the bolt [17].

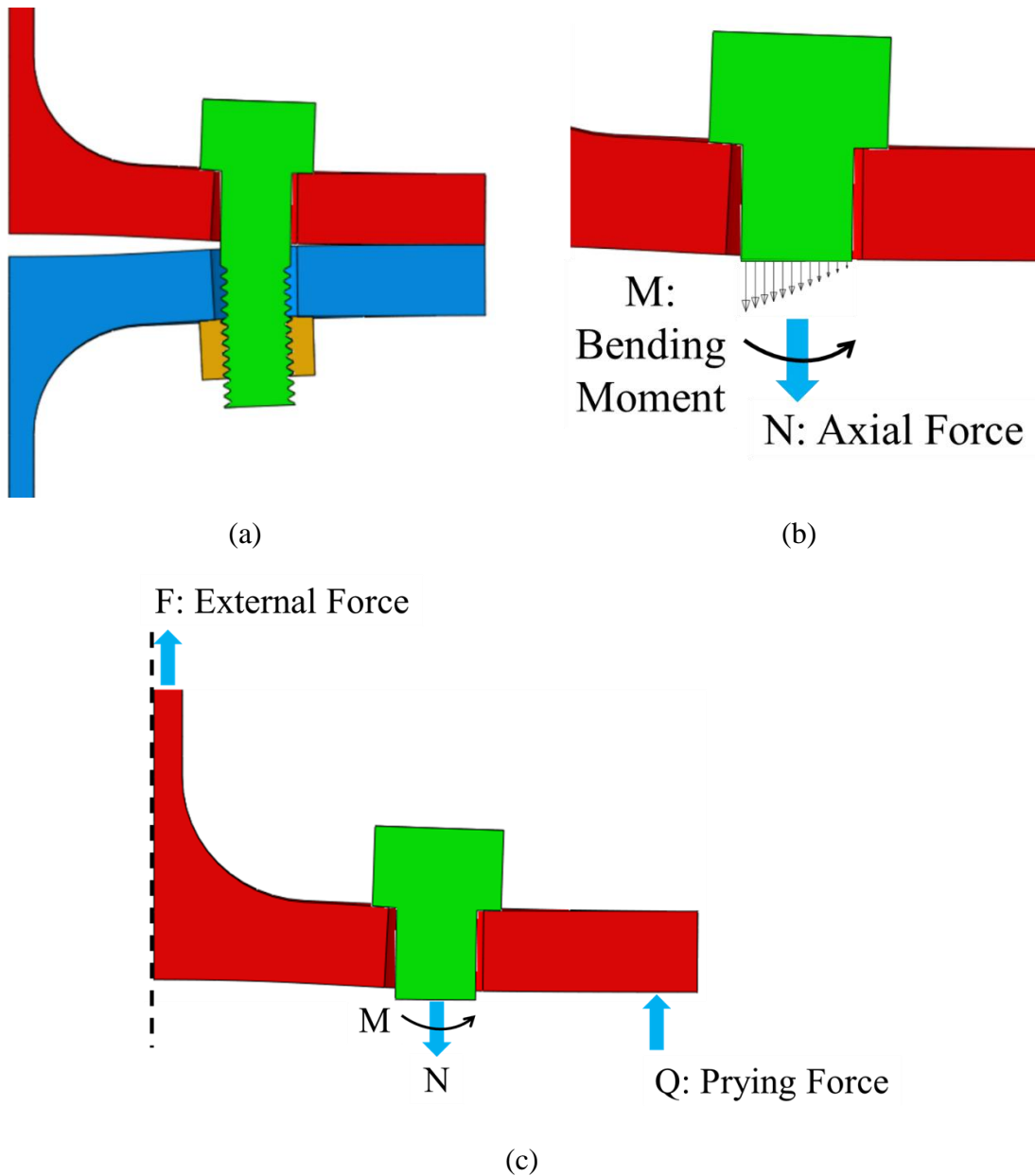


Figure 2.10. (a) Deformed situation of a bolted joint under prying action, (b) a schematic representation of the stress distribution of the bolt by mentioning the internal bending moment and axial force, (c) free-body diagram of the bolt and upper side member.



It is known that prying action and bolt bending decrease the strength of the joint which is under the eccentric loading. In the literature, there are studies which investigate the prying action at the eccentric loading by also considering the importance of the bolt bending. Ahmed et al. performed nonlinear finite element analyses for the top-angle and seat-angle bolted connections. It was mentioned that decreasing the member thickness develops a higher prying load at the bolt while indicating the presence of the bending moment at the bolt in addition to prying force [69]. Komuro et al. investigated the prying action in the top and seat-angle connections by performing nonlinear finite element analyses. They highlighted bending stiffnesses of the bolt and the members and the eccentricity as the factors for the prying action while mentioning that larger diameter of bolts, decreasing the member thickness, or increasing eccentricity develops higher prying forces [70]. El Kalash and Hantouche focused on secondary prying which is a little more complex phenomenon than conventional prying, and they observed also larger tensile force and bending deformation at the bolt due to prying action at the configuration that relatively small member thickness was used [71]. Apeland suggests stiffer geometric properties for the members having relatively lower material stiffness such as titanium and aluminum for minimizing the prying action. It was mentioned that bending moments may not be present according to VDI 2230 when the bolts are highly pre-tensioned, and the material of the members are steel but bending moments should be considered for custom designs such that softer materials were used for the members [4]. Huang et al. modified the formula for the prying force at the flange connections by considering the bending deformation of the bolts which are subjected to additional bending moment due to flexural deformation of the flange. They performed finite element analyses for the equation parameters used in the formulas, and they observed that the growing tendency of the prying force is negligible when the ratio of edge distance over the eccentricity is higher than one [72]. By mentioning the presence of the bolt bending deformation reducing the load capacity of the joint, Liu et al. stressed that the parameter causing the largest impact on the prying force is the flange thickness while the others affect less than the flange thickness [41].

The bolt bending phenomenon was considered in [4, 41, 69-72] in the presence of the prying action, however, these do not provide enough information to evaluate the bolt bending in terms of bolt bending moment or the effect of the parameters on the bending deformation of the bolts. Some evaluation has been made for the bolt bending while the prying action exists

in [62]. As mentioned previously, increasing the eccentricity rises the bolt bending moment while this moment decreases by increasing the member thickness. It was also showed that increasing the bolt diameter rises the bending moment but decreases the bending stress in the bolts [62].

Because the number of parameters affecting the bolted joint under the prying action is not low, it is essential to demonstrate the parameter effects on the outputs such as bolt force and bending moment while studying the prying action characteristics in terms of the flexural rigidity of the fastener. The influence of increasing the values of the parameters belonging to bolted joint under the prying action on the different evaluation items can be summarized as given in Table 2.1 [3-4, 29, 34-35, 37, 43, 61-62, 68, 70, 75-87]. As shown in Table 2.1 and related to bolt bending deformation, there is no information about the effects of the bolt preload on the bolt bending moment in the literature.

Table 2.1. The effects of increasing the parameter values on the different evaluation items.

Parameter	Eccentricity	Member Thickness	Elasticity Modulus of the Members	Bolt Diameter	Bolt Preload	Elasticity Modulus of the Bolt	Surface Flatness
Bolt Force	↑	↓	↓	↑	↓	↑	↑
Bolt Bending Moment	↑	↓	↓	↑	N/A	↓	↑
Prying Force	↑	↓	↑	↑	-	N/A	N/A
Stiffness of the Eccentric Joint	↓	↑	↑	↑	↑	↑	N/A

N/A: Not Applicable

## 2.5. Methods for Bolt Strength Evaluation

Because the eccentric loading may cause an additional bending moment at the bolted joint, it is important to evaluate the strength of the bolted joints under prying action, and it can be determined by using several test configurations. These can be summarized under two main configurations as the bolted flange joints and T-Stub connections. Four-point bending tests for the bolted flange joint and monotonic tensile tests for the T-Stub connection are widely used configurations in the literature. In addition, numerical studies such as performing finite element analysis can be also conducted for enhancing the strength evaluation in many studies. Moreover, bolt tensile tests and material characterization tests using tensile specimens may be conducted prior to joint evaluation tests because they provide the strength characteristics of the setup components separately.

Wang et al. studied the prying action of the bolts by using different flange connection types subjected to a four-point bending test, and they observed that prying action occurs at the bolted joint for both the unstiffened and stiffened joints. In addition to prying observation, they proposed a practical design procedure with the support of the finite element analyses which provides significant assistance for revealing the strength of the bolted joint more excellent [88]. Ibrahim et al. demonstrated the effect of the parameters on the deformation characteristics of the bolted flange joint with respect to the results of the four-point bending test. By the use of the finite element analysis, the deformation behaviour of the bolted joint under prying action was apparently demonstrated in this study, and failure modes including bolt bending were presented [89].

The T-Stub connection is considered as an equivalent model for studying the structural components in the Eurocode standard [86], and this feature provides that many studies included and considered this connection type while investigating the strength of the bolted joints under prying action. Similar to the studies including the bolted flange joints, the content of the experimental bolt strength evaluation studies involved supportive finite element analysis results.

## 2.6. Conclusion

To support the fact about the data absence for the influence of the bolt preload on the bolt bending moment, the items of the lack of information about the bolt bending deformation under the prying action are summarized as listed below:

- There is not any study about the effect of the finite element modelling technique of the bolted joint under the prying action on the bending-tension interaction of the bolted joint,
- There is not any study about the consideration of the critical cross-section of the fastener to determine the maximum bolt bending moment,
- The influence of the bolt preload on the bending-tension interaction of the bolted joint was not studied in the literature,
- The effects of the bolt preload on the bolt bending moment were not studied in the literature,
- There are studies indicating that the fastener carries a remarkable amount of bending moment under the prying action, but there is no clear evaluation of whether the failure of the bolted joint is caused by the bolt bending moment.

Lastly, it is worth to mention that the bolt bending deformation is not the only consideration item for the prying action studies. Fatigue and stress concentration topics are also investigated for the bolted joints under eccentric loading in the presence of the prying action. Because these topics are not the scope of the thesis, only one study will be expressed for each topic. Priaprez mentioned the influence of the additional tensile force occurred at the bolt due to prying action on the fatigue strength of the bolt because it reduces the number of cycles to failure. The bolt bending was also mentioned as a factor for the reduction of the number of cycles to failure of the bolted joint due to increased bending stress at the bolt [73]. Srinivasan and Lehnoff performed linear three-dimensional finite element analysis of the bolted pressure vessel joint to evaluate the stress concentrations at the bolt head fillet under the prying action. They observed higher stress concentration factors at the eccentric loading with respect to concentric loading, and as a result of this fact, it was mentioned that conventional stress concentration factors might not be satisfactory in the presence of the prying action due to additional bending moment and tensile force on the bolt [74].



### **3. EXPERIMENTAL STUDY**

The experimental program carried out for this thesis is introduced in this section. The experiments consist of three main sub-categories which are bolt tensile tests, material characterization tests, and prying tests.

Initially, the content of the tensile tests performed to evaluate the yield and ultimate strength of the bolts is described. Secondly, details of the tensile tests for characterization of the material used in prying tests are introduced. Lastly, the prying tests conducted for comparison with finite element analyses are demonstrated. The test configuration and results are shared under different sub-headings for each test program.

All tests were performed using an Instron test machine with  $\pm 150$  kN capacity. In this study, the loading was applied by displacement control with a 2 mm/min speed rate for each experiment in a quasi-static monotonic manner. A video extensometer was used to obtain displacement from the gauge length for more accurate results than the tensile test machine grip displacement at all specimens. Strain gauge sensors were instrumented for only one set of T-Stub samples for analysis comparisons. The details of the strain gauge instrumentation are given in the corresponding sections.

#### **3.1. Bolt Tensile Tests**

Several tensile tests on bolt material were performed to evaluate the strength properties of the fastener. ISO4762 partially threaded M10 size bolt produced by a local manufacturer was used in this study. The total length of the bolt is 45 mm with a shank length of 13 mm. The details of the experimental program configuration of the bolt tensile tests and the results are shared in the following sections. The whole experimental program conducted for the bolt tensile tests including the data processing is in accordance with the international standard of ISO 898 [90].

##### **3.1.1. Test Configuration**

The tensile tests of the bolts were performed by using a test setup consisting of two major components providing the threaded connection of the fasteners. Both the representative view

of the test apparatus assembled to the tensile test machine and the section view of the assembled test setup are shown in Figure 3.1. 4140 steel material was used for the test setup parts. A total of ten bolt tensile test samples were used in this study. Five specimens were 8.8-grade bolts while the other specimens were 12.9-grade bolts.

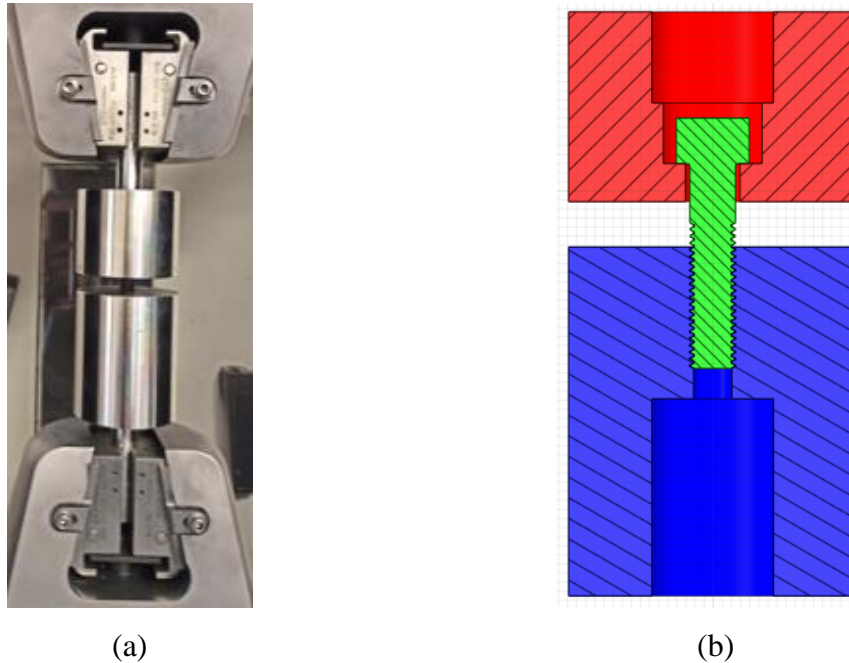


Figure 3.1. The views of the test configuration of the bolt tensile test, (a) assembly at the tensile test machine, (b) section view of the test setup.

### 3.1.2. Results

The force-displacement graph of the bolt tensile test specimens including the representative views of the destructed test samples, and the mechanical properties of bolt grades with average values are shared in this section. The force-displacement graph of both strength grades is shown in Figure 3.2, and the average force-displacement behaviour of both bolt strength grades is demonstrated in this graph. The average values of the mechanical properties which are strength and elongation parameters for both grades are shared in Table 3.1. As seen in the force-displacement graph and mechanical properties table, 8.8 grade has more ductile behaviour than the 12.9 grade. The strength values for both grades are also quite higher than the minimum recommended strength values for the corresponding bolt grades.

The strength values given in Table 3.1 are engineering values. True values are used while performing finite element analysis, and the corresponding values at the finite element models for the bolt materials will be introduced in the finite element analysis model section.

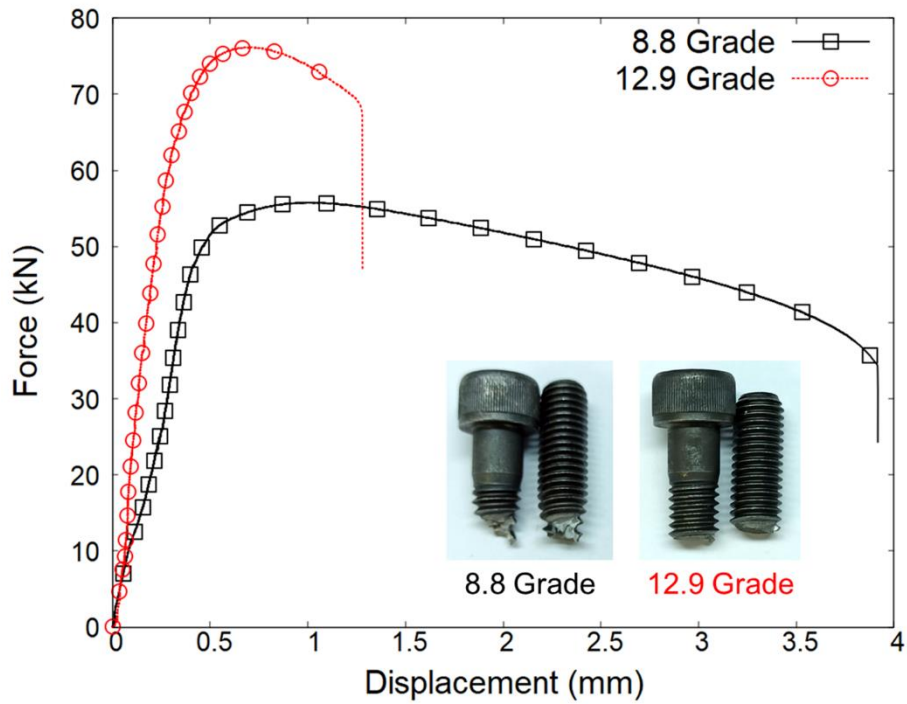


Figure 3.2. The force-displacement graph for both bolt strength grades including the representative views of the destroyed test samples.

Table 3.1. The mechanical properties of bolt grades with average values including standard deviation.

Bolt Grade	Yield Strength (MPa)	Ultimate Strength (MPa)	Elongation at the Ultimate Force (%)	Elongation at the Break (%)
8.8	$880 \pm 15$	$965 \pm 10$	$2.8 \pm 0.4$	$16.3 \pm 0.3$
12.9	$1185 \pm 10$	$1330 \pm 5$	$1.4 \pm 0.1$	$4.5 \pm 0.5$

### 3.2. Material Characterization Tests

Several tensile tests on setup material used in prying tests were performed to evaluate the strength properties. The details of the procedure applied to obtain the tensile specimens, experimental program and the results are shared in the following sections. The dogbone



sample geometries used in the experimental program conducted for the material characterization tests are in accordance with the ASTM A370 [91].

### 3.2.1. Test Configuration

S275JR steel material was used in this study. The samples were cut from a hot-rolled I-shaped beam produced by a local manufacturer by considering the rolling direction and section features. The water jet cutting process was used for cutting the samples from the I-shaped beam. The specimens cut from the web of the beam have three different orientations which are parallel, 45° inclined, and perpendicular to the rolling direction. On the other hand, the specimens cut from the flange are parallel to the rolling direction due to the geometric restrictions. The representation for this cutting process is shown schematically in Figure 3.3. The technical drawings of the dogbone specimens are given in Appendix A.

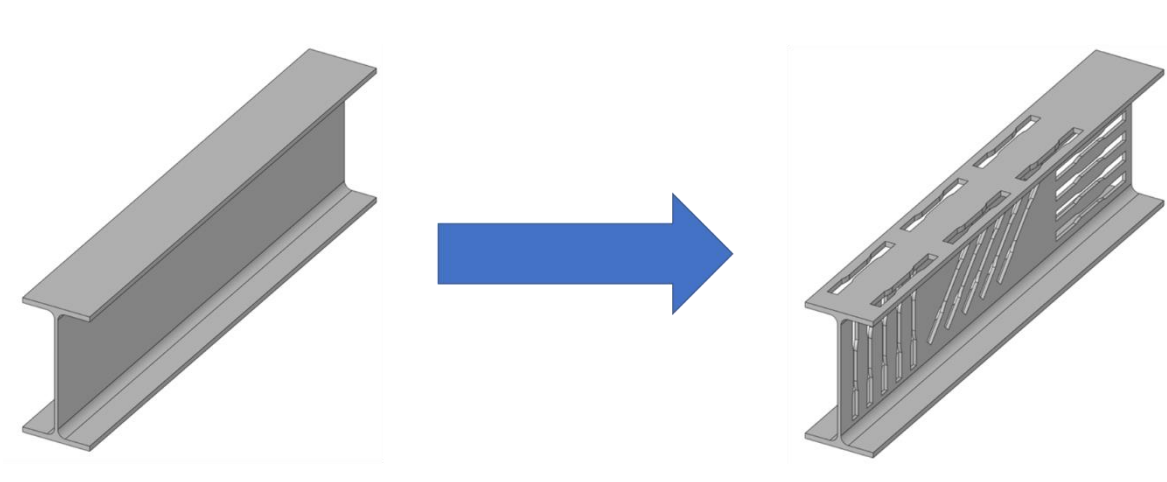


Figure 3.3. The demonstration of the manufacturing process applied for cutting the tensile specimens from an I-shaped beam.

The test matrix for the dogbone tensile specimens is given in Table 3.2. Because the samples were provided from different regions and orientations, each group was named as a specific code, and they can be seen in Table 3.2. These names are also used in the corresponding graphs and figures shared in the following results section.

Table 3.2. The test matrix for the dogbone tensile specimens.

Code	Number of Samples	Explanation
0-W	3	Region: Web Section Orientation: Parallel to Rolling Direction
45-W	3	Region: Web Section Orientation: 45° Inclined to Rolling Direction
90-W	4	Region: Web Section Orientation: Perpendicular to Rolling Direction
0-F	4	Region: Flange Section Orientation: Parallel to Rolling Direction

### 3.2.2. Results

The stress-strain graph of the dogbone tensile test specimens including the representative views of the destructed test samples, and the mechanical properties of each specimen category with average values are shared in this section. The stress-strain graphs of the specimen categories are shown in Figure 3.4, and the average stress-strain behaviour of both bolt strength grades is demonstrated in this graph. Because the nominal stress areas of the specimens from the web and flange section are different from each other, the stress-strain graphs are shared in this section. Lastly, the average values of the mechanical properties which are strength and elongation values for each category are shown in Table 3.3. Except for the hardening behaviour and elongation at the break parameter, a significant difference was not observed from the dogbone tensile specimen categories, and it was decided that an average parameter value set will be arranged at the material property assignment while performing finite element analyses.

As mentioned in the bolt tensile tests section, the strength values given in Table 3.3 are engineering values. True values are used while performing finite element analysis, and the corresponding values at the finite element models for the bolt materials will be introduced in the finite element analysis model section.

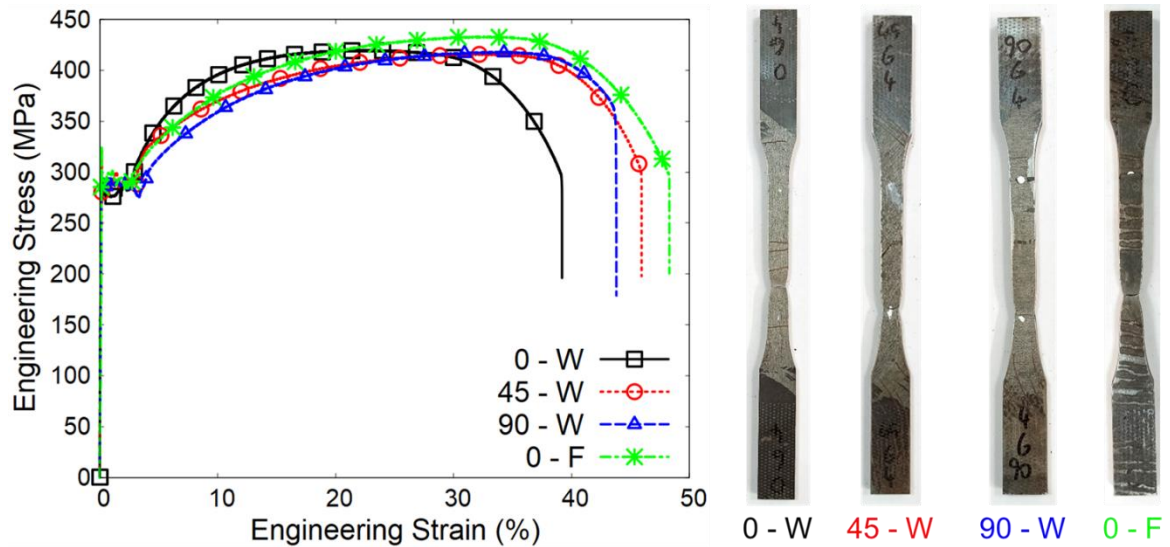


Figure 3.4. The stress-strain graph for each tensile specimen category including the representative views of the destroyed test samples.

Table 3.3. The mechanical properties of tensile dogbone test specimens with average values including standard deviation.

Code	Yield Strength (MPa)	Ultimate Strength (MPa)	Elongation at the Ultimate Force (%)	Elongation at the Break (%)
0-W	$297 \pm 10$	$417 \pm 5$	$27.3 \pm 1.3$	$37.7 \pm 1.3$
45-W	$283 \pm 2$	$413 \pm 2$	$33.3 \pm 2.5$	$44.0 \pm 1.6$
90-W	$288 \pm 3$	$414 \pm 2$	$32.5 \pm 2.2$	$40.8 \pm 2.4$
0-F	$298 \pm 3$	$421 \pm 7$	$32.5 \pm 3.0$	$46.3 \pm 1.5$

### 3.3. Monotonic T-Stub Tests

A total of 12 prying tests were conducted by using the T-Stub model which is a well-known configuration generally studied for the structural analysis of the beam-to-column connections in the civil engineering field [40]. A beam-to-column connection and its equivalent structural model called T-Stub can be seen in Figure 3.5. Single-row configuration for the bolted joint was used in this study. The details of the experimental program configuration of the monotonic T-Stub tests and the results are shared in the following sections.

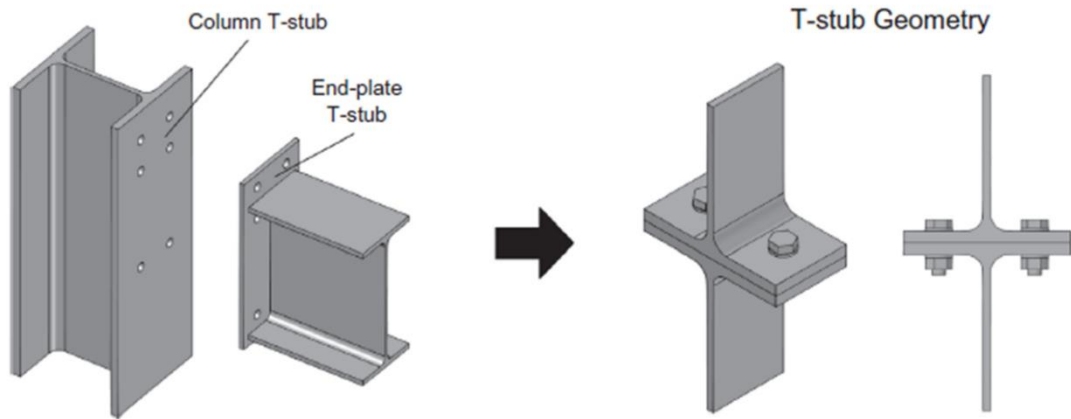


Figure 3.5. The end-plate connection and its equivalent T-Stub model [92].

### 3.3.1. Test Configuration

The test setup parts were cut from hot-rolled I-shaped beams produced by a local manufacturer. These beams are the same as the profiles used for the samples obtained from the material characterization tests. The initial cutting process used for obtaining the setup components from the I-shaped beam can be seen in Figure 3.6, respectively. After cutting the beam into particular portions, the parts were cut from the middle section to obtain two identical components. Then, the CNC operations such as drilling the holes were applied for the final shape. Two different eccentricity values were used in this study, and the final T-Stub model parts for both eccentricity values are seen in Figure 3.7. The final assembly of the T-Stub samples and the view of the assembled T-Stub samples on the tensile testing machine are shown in Figure 3.8. The technical drawings of the setup part designed according to IPE270 standard profile are given in Appendix B, and dimensions of the T-Stub assemblies are demonstrated in Figure 3.9 for both eccentricity values.

The test matrix for the T-Stub prying tests is given in Table 3.4. Because the samples include different bolt strength grades and eccentricity values, each group was named as a specific code, and they can be seen in Table 3.4. These names are also used in the corresponding graphs and figures shared in the following results section. One of the three tests from each category was performed with strain gauge sensors, and the details of the strain gauge instrumentation were given in the following section.



Figure 3.6. The representative view of the initial cutting process of the beam [93].

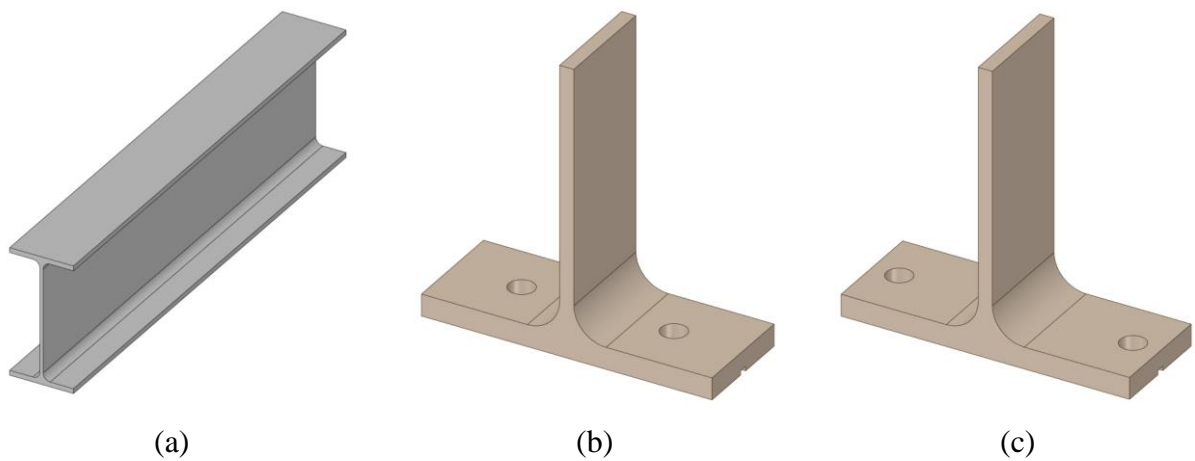
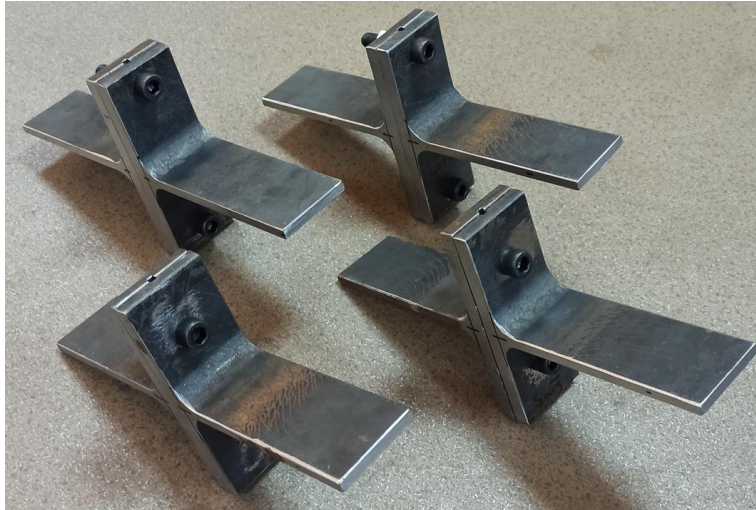


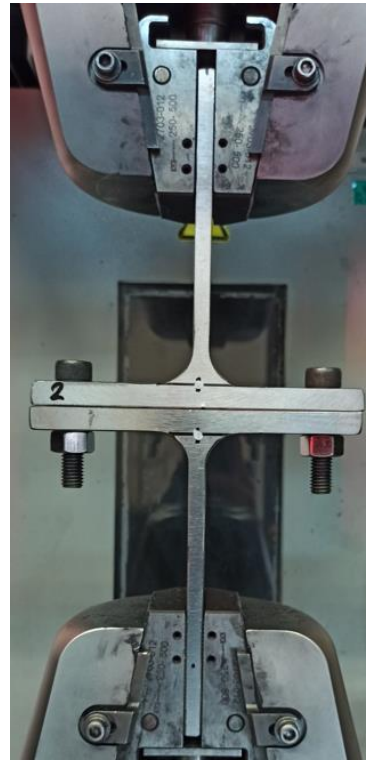
Figure 3.7. The whole process for obtaining the T-Stub components from an I-profile beam, (a) the raw shape of the beam, (b) the final shape of the T-Stub part with lower eccentricity, (c) the final shape of the T-Stub part with higher eccentricity.



(a)



(b)



(c)

Figure 3.8. (a) The view of the final assemblies of the T-Stub samples, (b) assembly at the tensile test machine of the T-Stub model with lower eccentricity, (c) assembly at the tensile test machine of the T-Stub model with higher eccentricity.

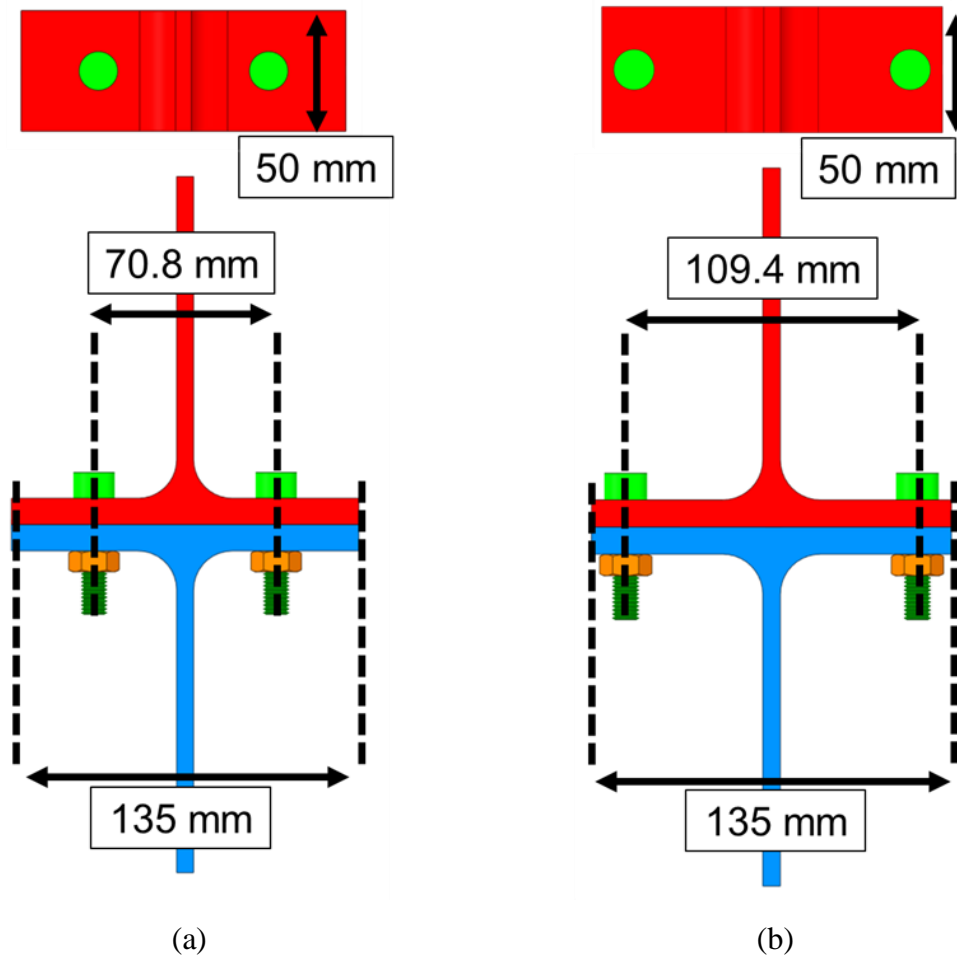


Figure 3.9. Dimensions of the T-Stub assemblies for (a) lower eccentricity, (b) higher eccentricity.

Table 3.4. The test matrix for the T-Stub prying tests.

Code	Number of Samples	Explanation
8.8 – E1	3	Bolt Grade: 8.8 Lower Eccentricity, 32.1 mm
8.8 – E2	3	Bolt Grade: 8.8 Higher Eccentricity, 12.8 mm
12.9 – E1	3	Bolt Grade: 12.9 Lower Eccentricity, 32.1 mm
12.9 – E2	3	Bolt Grade: 12.9 Higher Eccentricity, 12.8 mm

### **3.3.2. Strain Gauge Instrumentation**

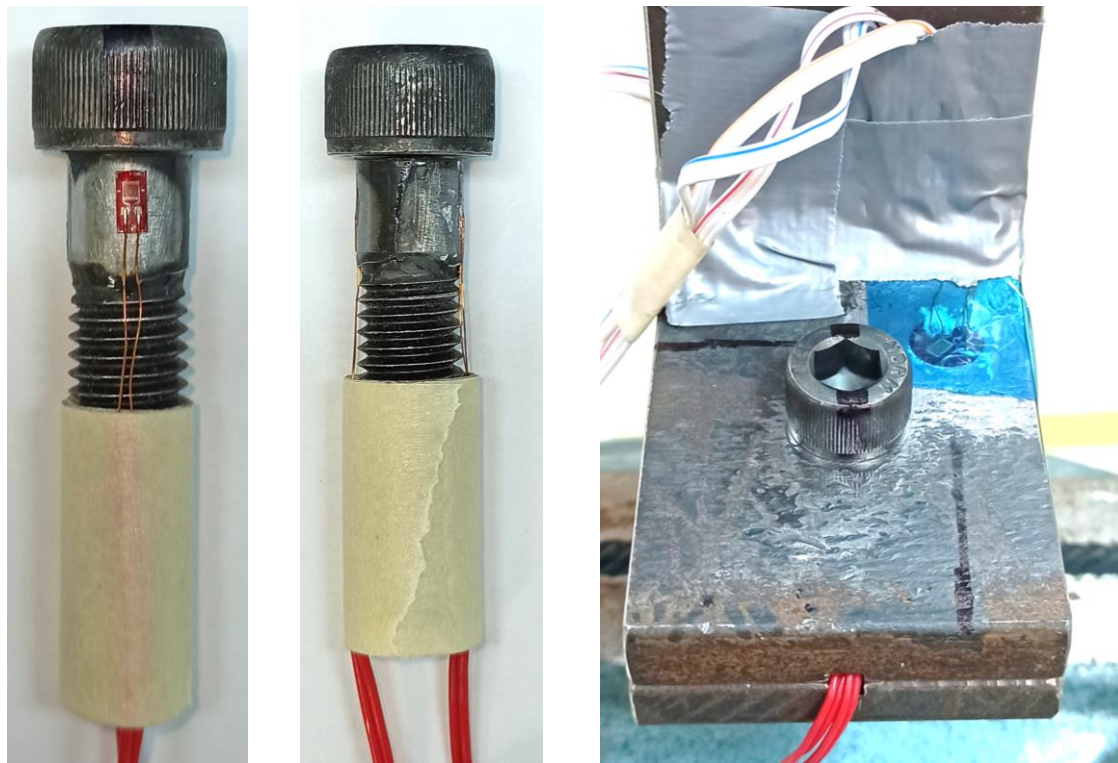
Strain gauge sensors were instrumented in T-Stub prying tests for comparing the experimental and finite element analysis results. TML strain gauges which are FLA-1-350-1LJB for the single-axis and FRAB-3-350-1LJBT-F for the three-axis were used in this study. The data was gathered via ESAM Traveller CF2 data acquisition system with quarter bridge configuration.

Two single-axis strain gauges for one bolt and two three-axis strain gauges for the upper part of the setup were used for one of each configuration. As mentioned earlier, one of three tests from each category was performed with strain gauge sensors, and four single-axis and two three-axis strain gauge sensors are used for each configuration.

Two single-axis strain gauges were bonded on each bolt used in each configuration. The angle between these sensors is provided as  $180^\circ$  for monitoring the bending deformation of the bolt, and the orientation was shown in Figure 3.10. The center of the resistance at the sensors is 5 mm away from the downside surface of the bolt head. The bolts were aligned by arranging the sensors perpendicular to the T-section. This alignment was controlled with the black marks on the bolt head as shown in Figure 3.10. The denomination of these sensors is demonstrated also in Figure 3.10.

Grooves were machined at the T-section parts to provide the cable connection. These grooves can be seen in the view of the T-Stub assembly as given in Figure 3.10 and 3.11, and the dimensions of the groove are also shared in Appendix B.

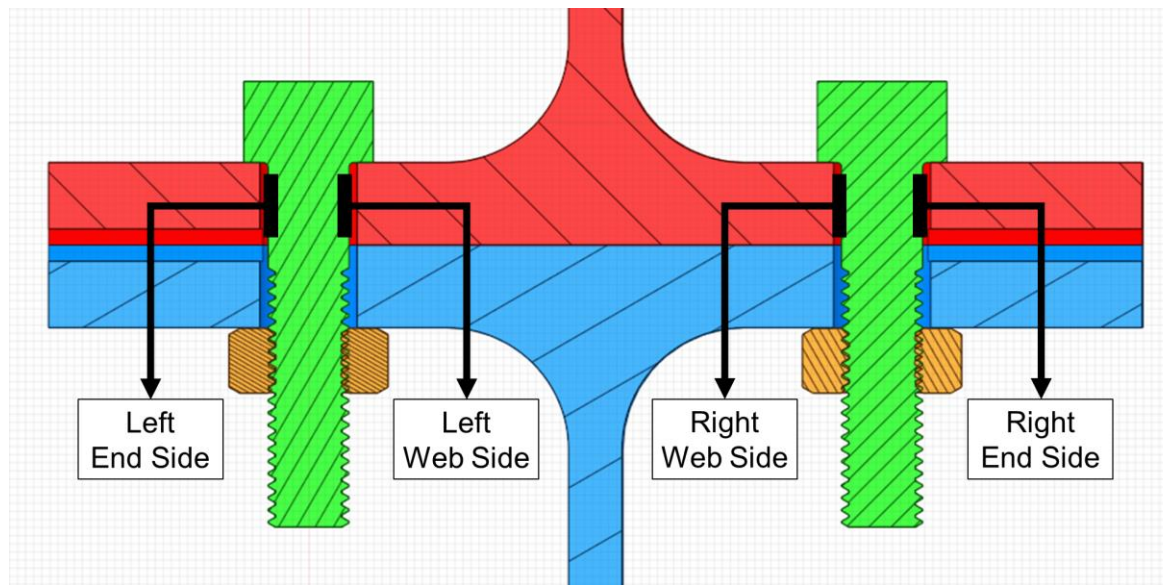




(a)

(b)

(c)



(d)

Figure 3.10. (a) The front view of the strain gauge bonded to the bolt, (b) the side view of the strain gauges, (c) the alignment of the strain gages by using the black marks on the bolt head, (d) the sensor denomination of the bolt strain gauges.

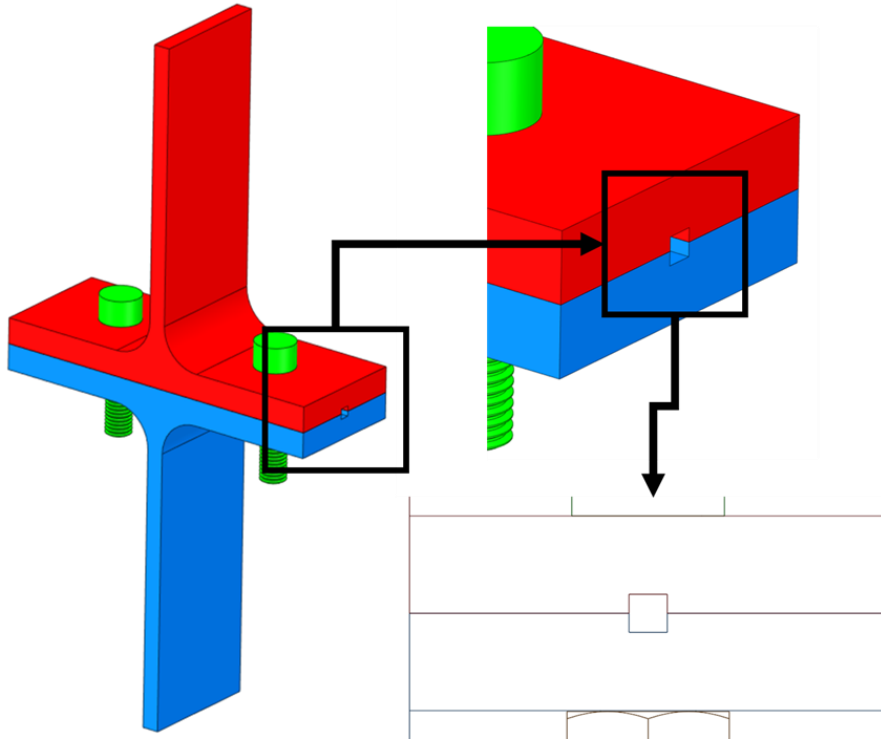


Figure 3.11. Schematically representation of the groove.

Two three-axis strain gauges were bonded on both sides of the T-section. The location of these sensors can be seen in Figure 3.12. The axes used for the finite element analysis comparison are presented in Figure 3.13. The longitudinal and transverse directions were used for the comparisons.

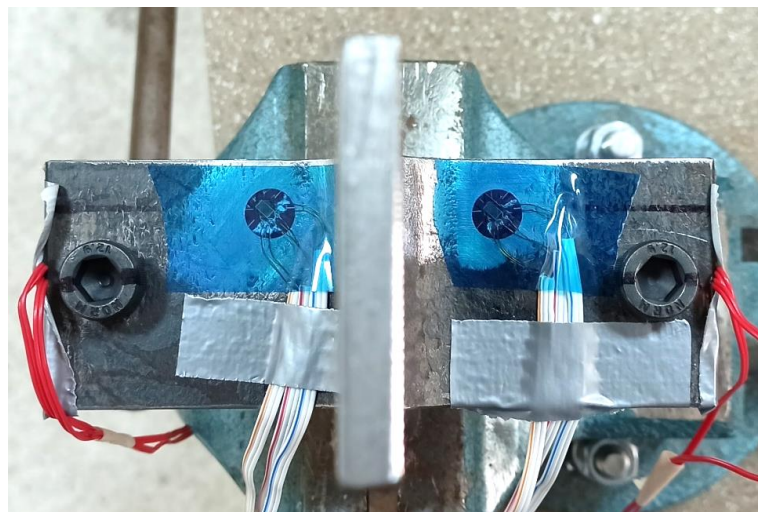


Figure 3.12. The location of the rosette strain gauges.

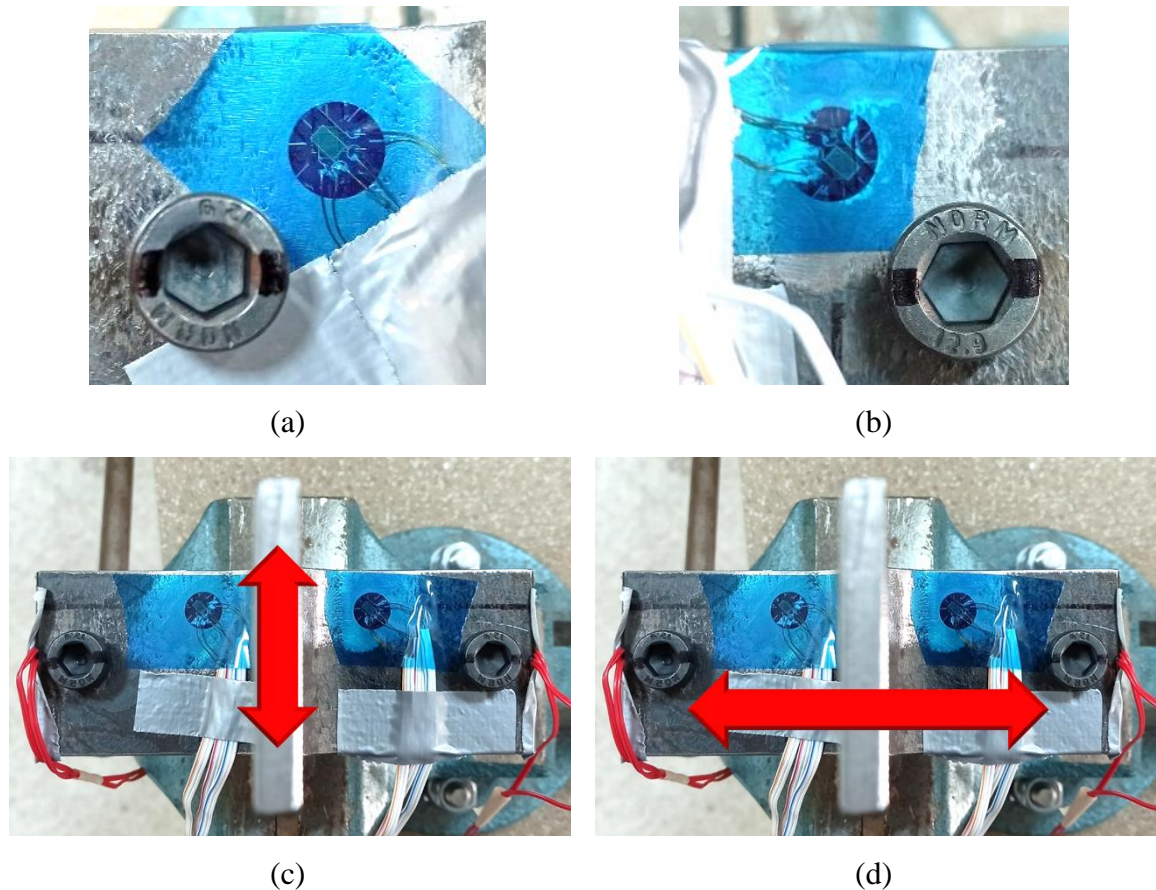


Figure 3.13. (a) The close view of the strain gauge bonded at the left side of the T-section, (b) the close view of the strain gauge bonded at the right side of the T-section, (c) the longitudinal direction of the strain gage, (d) the transverse direction of the strain gage.

### 3.3.3. Results

#### 3.3.3.1. Response of the T-Stub Samples

The force-displacement graph of the T-Stub test specimens including views of the destructed samples and the average results of the mechanical parameters are shared in this section. The force-displacement graph of each configuration is shown in Figure 3.14, and the average force-displacement behaviour of each configuration is demonstrated in this graph. The average results of the mechanical parameters which are initial stiffness, maximum force, and displacement at the maximum force are shared in Table 3.5.

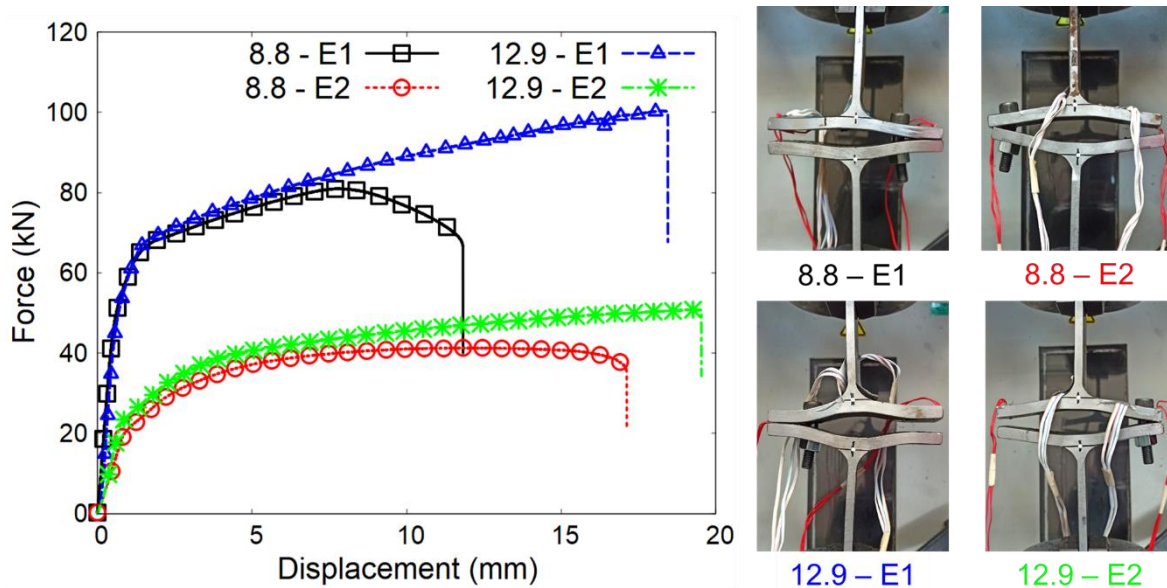


Figure 3.14. The force-displacement graph for each test configuration including the representative views of the destroyed test samples.

Table 3.5. The results of the mechanical parameters of each T-Stub prying test specimen.

Code	Initial Stiffness (kN/mm)	Ultimate Force (kN)	Displacement at the Ultimate Force (mm)
8.8 – E1	$92.3 \pm 0.9$	$81.1 \pm 0.2$	$7.6 \pm 0.3$
8.8 – E2	$27.1 \pm 1.6$	$41.7 \pm 0.4$	$11.2 \pm 0.4$
12.9 – E1	$90.5 \pm 0.3$	$99.2 \pm 0.8$	$16.8 \pm 1.1$
12.9 – E2	$36.1 \pm 0.9$	$50.0 \pm 1.1$	$19.3 \pm 1.2$

### 3.3.3.2. Strain Gauge Results

The results observed from the strain gauge sensors are shown in this section. The strain-force graphs are given in Figure 3.15 – 3.18. The results of the strain gauges bonded on the shank region of the bolt were plotted in Figure 3.15 and 3.16, and the sensor denomination used in Figure 3.13 was referenced for the data labels at the legend. Similarly, the results of the strain gauges bonded on the T-section were plotted in Figure 3.17 and 3.18, and the sensor positions were indicated as Left or Right at the legend. Because two of the web side sensors on the 8.8-grade bolts were damaged while assembling the setup on the tensile testing machine, the data belong to them is absent.

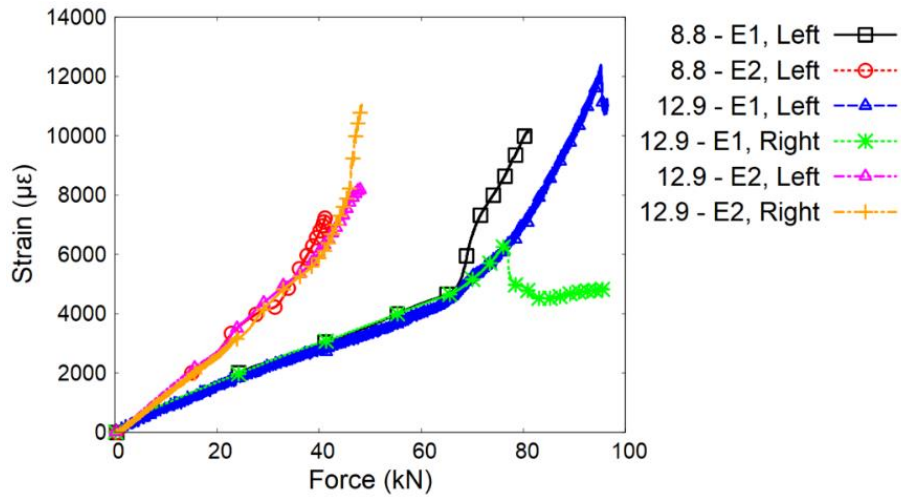


Figure 3.15. Strain-force graph for the strain gauge sensors from the web side of the bolt.

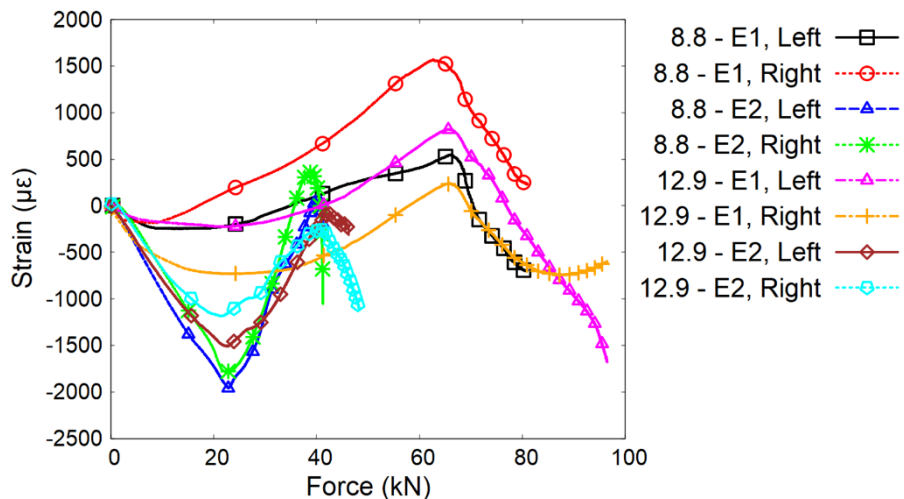


Figure 3.16. Strain-force graph for the strain gauge sensors from the end side of the bolt.

### 3.4. Conclusion

An experimental program was carried out to provide material properties as input information for finite element analysis models and evaluate the finite element analysis results. Firstly, the tensile tests of the bolts and dogbone specimens which material was used in prying tests were performed to obtain the mechanical features of the bolts and the setup material. After these characterization tests, several prying tests in the T-Stub configuration were accomplished by using different eccentricity levels of the bolted joint and bolt strength grades. The main goal of the prying tests is to provide experimental information for judging the results of the finite element analysis models. The results of the bolt tensile tests and the

material characterization tests contributed information on the material properties of the bolt and T-section material to the finite element analysis models. Besides the material properties input, the outcomes of the prying tests supported the comparison of the finite element modelling techniques of the bolted joints while evaluating the analysis results. These results can be found in the results section of this thesis.

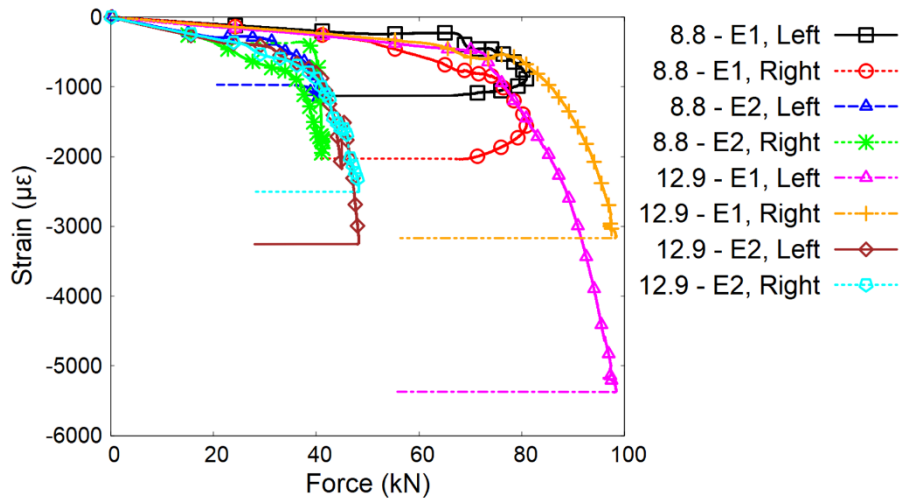


Figure 3.17. Strain-force graph in the longitudinal direction for the strain gauge sensors from the setup part.

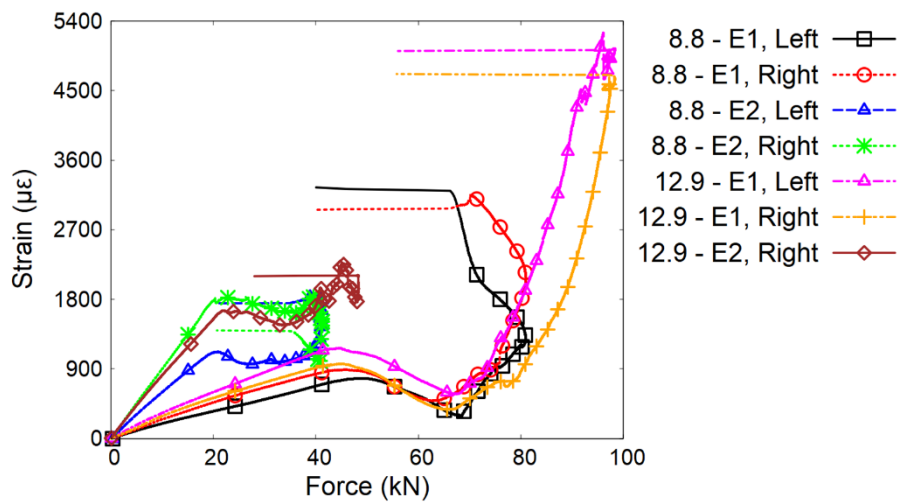


Figure 3.18. Strain-force graph in the transverse direction for the strain gauge sensors from the setup part.



## **4. FINITE ELEMENT ANALYSIS MODELS**

Finite element analysis models of the T-Stub geometries at the prying test configuration were constructed using the commercial software ABAQUS 2016, and several models were created for different bolt modelling techniques. The details of the models and bolted joint modelling techniques are mentioned in this section. Firstly, the analysis parameters used for each technique are introduced. These parameters include material models, assemblies, solver details, interactions, loads, boundary conditions, and mesh structure. Then, the details of the modelling techniques are demonstrated. Five different modelling techniques were used in this study, and the features of each of them are presented in the corresponding sections. These are presented in this study as V1, V2, V3, Proposed and Threaded.

### **4.1. Finite Element Analysis Parameters**

This section presents the common features of the finite element analysis models including material models, assemblies, solver details, interactions, loads, boundary conditions, and mesh structure.

#### **4.1.1. Material Models**

Three different material models for bolts and T-section parts were used in this study. The materials are assumed to be a homogenous, isotropic, linear elastic feature and have isotropic hardening plastic deformation capacity. Damage properties are excluded, and the fracture behaviour of the models was not simulated.

S275JR structural steel is the material of the T-section parts at the assemblies. Because significant differences in the results of the dogbone tensile test results were not observed, only one material property set was used for these parts. For bolts, 8.8-grade and 12.9-grade strength properties were applied. The mechanical properties used for the materials in true values are listed in Table 4.1. Because the materials of 8.8-grade and S275JR are ductile, their material models are trilinear while the material model of the 12.9-grade is bilinear due to its brittle behaviour. The stress values at the fracture point at the trilinear models were calculated by using energy equivalence [94]. The Young's Modulus and Poisson's Ratio for all materials are 200 GPa and 0.3.



Table 4.1. The mechanical properties used in this study.

Material Name	Yield Stress (MPa)	Ultimate Stress (MPa)	Strain at the Maximum Load (%)	Fracture Stress (MPa)	Fracture Strain (%)
S275JR	285	550	26	590	43
8.8-Grade	890	980	3.5	1150	16
12.9-Grade	1200	1340	1.5	1340	5

#### 4.1.2. Assembly

The general construction of the finite element analysis models is quite similar to each other. The assemblies consist of three components which are the upper T-section part, the lower T-section part, and the fastener as described in Figure 4.1. The fasteners consist of bolt and nut, and the part features of the fastener varies with respect to the modelling technique described as in the section of the bolted joint methods.

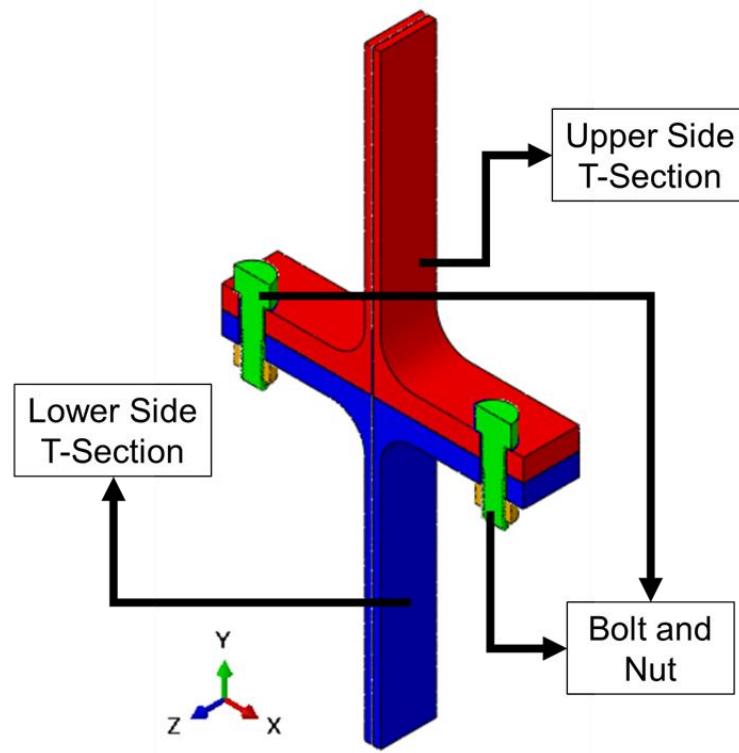


Figure 4.1. The demonstration of the T-Stub assembly components.

Because the geometry has symmetries, the whole model was reduced to a quarter model by using two symmetry planes. In several studies, three symmetry planes were used instead of two planes neglecting the difference between the bolt head and nut side of the bolted joint [61]. However, this assumption was not applied in this study because different modelling techniques including partially threaded bolts, and also threaded geometry, were investigated. The reduction from the whole geometry into the quarter model is demonstrated in Figure 4.2.

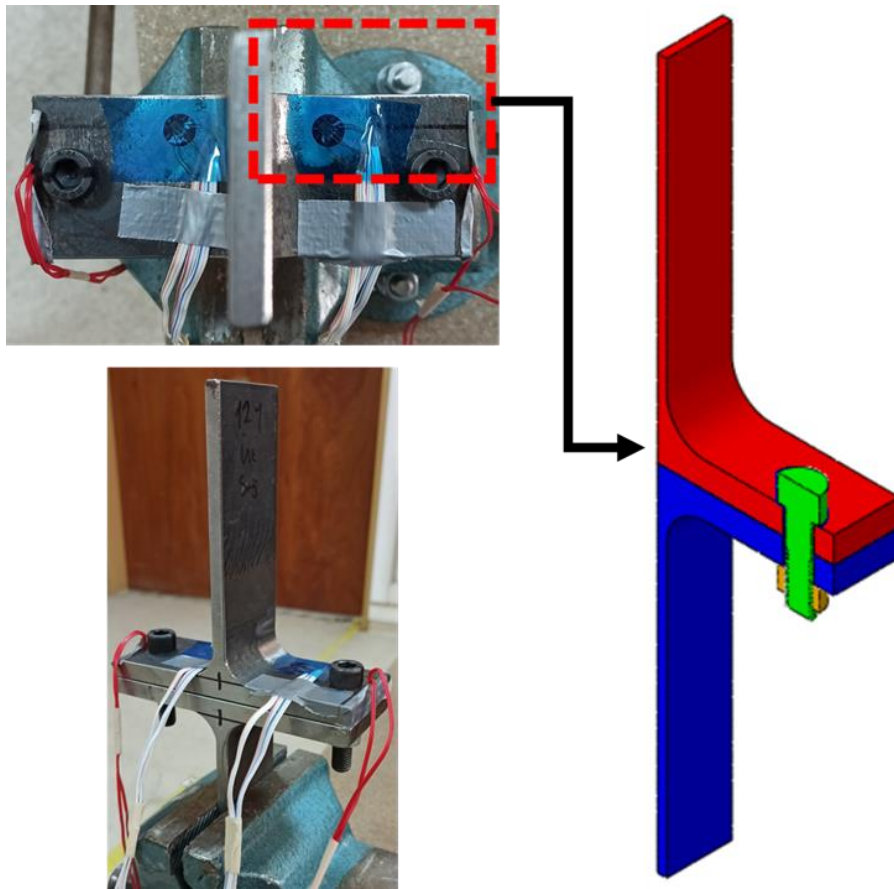


Figure 4.2. The reduction from the whole model into the quarter model.

#### 4.1.3. Steps

Two consecutive analysis steps were applied for the bolt preload and external loading stages. Static implicit solution strategy with Newton-Raphson solution technique was used for both steps by arranging to include the geometric nonlinearity. The reason behind the implicit solver selection is that this type of solver is suitable for problems including nonlinearities [76]. Additionally, the explicit solver was not necessary for this study because there was not

any condition which can compel the simulations such as element erosion and very large deformations.

#### **4.1.4. Interactions**

All analysis models include contact interactions between the pairs listed as follows:

- Upper and lower T-section parts,
- Bolt head and upper T-section part,
- Nut and lower T-section part.

Surface-to-surface contact was applied with penalty friction formulation with a 0.3 coefficient of friction by using the penalty method algorithm for the contacting surfaces, and different coefficient of friction values were not tried because this parameter does not affect the structural behaviour of this problem [2]. The default settings of the ABAQUS software were defined for the contact parameters except for the value of the coefficient of friction. Different contact algorithms were not attempted because a significant effect of the contact algorithm on the accuracy and computational effort was not observed for bolted flange connection in [95]. The contact pairs of the interactions containing all models are shown in Figure 4.3.

The default settings used for contact interactions are described as listed above:

- The finite sliding formulation was used.
- The discretization method is surface-to-surface.
- Separation was allowed after the contact.
- Isotropic directionality was applied for the penalty friction formulation.
- “Hard” contact was selected for the pressure-overclosure adjustment.

Two continuum-distributing coupling definitions were created for the load and boundary condition. These constraints were used for obtaining the reaction force and displacement increment in a practical way, and all degrees of freedom were constrained.

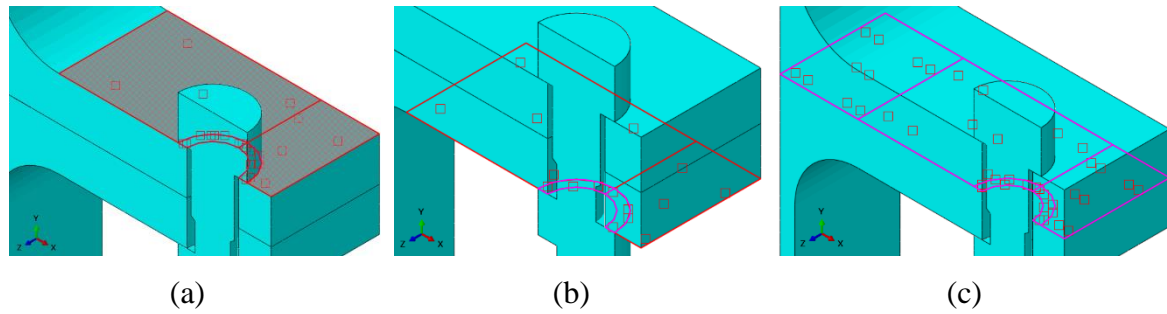


Figure 4.3. The common contact pairs between (a) the bolt head and upper T-section, (b) the nut and lower T-section, (c) the upper and lower T-section.

#### 4.1.5. Loads and Boundary Conditions

The loads were implemented separately in two consecutive analysis steps. The pretension force for the bolt was applied in the first step. Then, the external load was defined with displacement boundary condition from the master point of the continuum-distributing coupling definition for the upper T-section part. The displacement boundary conditions varied according to experimental results. To prevent the occurrence of the negative stiffness at the force-displacement response, primary calculations were performed to observe the displacement that occurred at the maximum reaction force, similarly in [79]. After obtaining them, the main analyses were run with these displacement values. The final values of the displacement boundary conditions for each model were shared in Table 4.2.

Comparisons between the modelling techniques and experimental results were performed for the non-preloaded condition. To overcome the convergence problems, a generic 10 N preload was applied for each analysis for the non-preloaded bolted joint configuration. Several preloaded bolted connection analyses were performed to investigate the effect of bolt pretension on bolt bending deformation. The preload values were arranged with respect to the bolt strength grade used in the analysis for each model, and the details of the preloaded configuration will be given in the corresponding results section.

Besides the displacement-controlled loading, three boundary conditions were defined to provide static equilibrium. Two of them were implemented by using the symmetry planes described at the assembly part of this section, and the boundary condition applied from the master point of the continuum-distributing coupling definition for the lower T-section part

constrained the model along the loading direction. The symmetry boundary conditions are shown in Figure 4.4 by stressing the constrained surfaces.

Table 4.2. Displacement boundary condition values.

Configuration Name	Model Name	Displacement Value (mm)
8.8 – E1	V1	6.9
	V2	16
	V3	5.8
	Proposed	6.4
	Threaded	9
8.8 – E2	V1	12.5
	V2	30
	V3	9.2
	Proposed	10.3
	Threaded	10
12.9 – E1	V1	14.8
	V2	24.3
	V3	16.5
	Proposed	14.1
	Threaded	15.4
12.9 – E2	V1	18.5
	V2	32
	V3	19
	Proposed	19
	Threaded	30

#### 4.1.6. Mesh

The mesh structure of the parts was constructed with the 8-node linear hexahedral three-dimensional stress elements named as C3D8 from the ABAQUS element library [18]. A mesh sensitivity analysis was not performed because a relatively fine mesh size was used. The relatively fine mesh size also provided that it was not required to use 8-node linear

hexahedral elements with incompatible modes for the bending-dominating problems dissimilar to the studies performed in the literature [63, 96].

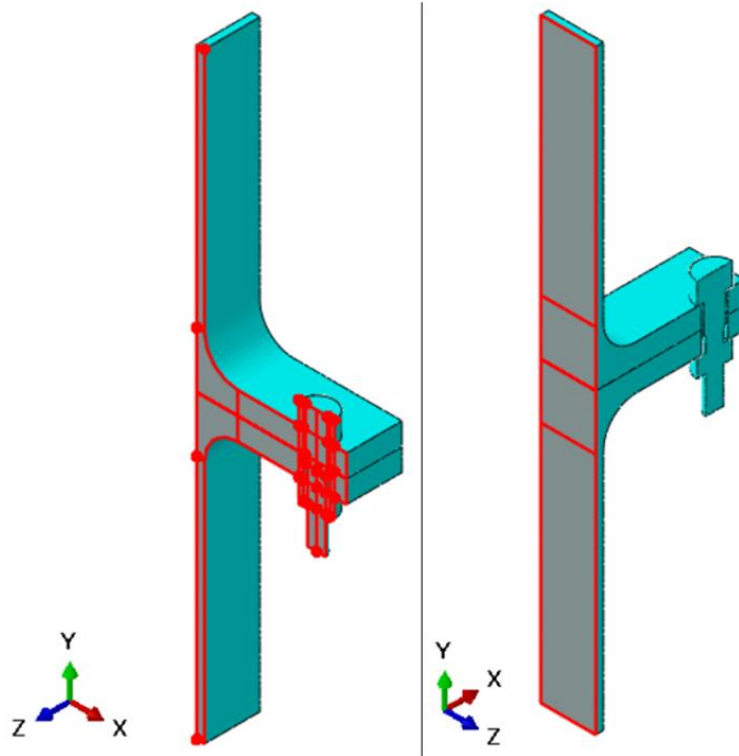


Figure 4.4. The surfaces where the symmetry boundary conditions were applied.

The mesh structure of the T-section components which are for the lower and higher eccentricities are shown in Figure 4.5. Five elements were used in the thickness direction at the region where bolted joint was placed. A finer mesh structure was created for the region where the bolt head and nut contact the T-section parts as demonstrated in Figure 4.5. The total element and node numbers was indicated in Table 4.3. A 2.5 mm average mesh size was applied for both components. The mesh details of the fasteners will be introduced in the section of bolted joint models because they have different geometries and features.

## 4.2. Bolted Joint Models

This section presents the bolted joint modelling techniques used in this study. These methods are commonly used techniques in the literature for modelling the bolted joint three-

dimensionally. The specific features are explained, and an overview of these modelling methods is made for comparison between each other.

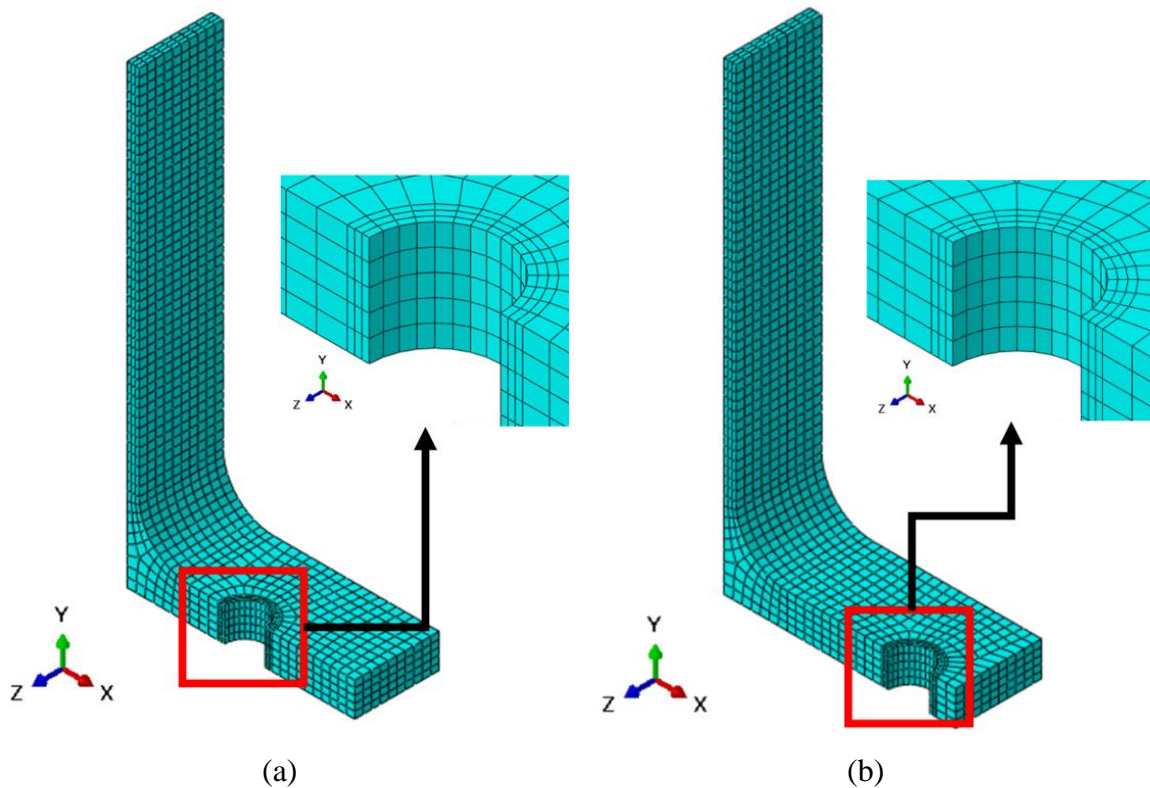


Figure 4.5. The mesh structure of the T-section parts for (a) lower eccentricity, (b) higher eccentricity.

Table 4.3. The total number of elements and nodes of the T-section parts.

Part Name	Total Number of Elements	Total Number of Nodes
T-section for Higher Eccentricity	2940	4200
T-section for Lower Eccentricity	2970	4244

#### 4.2.1. Three-Dimensional Models without Threads

Three different modelling techniques excluding the threads geometrically were created. The nut and bolt were modeled as one-piece part, and they are introduced with the mesh structure in Figure 4.6. The bolt was modeled in three different ways which are formed by using only the minor diameter, major diameter, and combining both major and minor diameters

respectively. A 1 mm average mesh size was applied for all of them by using C3D8 element type. The total element and node numbers was indicated in Table 4.4.

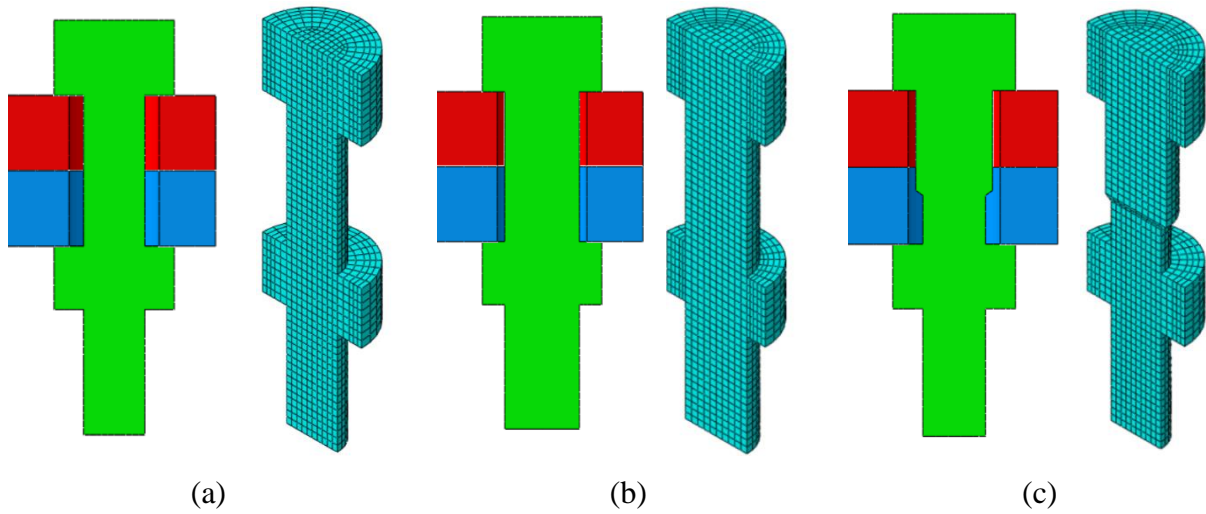


Figure 4.6. The representation and mesh structure of the bolted joints model of (a) V1, (b) V2, (c) V3.

Table 4.4. The total number of elements and nodes of the bolts of the three-dimensional models without threads.

Modelling Method	Total Number of Elements	Total Number of Nodes
V1	4080	5172
V2	4080	5172
V3	4128	5234

#### 4.2.2. Three-Dimensional Models with Threads

One of the studied methods has a threaded geometry. As shown in Figure 4.7, the threaded region of the fastener was modeled three-dimensionally by disregarding the run-out region and helix angle due to the high modelling efforts and computational costs. The mesh structures of the threads are also presented in Figure 4.7. A 1 mm average mesh size was applied for both bolt and nut while finer mesh structures were created for the threaded regions. C3D8 element type was used for both bolt and nut geometry. The total element and node numbers was indicated in Table 4.5. Because the end side of the bolt was not used structurally in the analyses, this region was not meshed. The contact features mentioned at the previous chapter are valid for the contact of the mating threads.



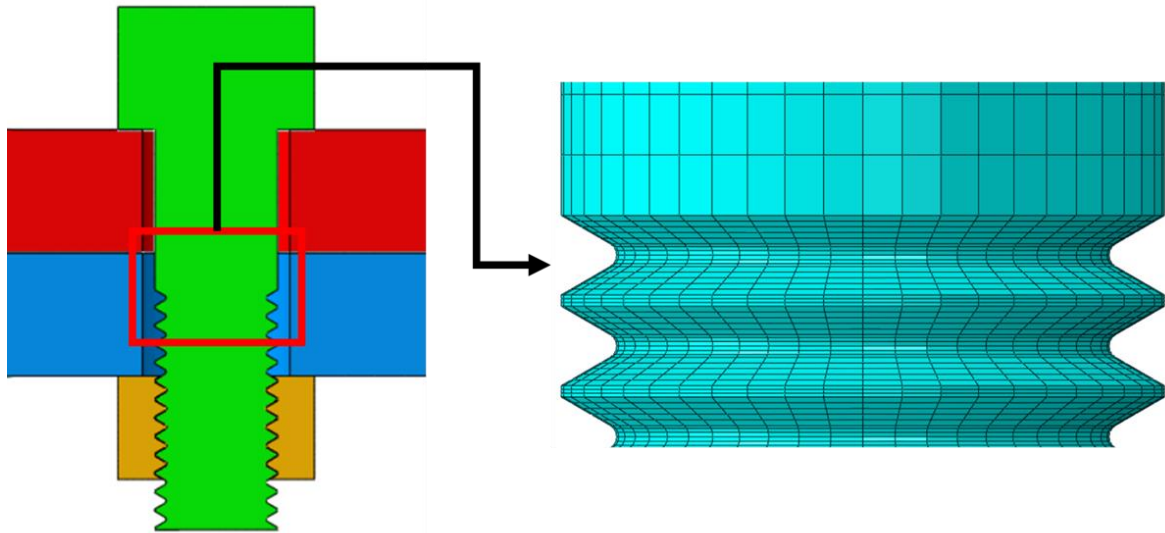


Figure 4.7. The threaded bolted joint modelling method with representing the mesh structure of the threads.

Table 4.5. The total number of elements and nodes of the parts of the three-dimensional model with threads.

Part Name	Total Number of Elements	Total Number of Nodes
Bolt	27144	32676
Nut	18144	21800

### 4.2.3. Proposed Model

A novel modelling technique was proposed for the finite element analysis of the bolted joints. This technique was inspired by the load distribution at the mating threads of the bolted joint. As presented in Figure 4.8, more than 70% of the bolt load is carried by the first three mating threads from the bolt head side [97]. Because modelling the bolt and nut as a one-piece part causes relatively higher stiffness than the threaded connection while performing static structural finite element analysis., this one-piece part assumption needs a stiffness revision. This stiffness update was attempted in this study by using the phenomenon described above, and three corresponding threads inasmuch as pitch size were removed geometrically as demonstrated in Figure 4.9. Similar to the three-dimensional models without threads, the nut and bolt were modeled as one-piece part, and they are introduced

with the mesh structure in Figure 4.10. A 1 mm average mesh size was applied for all of them by using the C3D8 element type.

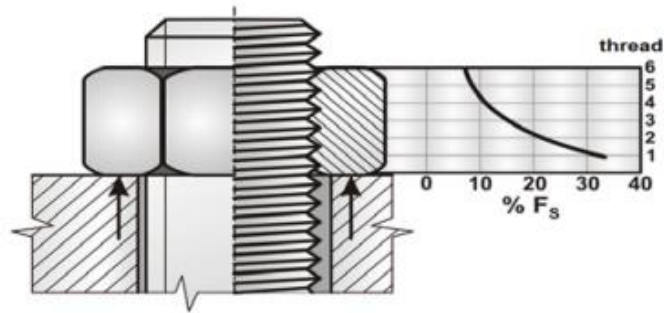


Figure 4.8. Load distribution at the mating threads of a bolted joint [98].

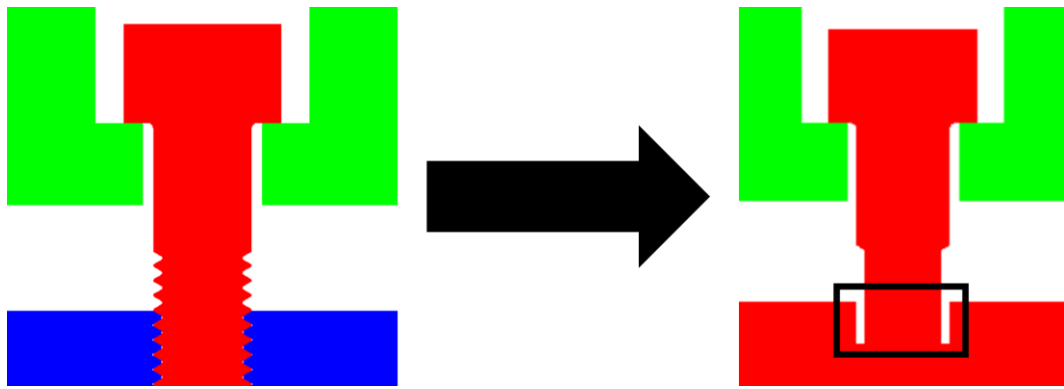


Figure 4.9. The stiffness arrangement by removing the threads.

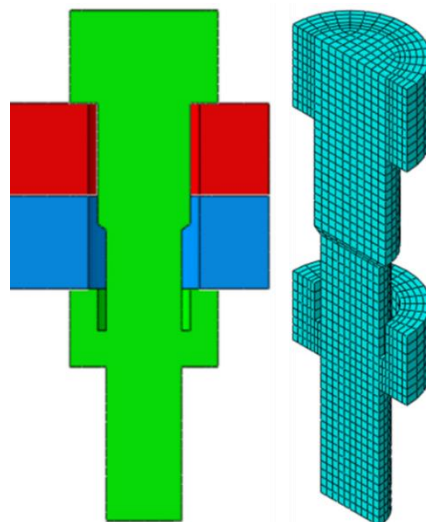


Figure 4.10. The representation and mesh structure of the proposed bolted joints modelling technique.



## 5. RESULTS

The results observed from the finite element analyses are described in this chapter. Firstly, the results of the non-preloaded bolted joint models were compared with the corresponding experimental outcomes in terms of the force-displacement and force-strain variations, and structural parameters such as initial stiffness and maximum force. Secondly, the studied modelling techniques were compared with each other in terms of the bolt bending distribution throughout the clamped region and bending-tension interaction at a specific cross-section. Moreover, an overview was presented of the studied bolted joint modelling techniques in terms of the characteristics and computational parameters. Lastly, the results of the bolt bending distribution throughout the clamped region and bending-tension interaction at a specific cross-section were shared for the preloaded bolted joint analyses.

### 5.1. Non-Preloaded Bolted Joint Models

#### 5.1.1. Comparison with Experimental Results

The force-displacement response and strain values from where strain gauges were instrumented at the experimental study were compared with the experimental results. The mechanical parameters are demonstrated in Figure 5.1. The force-displacement graphs for all configurations are shared in Figure 5.2 and 5.3 while the force-strain curves are plotted for all configurations in Figure 5.4 – 5.11. The closer views of the strain-force graphs are given for each figure by using the rectangles with black dashed line demonstrating the corresponding region.

The initial stiffness results of the modelling techniques for all configurations are quite compatible with the experimental results, however, the plastic deformation region at the force-displacement curves is different for each modelling technique, especially in the models in which the 8.8 bolt strength grade was used. The force-displacement variation at the plastic deformation region for the models in which the 12.9 bolt strength grade was used is more consistent than the models in which the 8.8 bolt strength grade was used. Additionally, the numerical and experimental results of the secondary stiffness are not coherent as seen in force-displacement graphs. The plastic deformation response obtained at the lower eccentricity configuration for both bolt strength grades is more suitable with the

experimental results, and the configuration of the lower eccentricity with 12.9 bolt strength grade can be considered as the most compatible one. In despite of the inconsistency between the results of the numerical and experimental secondary stiffness behaviour and yield force, the modelling techniques provided sufficient results for the initial stiffness, maximum force, and displacement at the maximum force. The strain values acquired from the web side strain gauges on the bolts are consistent with the experimental results, and the strain values acquired from the end side strain gauges on the bolts are not compatible with the experimental results. This inconsistency might be caused by the initial tightening of the bolts. For the models in which the 8.8 bolt strength grade was used, the proposed modelling technique can be considered as the most compatible one while M1 and M2 techniques are the least compatible methods for all models. The strain values acquired from the T-sections were in longitudinal and transverse directions. The strain values in the longitudinal directions for all models are more consistent with the experimental results than in the transverse direction. Similar to the bolt strain values, the models in which the M2 technique was used are the least compatible for strain values in the longitudinal direction at all configurations. The results of the mechanical parameters which are initial stiffness, maximum force, and displacement at the maximum force for all configurations were compared and introduced in Table 5.1 – 5.12. The ratios of the numerical result over the experimental result for each configuration and parameter are also indicated in these tables. As seen in the tables, all studied methods excluding the M2 technique provide compatible ratios with compared the experimental results. Some inconsistent results were observed for the displacement at maximum force in the models in which the threaded method was used as an exception.

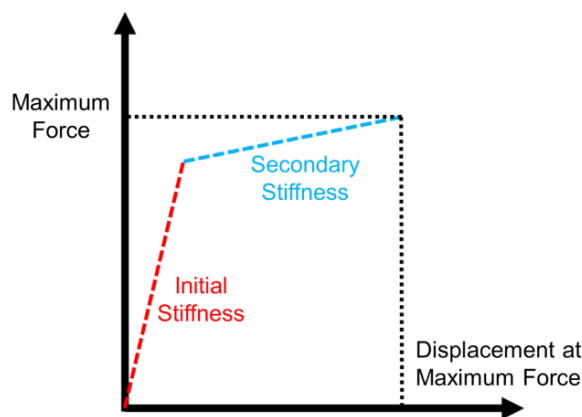
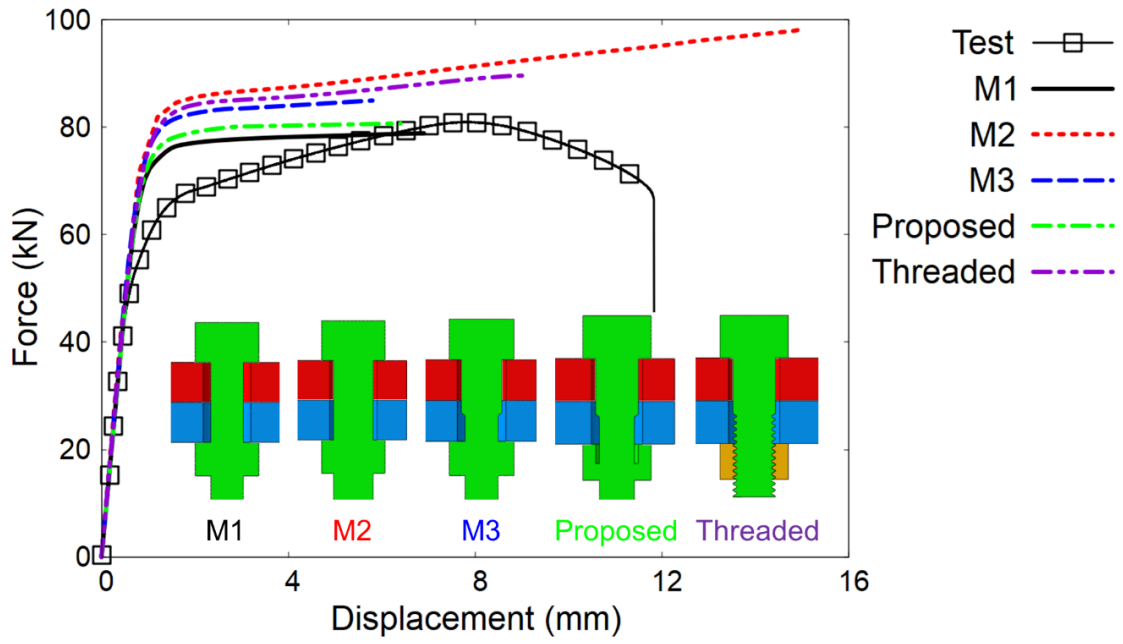
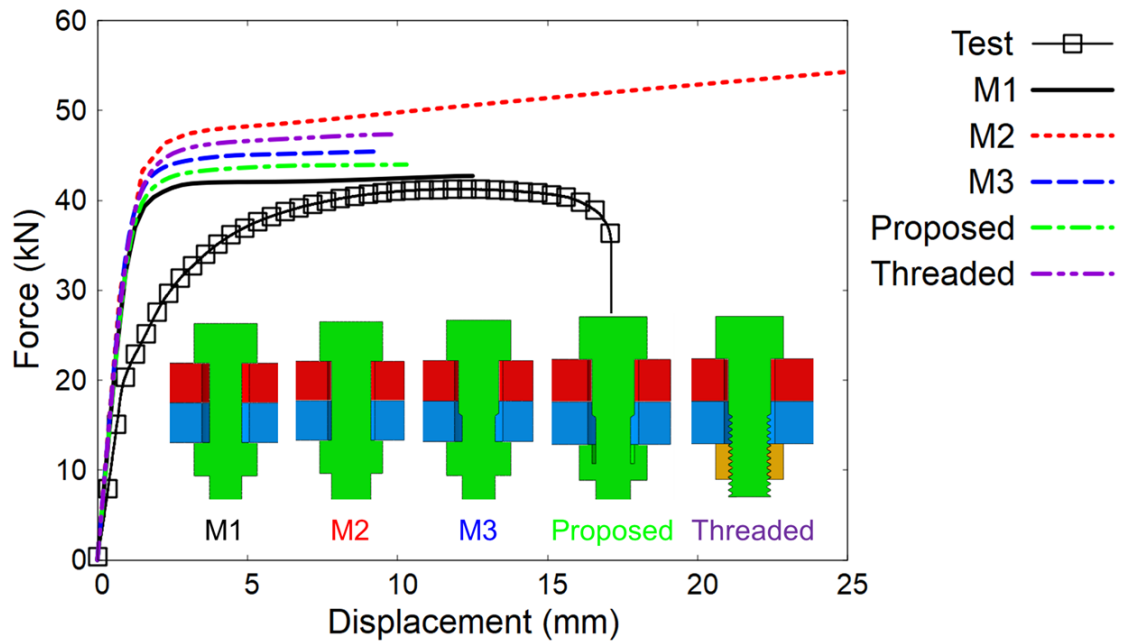


Figure 5.1. Representation of the mechanical parameters of the force-displacement behaviour.

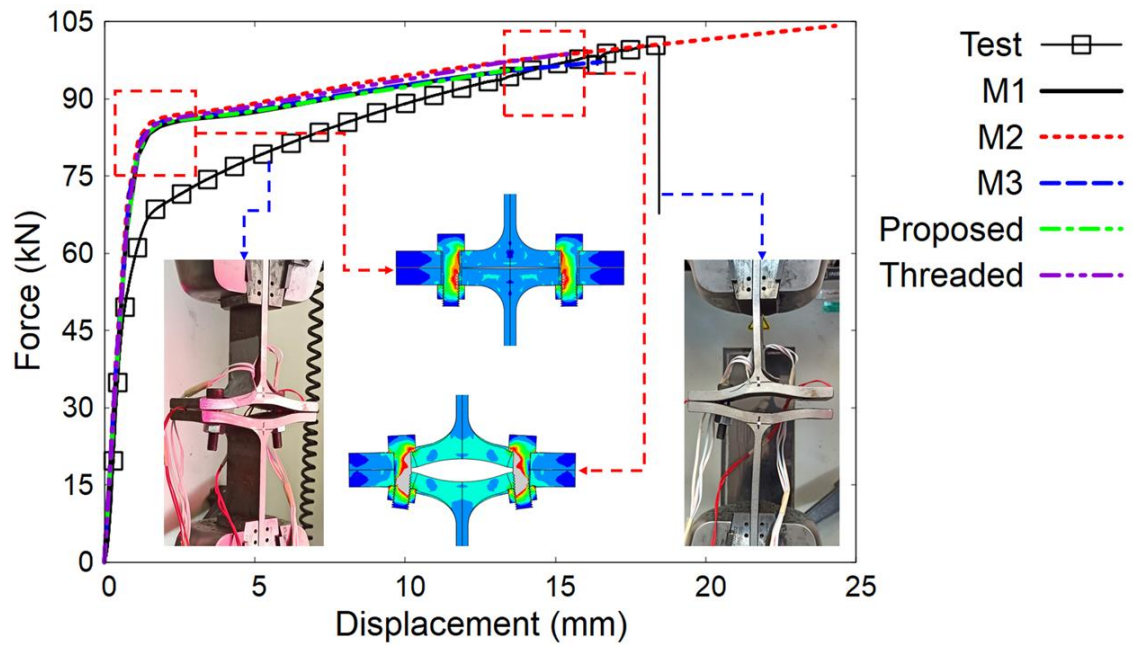


(a)

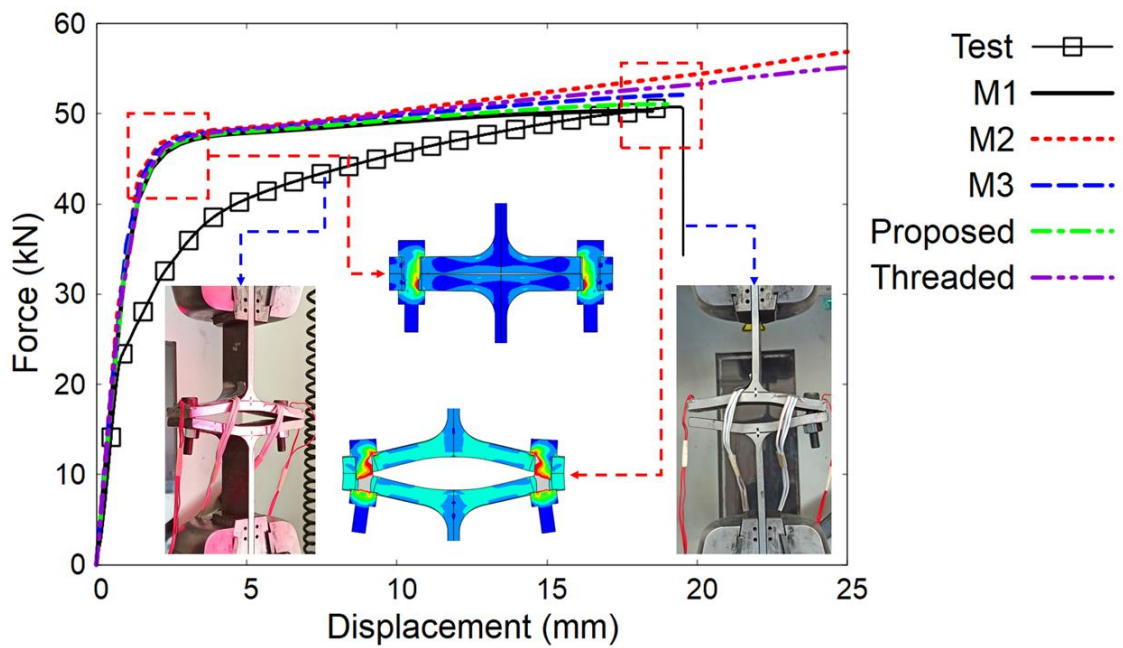


(b)

Figure 5.2. The force-displacement graphs of the configuration of (a) 8.8 – E1, (b) 8.8 – E2.

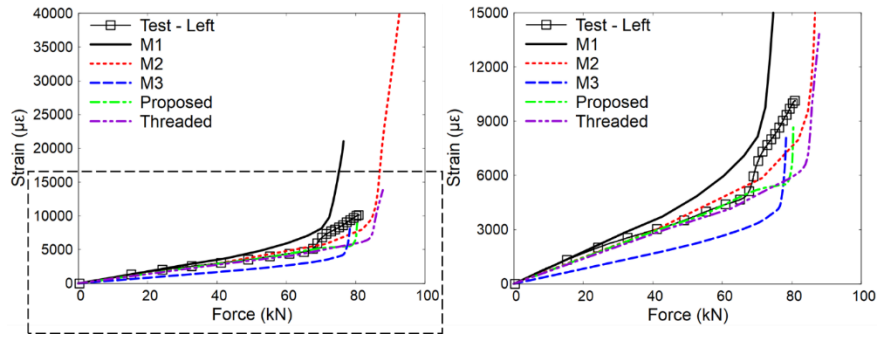


(a)

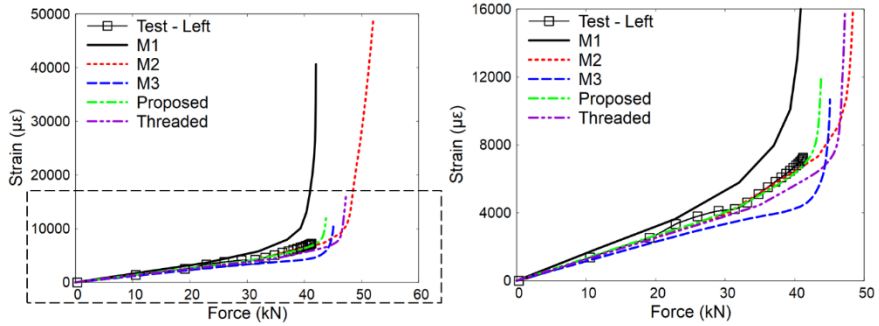


(b)

Figure 5.3. The force-displacement graphs of the configuration of (a) 12.9 – E1, (b) 12.9 – E2.

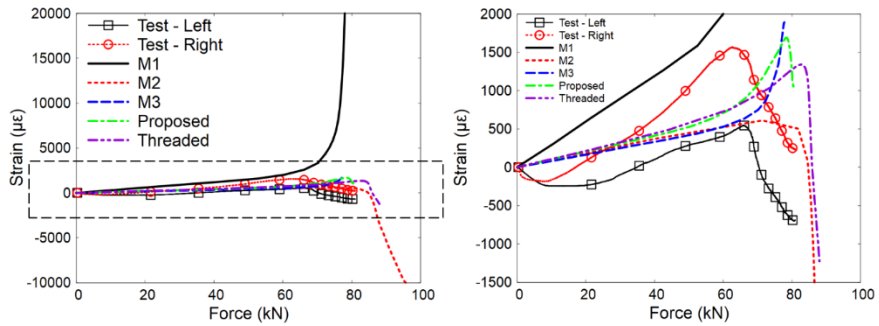


(a)

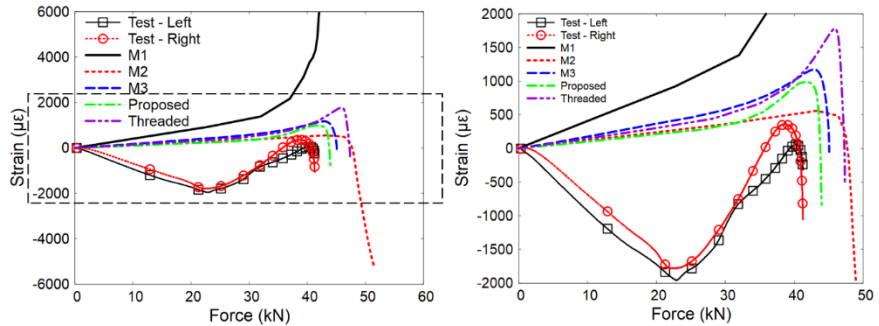


(b)

Figure 5.4. The strain-force curves created from the web side strain gauge location of the bolts for the configuration of (a) 8.8 – E1, (b) 8.8 – E2.



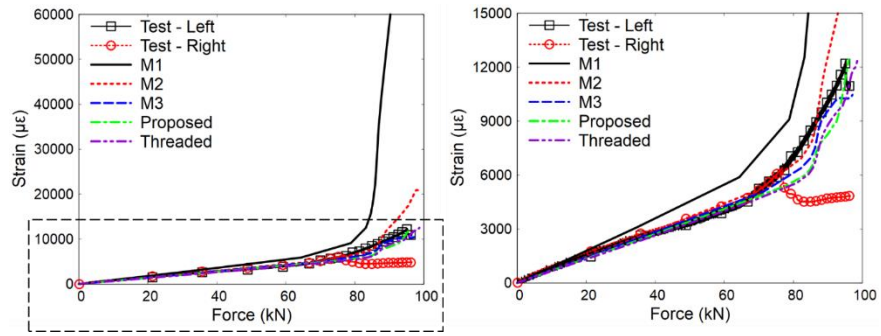
(a)



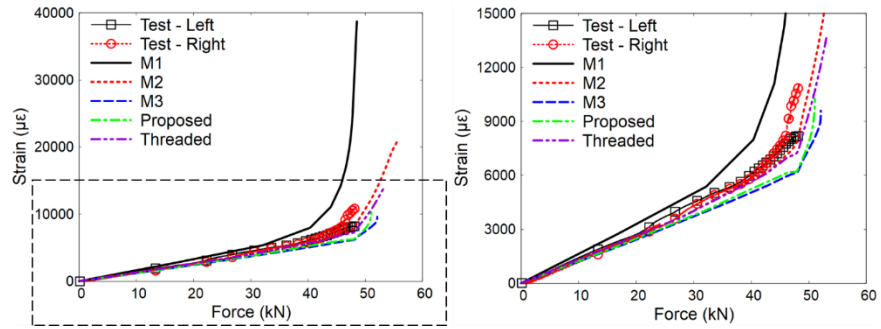
(b)

Figure 5.5. The strain-force curves created from the end side strain gauge location of the bolts for the configuration of (a) 8.8 – E1, (b) 8.8 – E2.



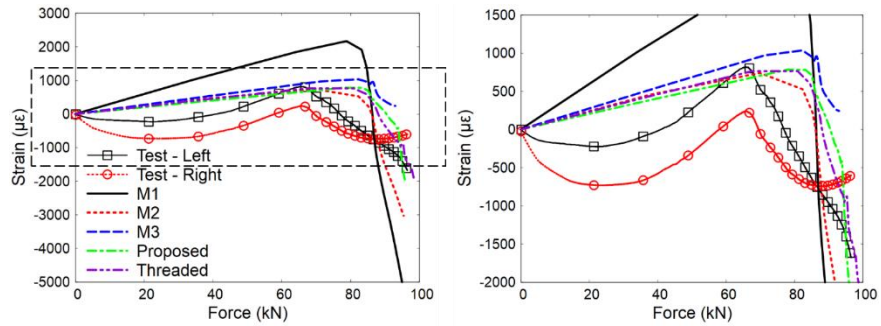


(a)

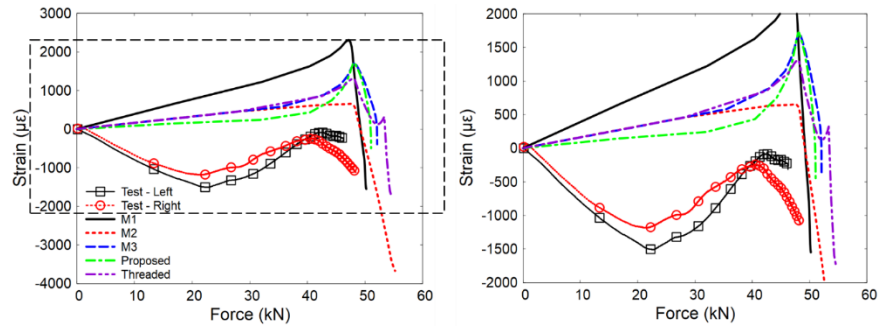


(b)

Figure 5.6. The strain-force curves created from the web side strain gauge location of the bolts for the configuration of (a) 12.9 – E1, (b) 12.9 – E2.

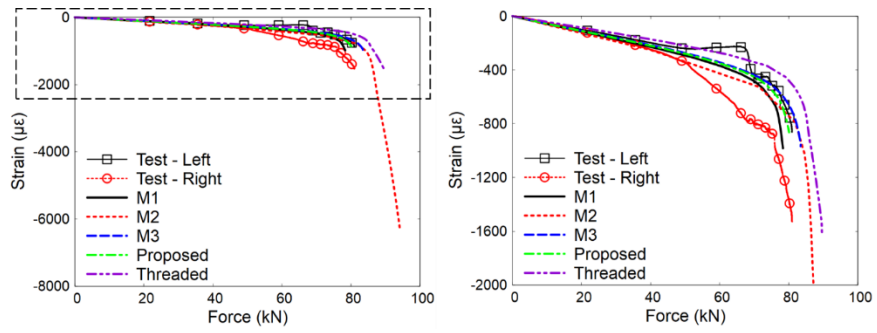


(a)

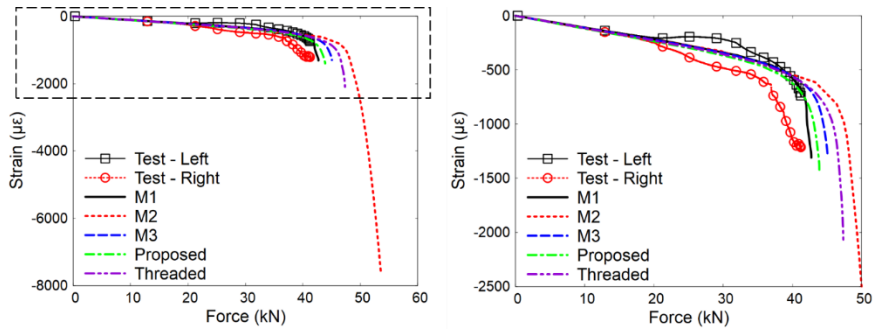


(b)

Figure 5.7. The strain-force curves created from the end side strain gauge location of the bolts for the configuration of (a) 12.9 – E1, (b) 12.9 – E2.

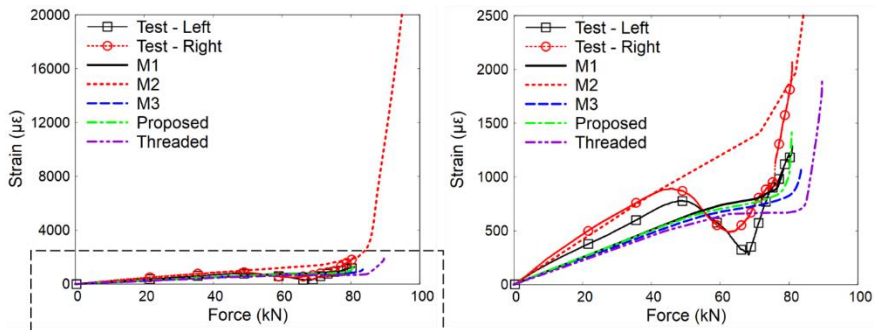


(a)

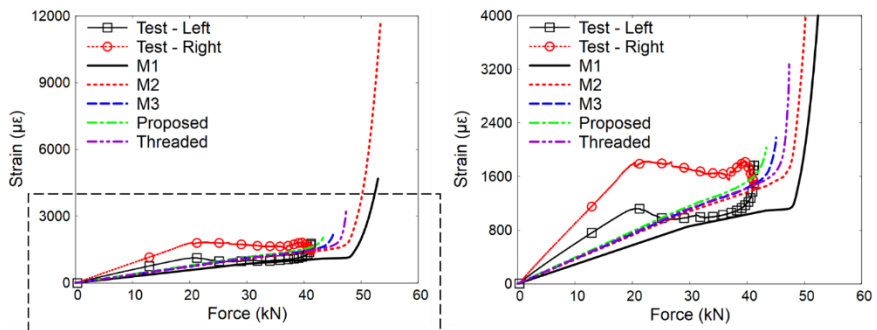


(b)

Figure 5.8. The strain-force curves created from the strain gauge location of the T-sections for the longitudinal direction of the configuration of (a) 8.8 – E1, (b) 8.8 – E2.

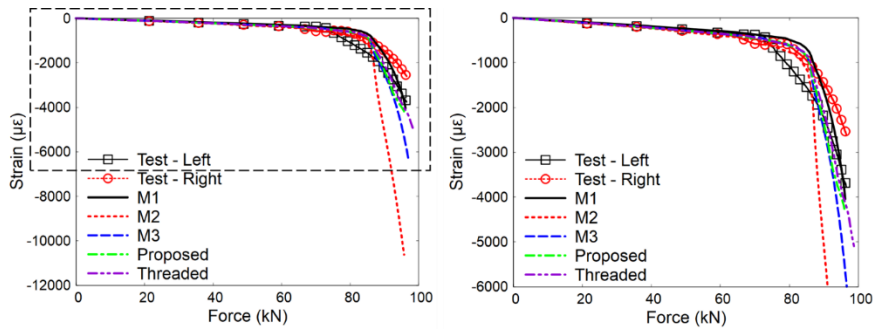


(a)

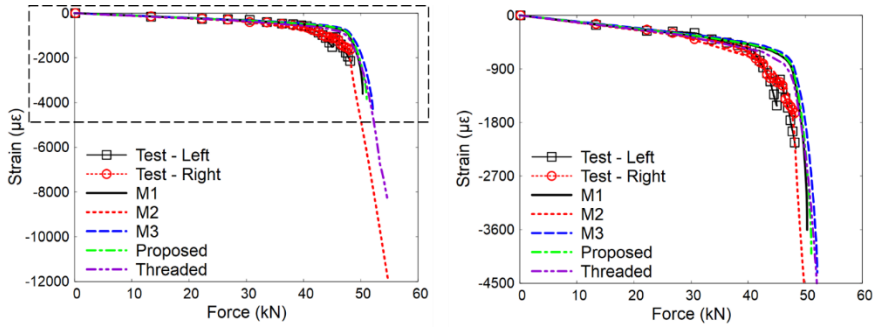


(b)

Figure 5.9. The strain-force curves created from the strain gauge location of the T-sections for the transverse direction of the configuration of (a) 8.8 – E1, (b) 8.8 – E2.

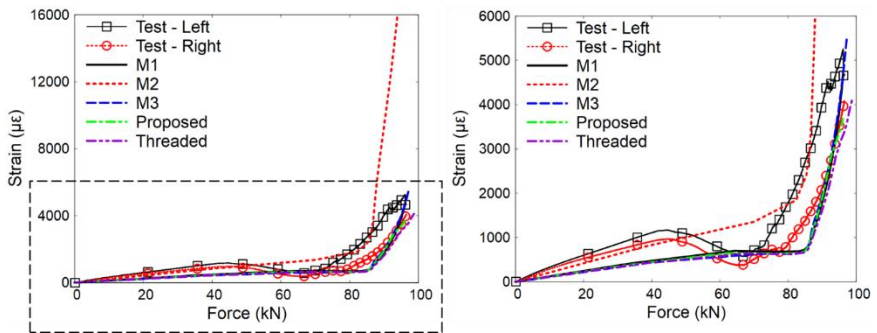


(a)

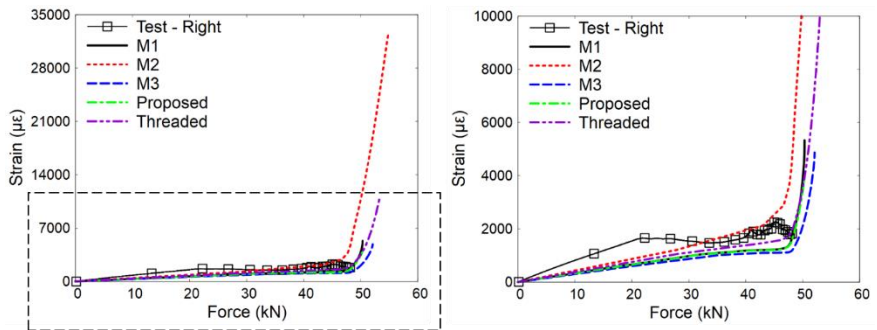


(b)

Figure 5.10. The strain-force curves created from strain gauge location of the T-sections for the longitudinal direction of the configuration of (a) 12.9 – E1, (b) 12.9 – E2.



(a)



(b)

Figure 5.11. The strain-force curves created from the strain gauge location of the T-sections for the transverse direction of the configuration of (a) 12.9 – E1, (b) 12.9 – E2.

Table 5.1. Comparison at the 8.8 – E1 configuration for the initial stiffness between numerical and experimental results.

Model Name	Analysis Result (kN/mm)	Average of Experimental Results (kN/mm)	FEM/Test
V1	92.2		0.999
V2	100.7		1.091
V3	95.7	92.3	1.039
Proposed	91.2		0.988
Threaded	93.1		1.009

Table 5.2. Comparison at the 8.8 – E2 configuration for the initial stiffness between numerical and experimental results.

Model Name	Analysis Result (kN/mm)	Average of Experimental Results (kN/mm)	FEM/Test
V1	35.4		1.305
V2	39.6		1.460
V3	38	27.1	1.403
Proposed	36		1.328
Threaded	35.4		1.307

Table 5.3. Comparison at the 12.9 – E1 configuration for the initial stiffness between numerical and experimental results.

Model Name	Analysis Result (kN/mm)	Average of Experimental Results (kN/mm)	FEM/Test
V1	91.7		1.013
V2	100.6		1.112
V3	97.2	90.5	1.074
Proposed	92.4		1.021
Threaded	92.2		1.019

Table 5.4. Comparison at the 12.9 – E2 configuration for the initial stiffness between numerical and experimental results.

Model Name	Analysis Result (kN/mm)	Average of Experimental Results (kN/mm)	FEM/Test
V1	36.5		1.011
V2	39.9		1.104
V3	38.5	36.1	1.067
Proposed	36.9		1.023
Threaded	36.6		1.015

Table 5.5. Comparison at the 8.8 – E1 configuration for the maximum force between numerical and experimental results.

Model Name	Analysis Result (kN)	Average of Experimental Results (kN)	FEM/Test
V1	78.9		0.973
V2	98.8		1.218
V3	85	81.1	1.048
Proposed	80.7		0.995
Threaded	89.6		1.105

Table 5.6. Comparison at the 8.8 – E2 configuration for the maximum force between numerical and experimental results.

Model Name	Analysis Result (kN)	Average of Experimental Results (kN)	FEM/Test
V1	42.7		1.024
V2	55.9		1.341
V3	45.4	41.7	1.089
Proposed	44		1.055
Threaded	47.3		1.134

Table 5.7. Comparison at the 12.9 – E1 configuration for the maximum force between numerical and experimental results.

Model Name	Analysis Result (kN)	Average of Experimental Results (kN)	FEM/Test
V1	96.2		0.970
V2	104.2		1.050
V3	97.1	99.2	0.979
Proposed	96		0.968
Threaded	98.7		0.995

Table 5.8. Comparison at the 12.9 – E2 configuration for the maximum force between numerical and experimental results.

Model Name	Analysis Result (kN)	Average of Experimental Results (kN)	FEM/Test
V1	50.3		1.006
V2	55.2		1.104
V3	52.1	50	1.042
Proposed	51.1		1.022
Threaded	54.3		1.086

Table 5.9. Comparison at the 8.8 – E1 configuration for the displacement at the ultimate force between numerical and experimental results.

Model Name	Analysis Result (mm)	Average of Experimental Results (mm)	FEM/Test
V1	6.9		0.919
V2	16		2.130
V3	5.8	7.5	0.772
Proposed	6.4		0.852
Threaded	9		1.198

Table 5.10. Comparison at the 8.8 – E2 configuration for the displacement at the ultimate force between numerical and experimental results.

Model Name	Analysis Result (mm)	Average of Experimental Results (mm)	FEM/Test
V1	12.5		1.116
V2	30		2.679
V3	9.2	11.2	0.821
Proposed	10.3		0.920
Threaded	10		0.893

Table 5.11. Comparison at the 12.9 – E1 configuration for the displacement at the ultimate force between numerical and experimental results.

Model Name	Analysis Result (mm)	Average of Experimental Results (mm)	FEM/Test
V1	14.8		0.881
V2	24.3		1.446
V3	16.5	16.8	0.982
Proposed	14.1		0.839
Threaded	15.4		0.917

Table 5.12. Comparison at the 12.9 – E2 configuration for the displacement at the ultimate force between numerical and experimental results.

Model Name	Analysis Result (mm)	Average of Experimental Results (mm)	FEM/Test
V1	18.5		0.959
V2	32		1.658
V3	19	19.3	0.984
Proposed	19		0.984
Threaded	30		1.554

### 5.1.2. Modelling Technique Comparison

The bolt bending distribution throughout the clamped region and bending-tension interaction at a particular cross-section were compared between the modelling techniques. The bolt bending moment diagrams for the clamped region for all configurations are shared in Figure 5.12 – 5.15. These diagrams were given for both the elastic limit and ultimate strength point of the T-Stub joint to evaluate the bolt bending behaviour at both the elastic and plastic regions. The bending-tension interaction curves for all configurations are plotted in Figure 5.16 and 5.17.

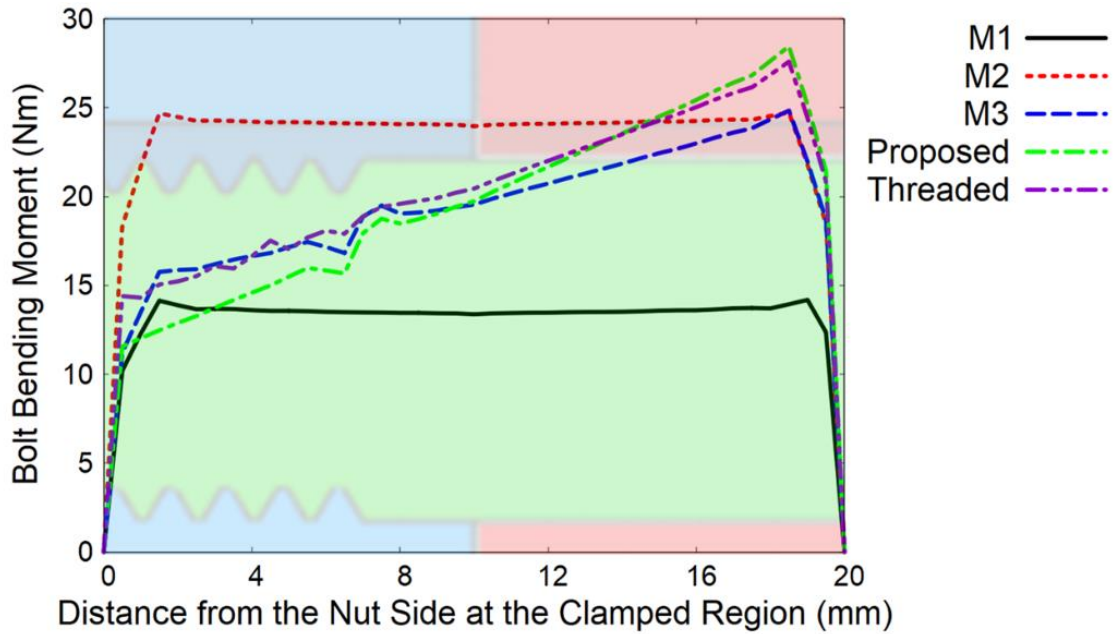
For the elastic limit of the bolt, the bending moment value is constant at the modelling techniques having uniform cross-section while the methods which the major and minor diameters of the bolt were modeled separately have a varying bending moment throughout the clamped region. The M3, the proposed, and the threaded modelling techniques have similar bending moment diagrams at the clamped region for the elastic limit of the bolt.

Bolt bending moment distributions for the modelling techniques at the ultimate load point of the T-Stub connection fastener were observed similarly with the results for the elastic limit of the fastener. For the ultimate point, the bending moment diagram for the modelling techniques with uniform cross-section mimics an arch while the methods which the major and minor diameter of the bolt were modeled separately have abruptly increasing bending moment towards to bolt head from the nut side where the bending moment is approximately zero. This situation shows that the threaded portion does not carry a bending moment at the plastic region because this area yields completely prior to the shank region where a complete yielding did not happen.

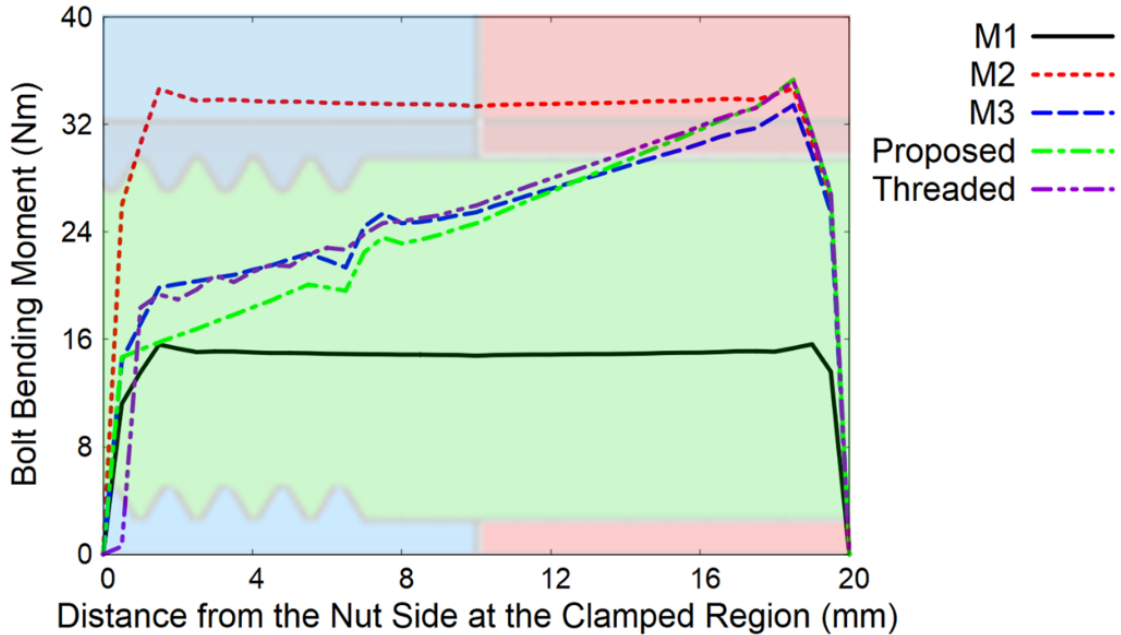
The bolt bending moment and the axial force on the bolt can be monitored together for a particular cross-section by using the bending-tension interaction curves. As seen in Figure 5.16 and 5.17, the interaction curve of the M1 technique showed different variations with respect to the others, and it can be said that the M1 Modelling technique provides a lower amount of bolt bending moment than the other techniques for elastoplastic region at all configurations. Because the area of the interested section is equal for the Modelling techniques except for the M1 technique, the interaction curve was obtained similarly for them, especially in the models in which the 12.9 bolt strength grade was used. It can be



stressed that the interaction curves for the modelling techniques except the M1 technique vary at the plastic region at the configuration in which the 8.8 bolt strength grade was used due to the high ductility of the 8.8 strength grade.

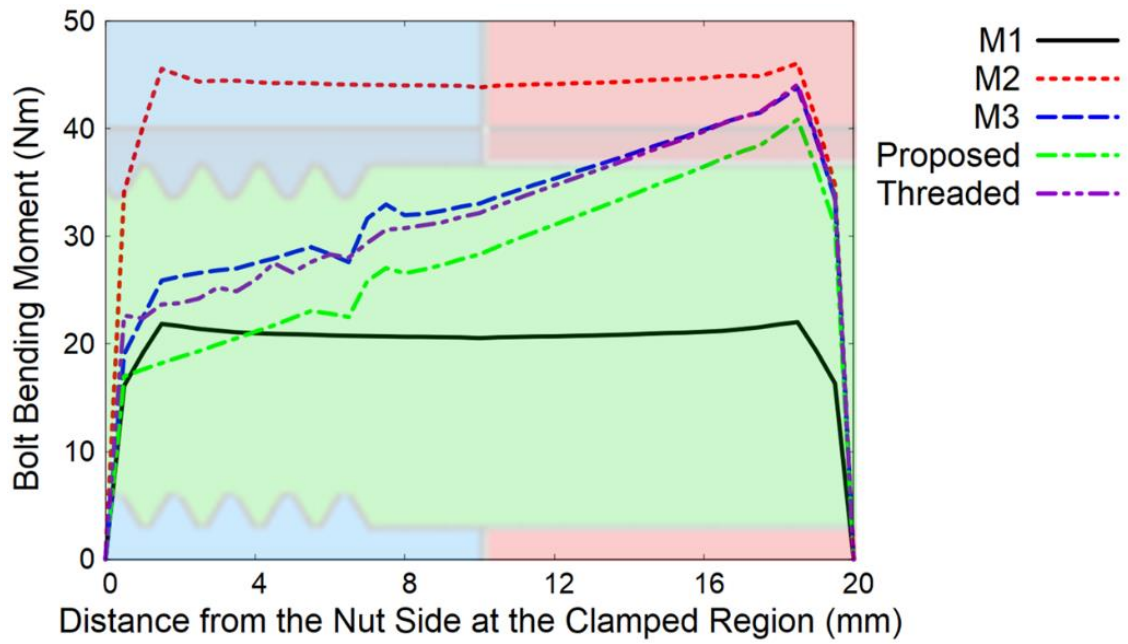


(a)

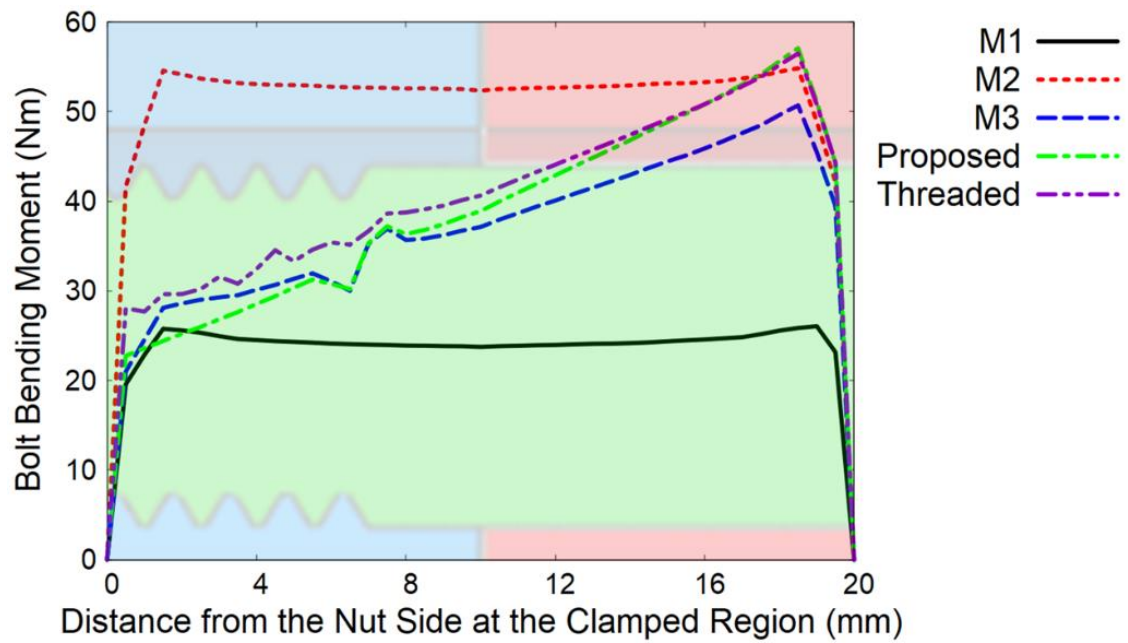


(b)

Figure 5.12. The bolt bending moment diagram at the elastic limit of the T-Stub connection for the clamped region of the configuration of (a) 8.8 – E1, (b) 8.8 – E2.

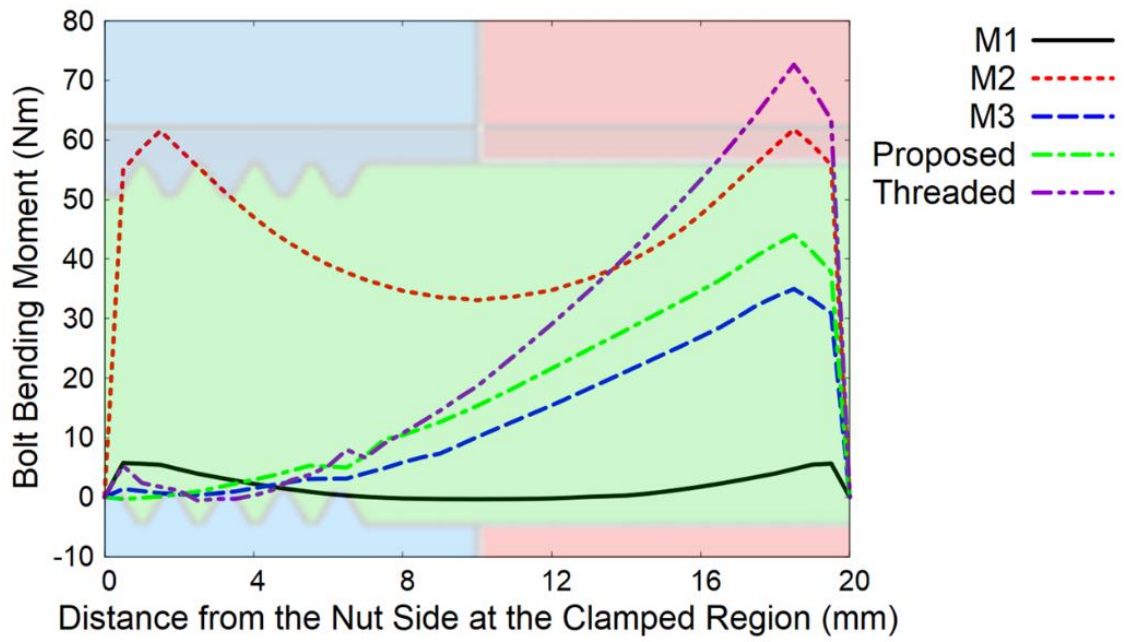


(a)

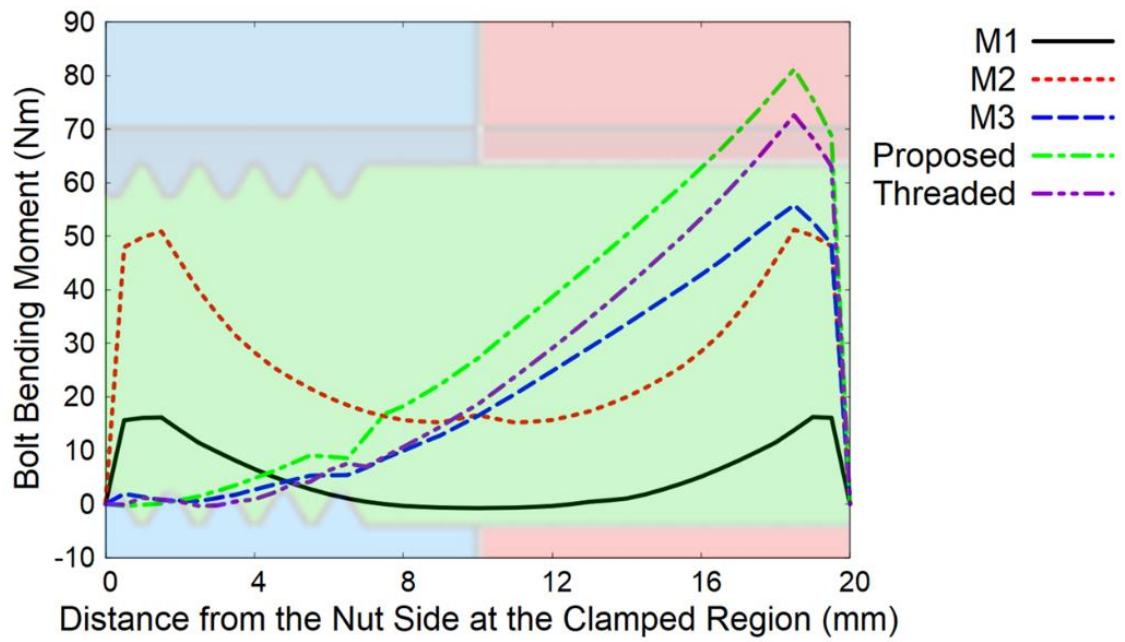


(b)

Figure 5.13. The bolt bending moment diagram at the elastic limit of the T-Stub connection for the clamped region of the configuration of (a) 12.9 – E1, (b) 12.9 – E2.

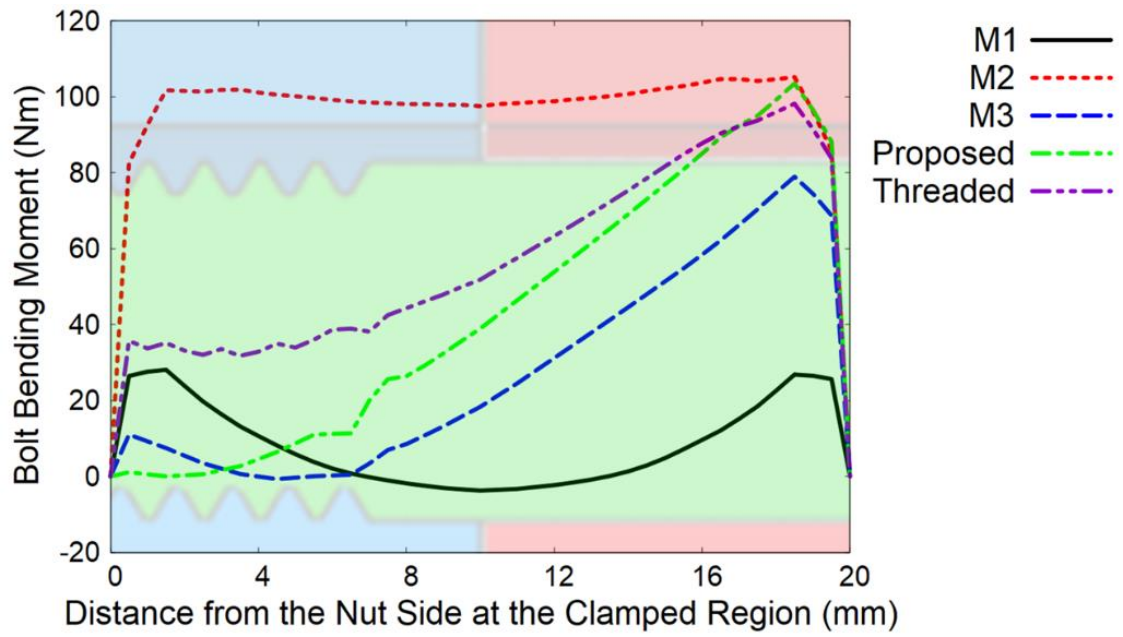


(a)

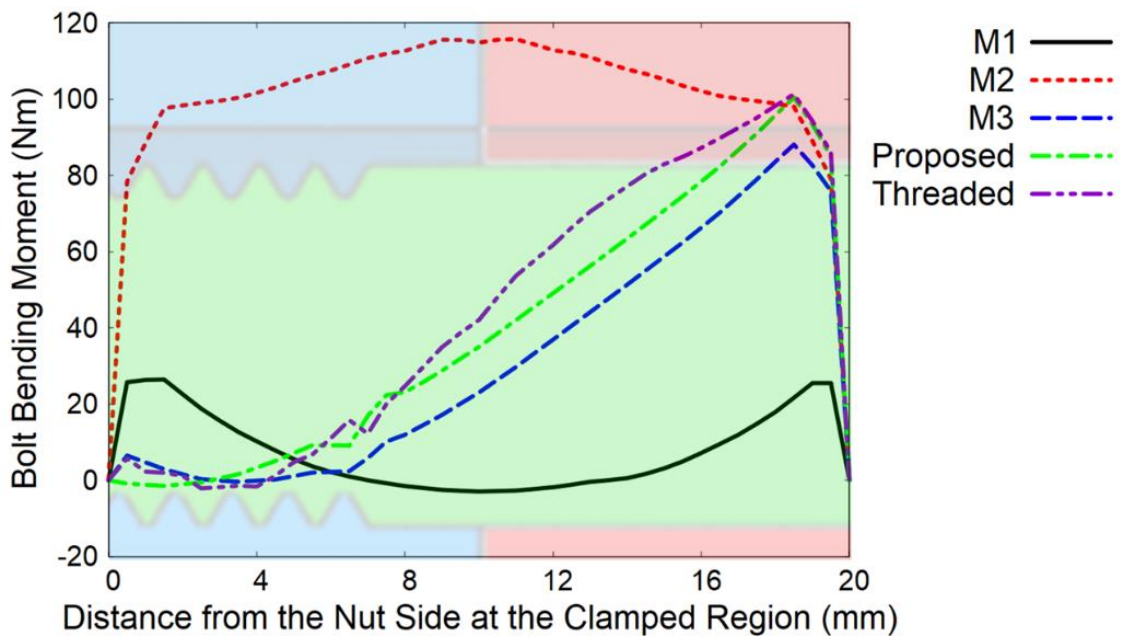


(b)

Figure 5.14. The bolt bending moment diagram at the ultimate strength of the T-Stub connection for the clamped region of the configuration of (a) 8.8 – E1, (b) 8.8 – E2.

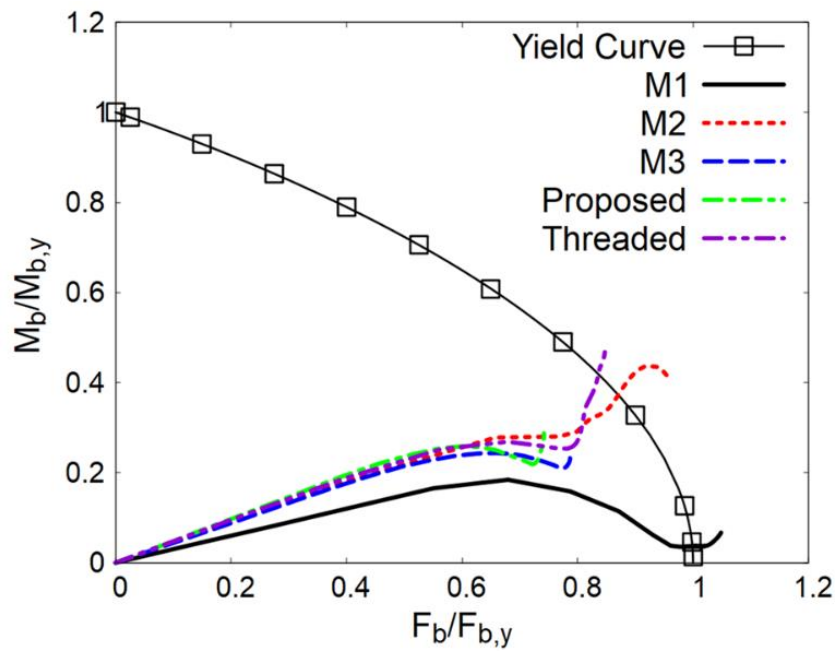


(a)

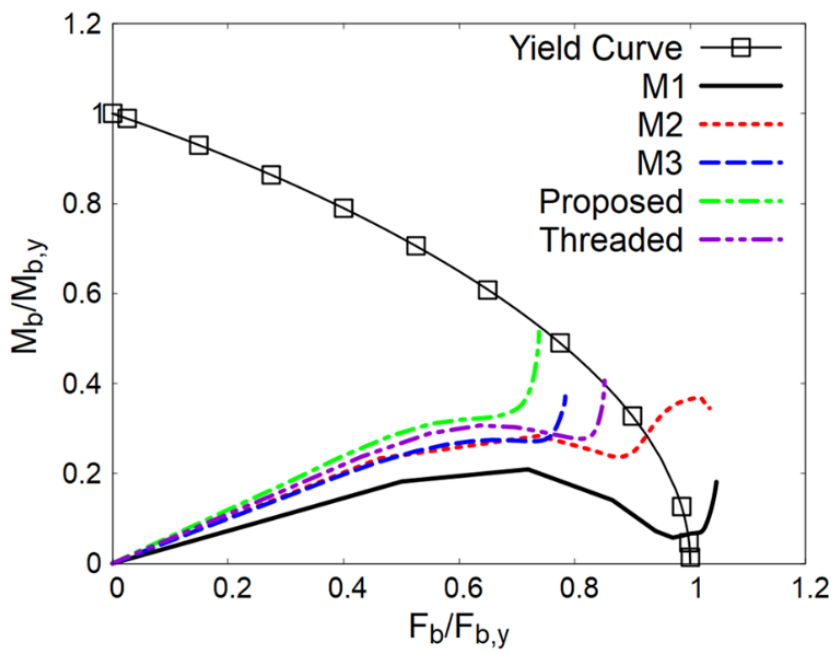


(b)

Figure 5.15. The bolt bending moment diagram at the ultimate strength of the T-Stub connection for the clamped region of the configuration of (a) 12.9 – E1, (b) 12.9 – E2.

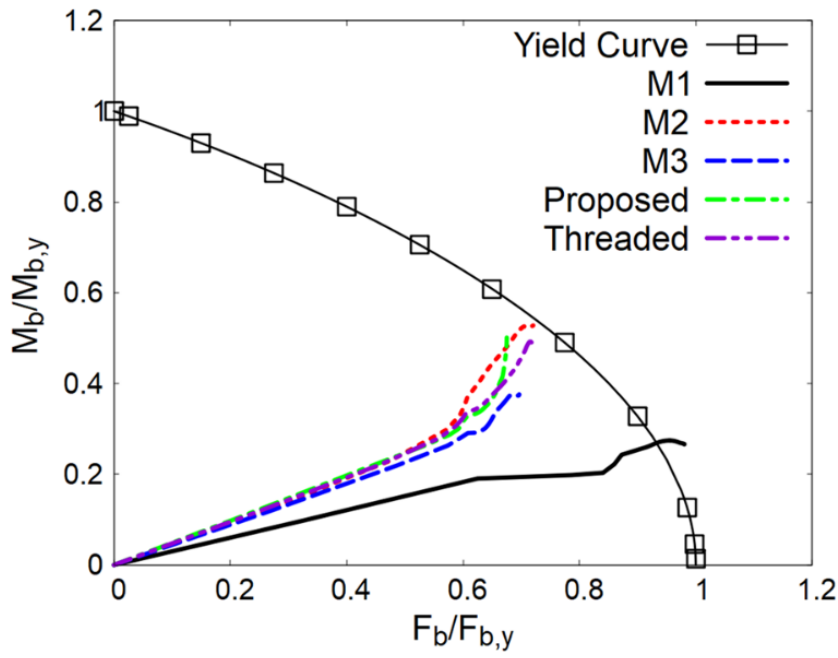


(a)

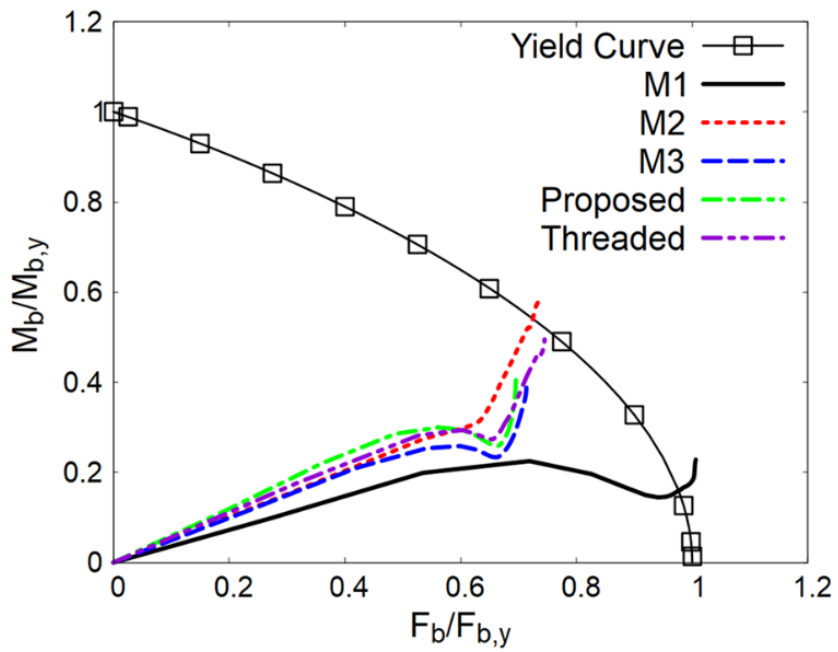
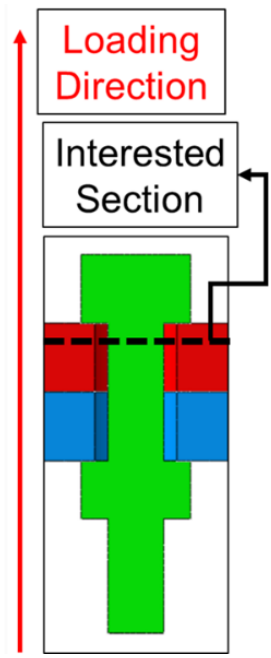


(b)

Figure 5.16. The bending-tension interaction curves of the bolt at the configuration of (a) 8.8 – E1, (b) 8.8 – E2.



(a)



(b)

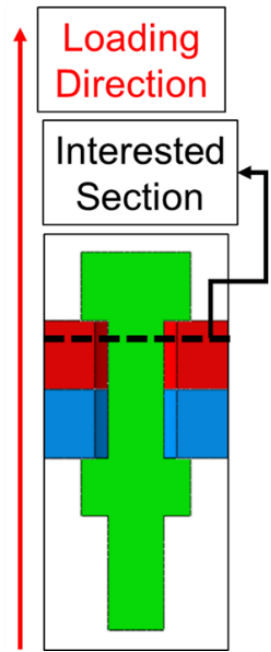


Figure 5.17. The bending-tension interaction curves of the bolt at the configuration of (a) 12.9 – E1, (b) 12.9 – E2.

## 5.2. Overview of the Modelling Techniques

The characteristics and the computational features of the finite element modelling techniques of the bolted joints are presented in this section. When the force-displacement and strain force variations, mechanical parameters, bolt bending moment distribution, and bending-tension interaction curves are evaluated, it can be approached that the M2 modelling technique shows the highest stiffness behaviour among the studied methods. In addition to this fact, the M1 and M2 methods could not reflect varying bolt bending moment distribution throughout the clamped region. As a result, the M1 and M2 techniques are not suitable for evaluating the bending deformation of the bolted joint under prying action.

The modelling methods which arrange the geometry of the partially-threaded bolts with both major and minor diameters showed consistent results between each other and with respect to experimental results. The stiffness arrangement applied for the proposed method provided a slight improvement in terms of the mechanical parameters with respect to the M3 technique. Moreover, the threaded modelling technique causes a remarkable amount of computation effort, and this fact compels the usage of this technique. In conclusion, it was decided to use the proposed method for the preloaded analyses because it seemed the most suitable modelling technique among the studied methods according to the results.

The computation effort of the modelling techniques was also evaluated quantitatively, and the results were shared in Table 5.13 – 5.16. All analyses were performed by using an Intel® Core™ i7-7700HQ 2.8 GHz processor with 8 cores.

Table 5.13. The computation effort comparison of the modelling techniques for 8.8 – E1 configuration.

Method Name	Simplified Model Result (second)	Threaded Model Results (second)	Threaded Model /Simplified Model
V1	755		13.179
V2	1219	9949	8.161
V3	822		12.099
Proposed	814		12.216

Table 5.14. The computation effort comparison of the modelling techniques for 8.8 – E2 configuration.

Method Name	Simplified Model Result (second)	Threaded Model Results (second)	Threaded Model /Simplified Model
V1	868		10.089
V2	1001	8761	8.748
V3	843		10.391
Proposed	872		10.049

Table 5.15. The computation effort comparison of the modelling techniques for 12.9 – E1 configuration.

Method Name	Simplified Model Result (second)	Threaded Model Results (second)	Threaded Model /Simplified Model
V1	1057		12.761
V2	1342	13482	10.048
V3	1039		12.977
Proposed	1107		12.178

Table 5.16. The computation effort comparison of the modelling techniques for 12.9 – E2 configuration.

Method Name	Simplified Model Result (second)	Threaded Model Results (second)	Threaded Model /Simplified Model
V1	942		11.795
V2	997	11116	11.152
V3	897		12.398
Proposed	915		12.143

### 5.3. Preloaded Bolted Joint Results

In addition to the finite element analyses with non-preloaded bolted joints, three different pre-tightening force levels were applied for the preloaded analyses. The preload values were



provided from Bossard Technical Documentation [99], and these are given in Table 5.17 for each bolt strength grade. 30.3 kN and 52.1 kN tensile forces were selected as the maximum admissible preload values for 8.8 and 12.9 bolt strength grades with 0.1 coefficient of friction value [99]. 30% and 60% of these values were used for the preloaded analyses in addition to the maximum preload values.

Table 5.17. Preload values for the bolted joint analyses.

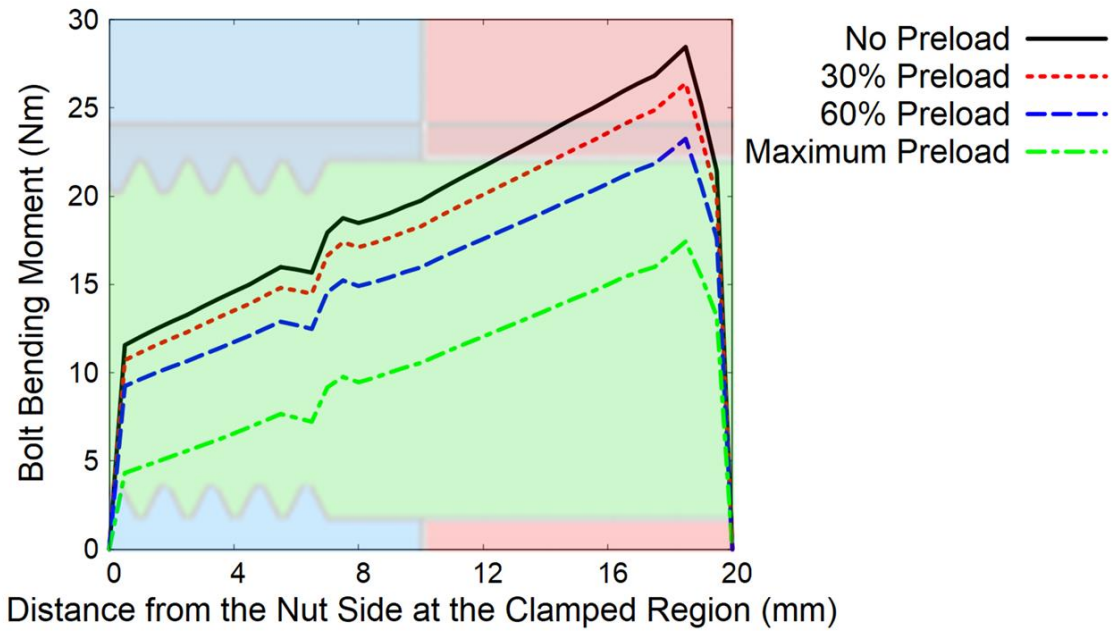
Bolt Strength Grade	Preload Value (kN)	Comment
8.8	9.09	30% Percent of the Maximum Admissible Preload Value for 8.8 Bolt Strength Grade
	18.18	60% Percent of the Maximum Admissible Preload Value for 8.8 Bolt Strength Grade
	30.3	Maximum Admissible Preload Value for 8.8 Bolt Strength Grade
12.9	15.63	30% Percent of the Maximum Admissible Preload Value for 12.9 Bolt Strength Grade
	31.26	60% Percent of the Maximum Admissible Preload Value for 12.9 Bolt Strength Grade
	52.1	Maximum Admissible Preload Value for 12.9 Bolt Strength Grade

The bolt bending distribution throughout the clamped region and bending-tension interaction at a specific cross-section were compared between the preload levels. The bolt bending moment diagrams for the clamped region for all configurations are shared in Figure 5.18 – 5.21. These diagrams were given for both the elastic limit and ultimate strength point of the T-Stub joint to evaluate the bolt bending behaviour at both the elastic and plastic regions. The bending-tension interaction curves for four configurations are plotted in Figure 5.22.

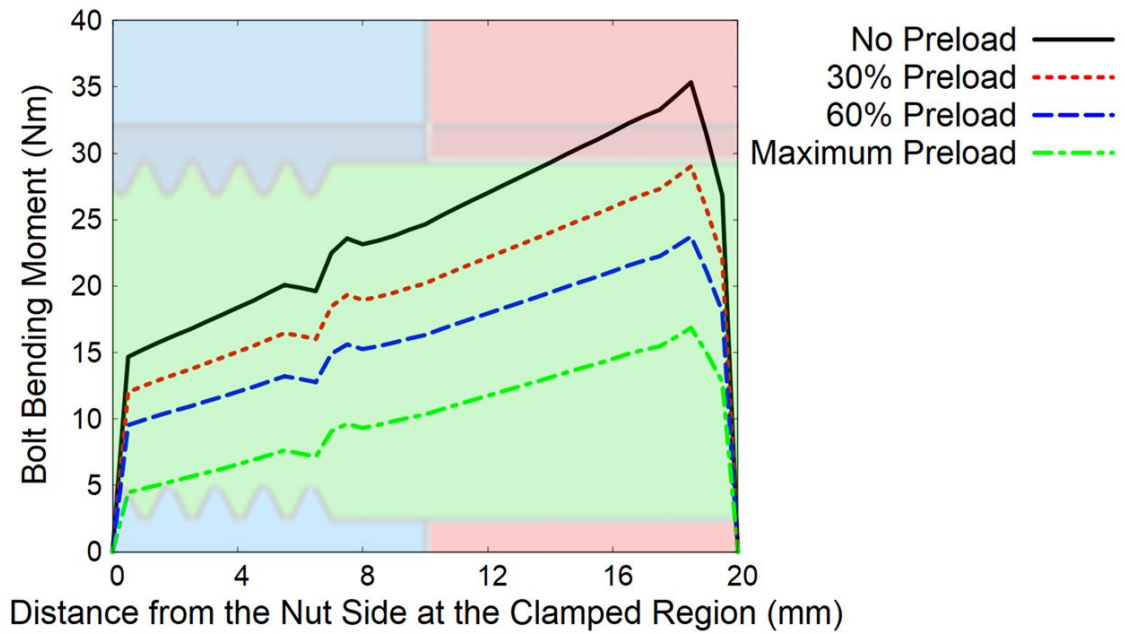
The variation of the bolt bending moment diagram throughout the clamped region for all configurations at the elastic limit of the bolt did not change with respect to the different preload levels, and the diagrams shifted as each other's offset. For the configurations of lower eccentricities, approximately 7% reduction for the 30% preload level, 17% reduction

for the 60% preload level, and 38% reduction for the maximum preload level were observed at the maximum bolt bending moment value of the non-preloaded analyses. Furthermore, approximately 17% reduction for the 30% preload level, 33% reduction for the 60% preload level, and 53% reduction for the maximum preload level were observed at the maximum bolt bending moment value of the non-preloaded analyses of the configurations of higher eccentricities. For the ultimate limit of the fastener, the bolt bending moment diagrams are approximately the same for each configuration. Slight differences were obtained at the maximum bolt bending moment values, but these differences can be negligible. It can be said that the preload effects disappeared after the clamped region was plastically deformed.

For all bending-tension interaction curves for the section specified in Figure 5.16 and 5.17, the variation at the curves is different for each preload level. The curves merge at the elastic limit, and similar to the bolt bending moment diagram at the ultimate point, they proceed in a single path to the ultimate point at the plastic region. Because the yield and ultimate strength of the bolts are quite higher than the conventional minimum strength values, the initial point of the curves is not consistent with the preload levels.

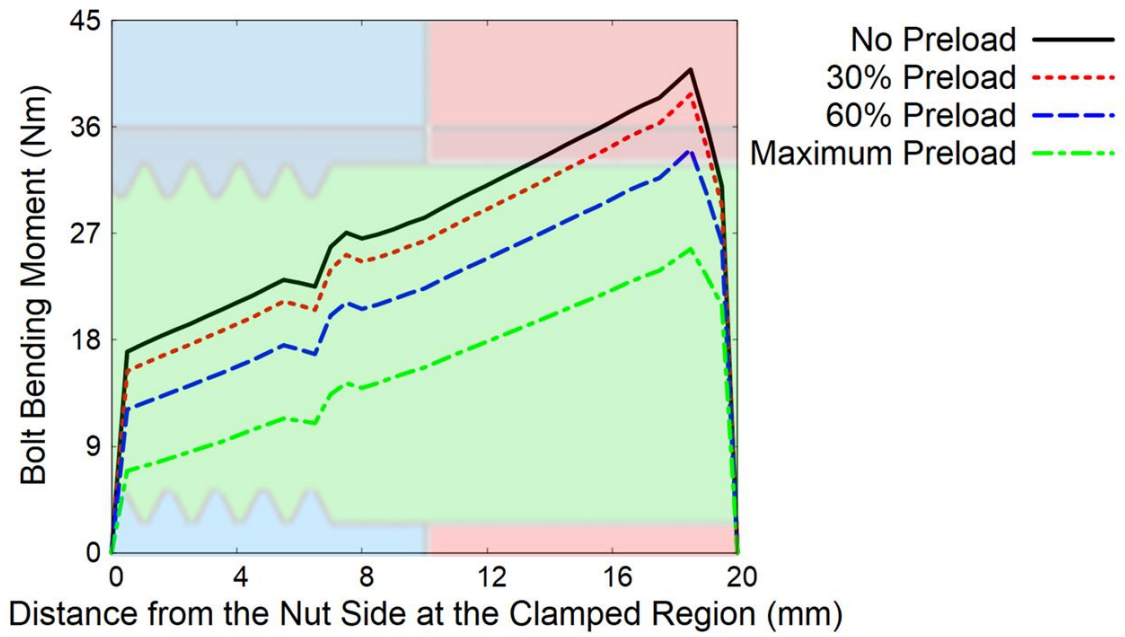


(a)

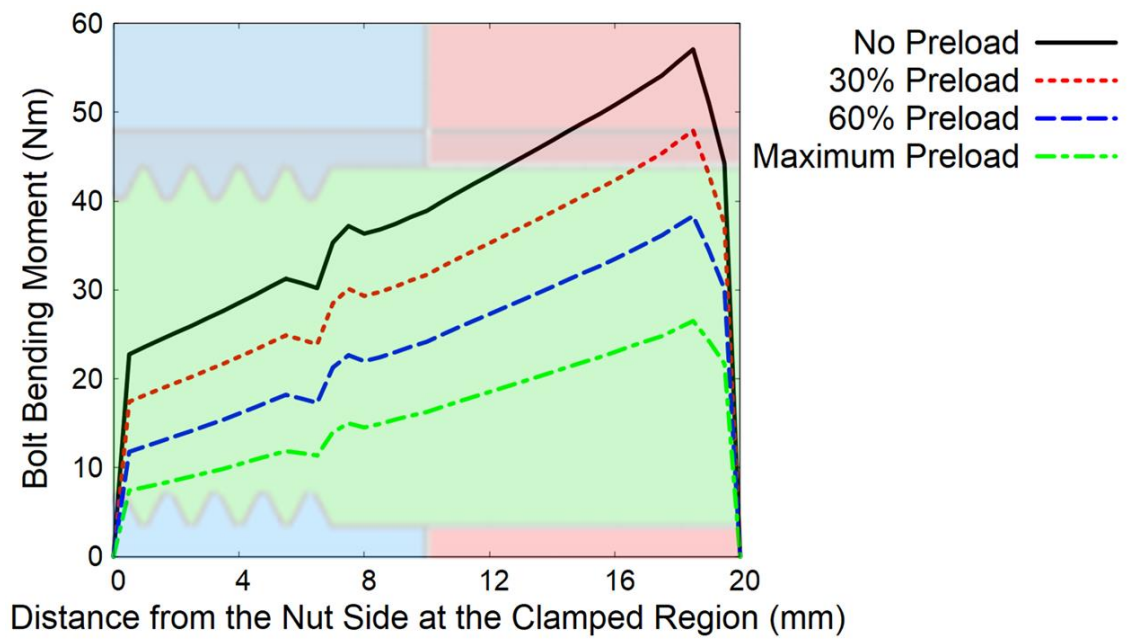


(b)

Figure 5.18. The preloaded bolt bending moment diagram at the elastic limit of the T-Stub connection for the clamped region of the configuration of (a) 8.8 – E1, (b) 8.8 – E2.

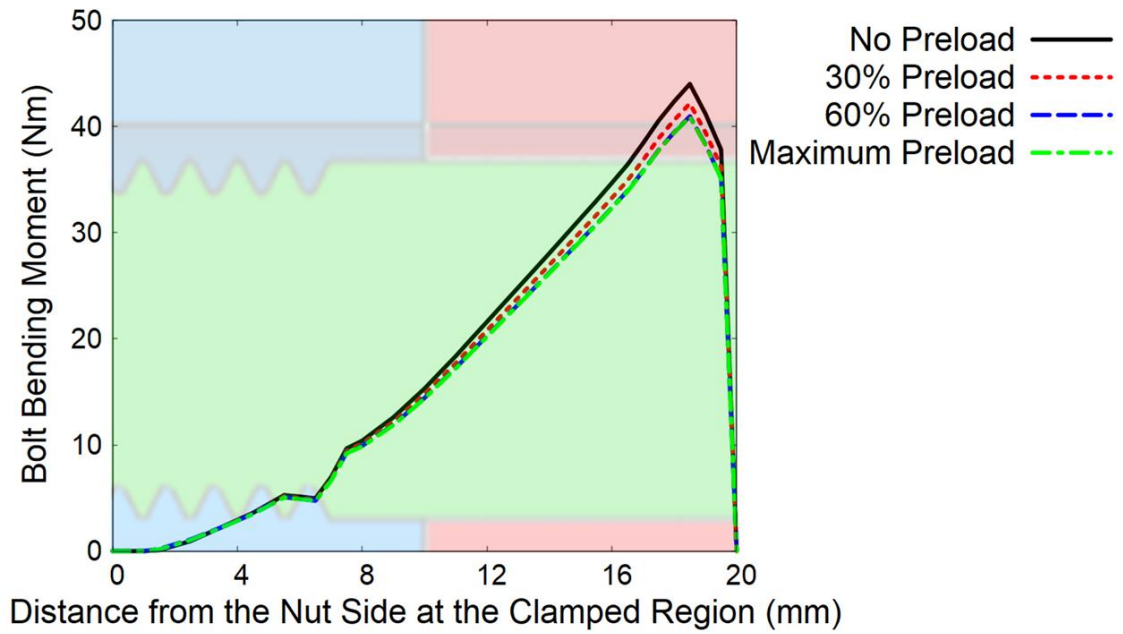


(a)

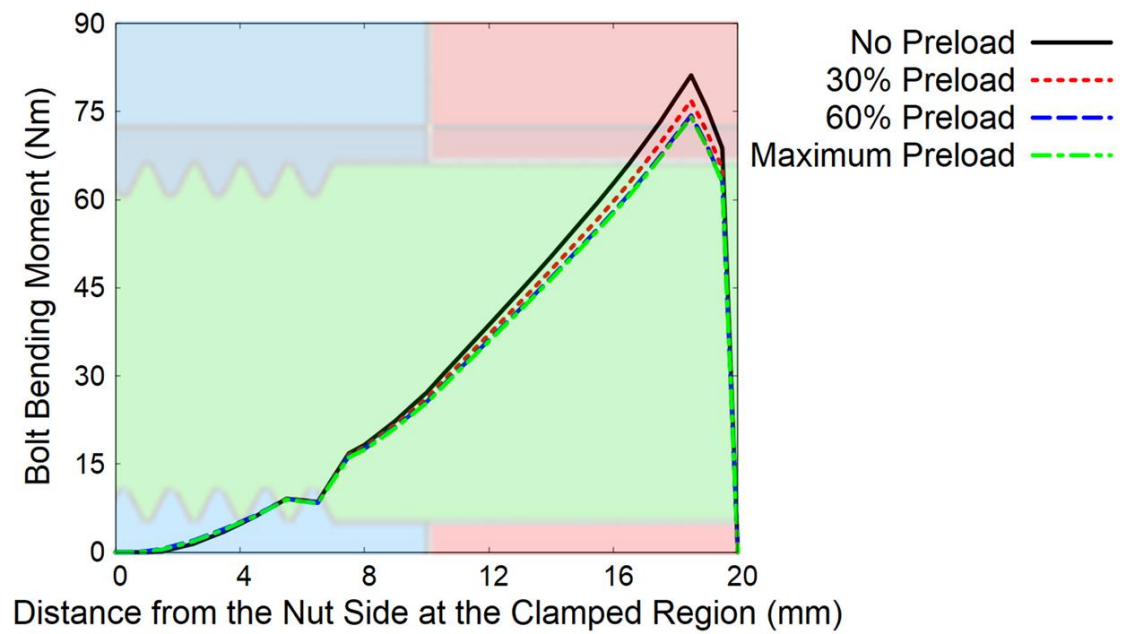


(b)

Figure 5.19. The preloaded bolt bending moment diagram at the elastic limit of the T-Stub connection for the clamped region of the configuration of (a) 12.9 – E1, (b) 12.9 – E2.

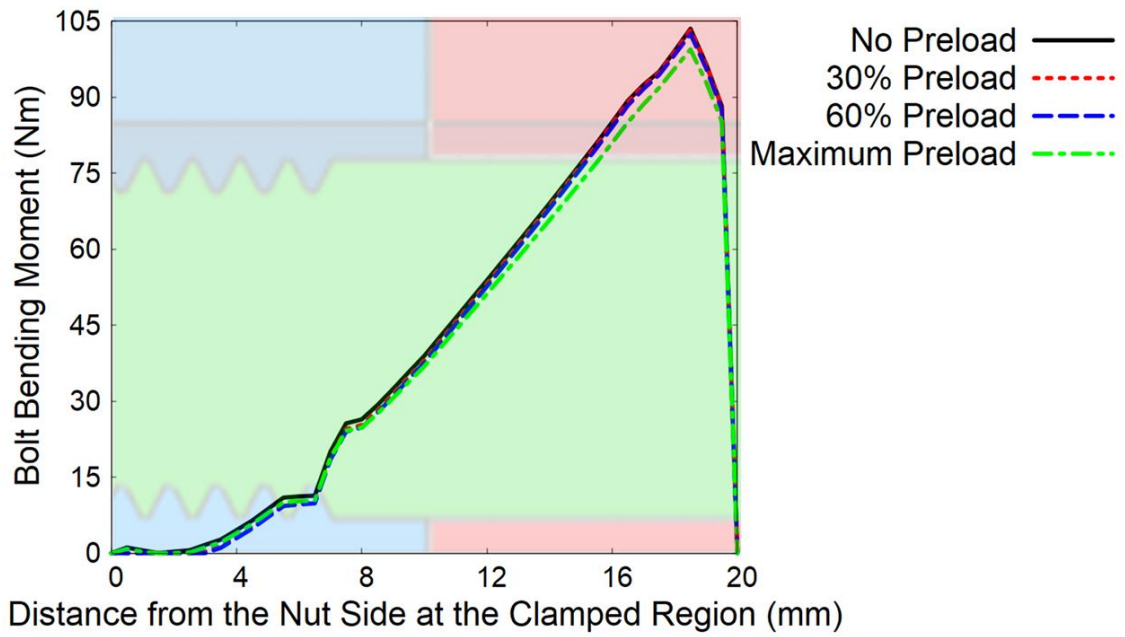


(a)

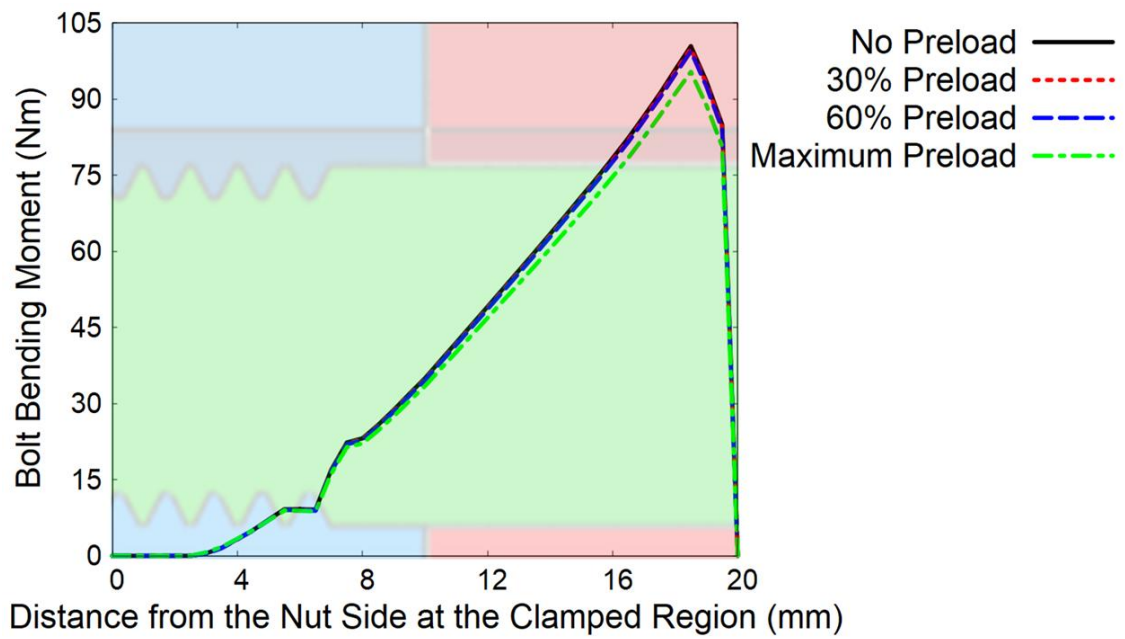


(b)

Figure 5.20. The preloaded bolt bending moment diagram at the ultimate strength of the T-Stub connection for the clamped region of the configuration of (a) 8.8 – E1, (b) 8.8 – E2.



(a)



(b)

Figure 5.21. The preloaded bolt bending moment diagram at the ultimate strength of the T-Stub connection for the clamped region of the configuration of (a) 12.9 – E1, (b) 12.9 – E2.

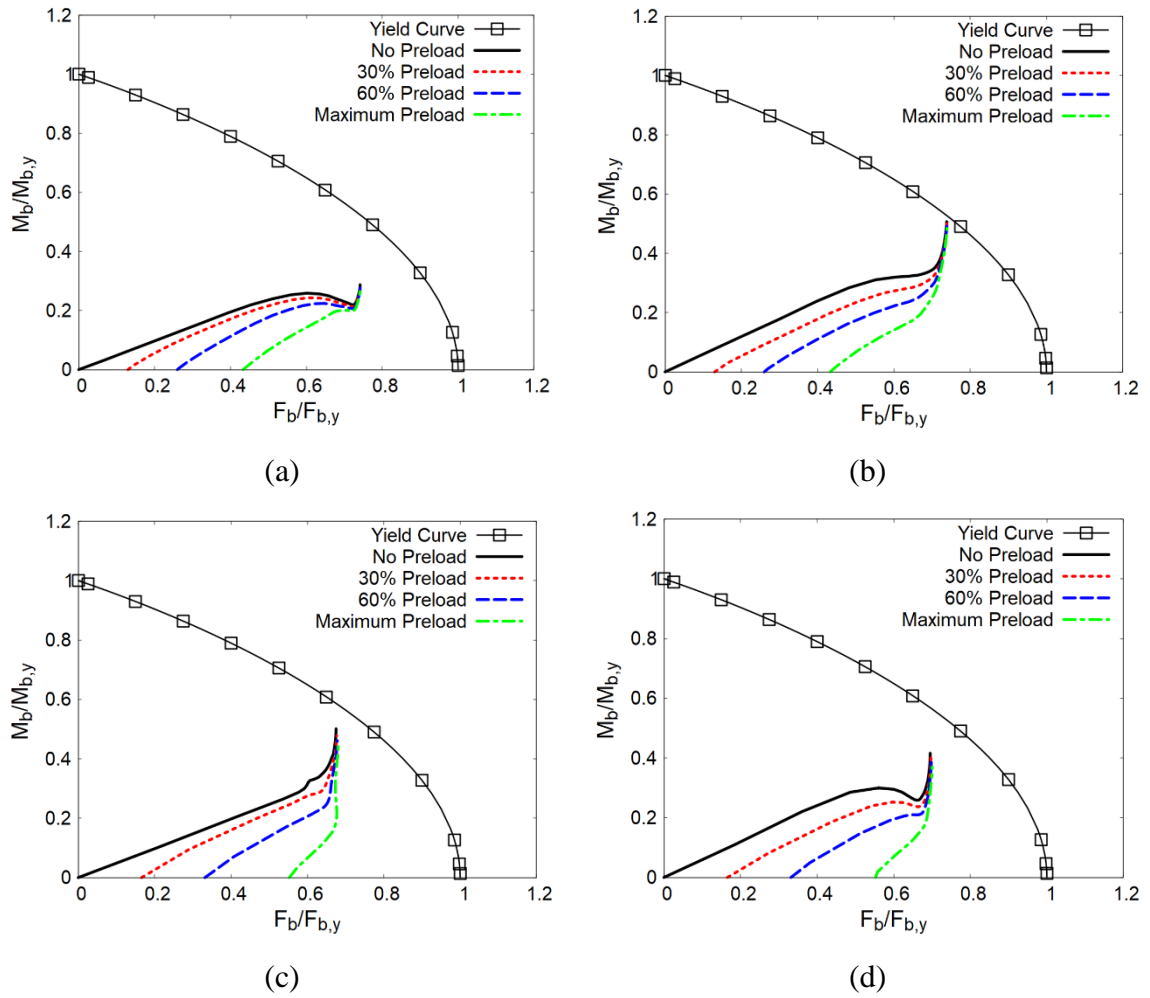


Figure 5.22. The bending-tension interaction curves of the preloaded bolt at the configuration of (a) 8.8 – E1, (b) 8.8 – E2, (c) 12.9 – E1, (d) 12.9 – E2.

## 6. CONCLUSION

This chapter introduces the observations from both numerical and experimental work done in this study. The bending deformation phenomenon of the bolted joints under prying action was investigated in this thesis. After introducing a brief background about the bolted joints under the eccentric loadings and prying action, a comprehensive literature survey was presented. The studies in the literature about the three-dimensional finite element modelling techniques of the bolted joints, bolt bending, and prying action were explained in detail. As a consequence of the content of the literature survey, several outcomes were identified for the major objectives of this study. The proposals of this thesis were constructed with respect to these observations, and they can be described as follows similarly shared at the end of the literature search chapter of this thesis. The overall outcome includes that the literature has lack of information about the following items, and the objectives of this study were assigned with respect to the facts mentioned above:

- The effect of the finite element modelling technique of the bolted joint under the prying action on the bending-tension interaction of the bolted joint,
- The consideration of the critical cross-section of the fastener to determine the maximum bolt bending moment,
- The influence of the bolt preload on the bending-tension interaction of the bolted joint and the bolt bending moment distribution throughout the clamped region of the fastener,
- Bolt failure mechanism where bolt bending moment exists in a remarkable amount.

The experimental and numerical programs were planned in accordance with the objectives. Experimental studies were performed prior to finite element analyses to provide required inputs such as material properties and displacement boundary conditions. The mechanical properties of bolts with different strength grades and setup material were shared in the corresponding chapter. It was obtained that the yield and ultimate strength values of the 8.8 and 12.9 bolt strength grades were quite higher than the minimum allowable strength values. The mechanical properties of the setup material of S275 were quite similar to the standard values except for the elongation parameters which show different behaviour for specimen



location and the angle with respect to the rolling direction. The results of the mechanical parameters from the T-Stub tests were consistent for each configuration. One of three tests performed for each configuration was performed by using strain gauges bonded at the bolt and the T-section parts, and the strain data for every enduring gauge were shared at the corresponding section.

Before presenting the results, the construction of the finite element analysis models was represented in detail. The mechanical properties obtained from the experimental study, the geometries used for the analyses, interactions, loads, and boundary conditions were stressed for all configurations. The mesh structures were indicated with the number of elements and nodes. The finite element modelling techniques of the bolted joints used in this thesis study were demonstrated. Moreover, the features and construction philosophy of the proposed modelling technique were explained.

The results obtained from the finite element analyses were presented in four different sections. Initially, the results of the non-preloaded bolted joint models were compared with the corresponding experimental outcomes in terms of the force-displacement and strain-force variations, and structural parameters such as initial stiffness and maximum force. Secondly, the studied modelling techniques were compared with each other in terms of the bolt bending distribution throughout the clamped region and bending-tension interaction at a specific cross-section. Furthermore, an overview was presented of the studied bolted joint modelling techniques in terms of the characteristics and computational parameters. Finally, the results of the bolt bending distribution throughout the clamped region and bending-tension interaction at a specific cross-section were shared for the preloaded bolted joint analyses. The force-displacement response and strain values from where strain gauges were instrumented at the experimental study were compared with the experimental results. Because the experimental studies were performed with non-preloaded bolts, the comparisons were also accomplished with the finite element analyses including non-preloaded bolted joint. The results of the mechanical parameters which are initial stiffness, maximum force, and displacement at the maximum force for all configurations of the non-preloaded finite element analyses were compared and introduced in the corresponding section.

The force-displacement behaviour, strain-force variations throughout the loading, and results of the mechanical parameters for all configurations and modelling techniques were compared with the experimental results. It was observed that the initial stiffness results of the modelling techniques for all configurations are quite compatible with the experimental results, however, the plastic deformation region at the force-displacement curves is different for each modelling technique. For the strain results of the bolts, it can be commented that the strain values acquired from the web side strain gauge sensors on the bolts can be admitted as consistent with the experimental results whereas the strain values acquired from the end side strain gauges on the bolts are not compatible with the experimental results. Moreover, the strain values acquired from the T-sections were in longitudinal and transverse directions, and the strain values in the longitudinal directions for all models are more consistent with the experimental results than in the transverse direction. Lastly, the results of the mechanical parameters which are initial stiffness, maximum force, and displacement at the maximum force for all configurations and modelling techniques provided compatible ratios with compared the experimental results excluding the M2 technique. The essential statements on the differences observed at all comparison items were mentioned in the corresponding sections in detail. For the sake of clarification, they can be defined as listed below. The following outcomes may be related to the discrepancy observed at the plastic region response of the force-displacement curves. However, they were neglected because most of the comparison results and the ratios of the main mechanical parameters were in compliance.

- The initial tightening of the bolted joints affected the strain gauge data from the end side sensors, and differences in a remarkable amount were observed between the numerical and experimental results.
- The transverse direction data of the strain gauge sensors on the T-section part could not provide sufficient similarities with the numerical results.

After comparing the experimental and numerical results in the results section, the modelling techniques were analyzed in terms of the bending deformation capability, and this feature was evaluated by using the bolt bending moment results throughout the clamped region and bending-tension interaction curves. Because there is not any supportive data from the experimental study about the bolt bending moment, the modelling techniques were examined

by accepting the threaded technique as the reference model. Despite the fact that the modelling techniques did not show significant differences at the bending-tension interaction curves except the M1 modelling technique, the proposed modelling technique provided the most suitable bolt bending moment diagrams throughout the clamped region for both elastic limit and ultimate capacity of the bolted joint among the modelling techniques. In conjunction with the advantage about the computational effort against the threaded model, it was decided to select the proposed model because of its overall results while performing finite element analyses including preloaded bolted joint.

The bolted joint configurations were also analyzed by using three different pre-tightening force levels. 30% and 60% of the maximum recommended preload values for 8.8 and 12.9 bolt strength grades were used for the preloaded analyses in addition to the maximum preload values, but these stages remained low because the strength of the fasteners used in the experimental study was relatively higher than the catalog levels. The bolt bending distribution throughout the clamped region and bending-tension interaction at a specific cross-section were compared between the preload levels. For the elastic limit of the bolted joint, the fastener carries less bending moment as the pre-tightening force value increases, and the bolt bending moment carrying situation was approximately the same for each configuration for the ultimate limit of the fastener. Those phenomena can be seen clearly from both bolt bending moment diagrams and bending-tension interaction curves.

In conclusion, the structural response of a bolted joint involving a partially threaded fastener under prying action was comprehensively evaluated by considering the bending deformation capacity. For the flexural features of the studied bolted joint type under prying action, finite element analysis modelling issues and design considerations are listed below:

- The constant diameter modelling technique for a partially threaded fastener cannot acquire the correct bending deformation characteristic for both elastic and plastic regions while performing finite element analyses.
- The piecewise modelling technique which contains both minor and major diameters of the bolt is able to reflect the bolt bending deformation at the results of the finite element analyses, however, a relief, with the size of a thread in the radial direction, at the thread engagement for the first three pairs of mating threads can represent the

bending deformation more suitable than the piecewise modelling technique not including a relief.

- The pre-tightening force applied to the bolt affects inversely proportional the bolt bending moment for the elastic region, the bolt bending moment decreases as the pre-tightening force increases.
- Beyond the elastic limit of the bolt, the preload effects on the bolt bending moment disappear.
- The initial complete plastically deformed region of the bolts is the threaded portion due to the effective diameter dimension. For both non-preloaded and preloaded bolted joint configurations, the amount of bending deformation at the threads decreases after the plastic deformation starts at this region. In addition, this region carries nearly tensile force only at the yielding region, and the damage starts in the presence of tensile force alone. As a result of this fact, the main plastic deformation mechanism occurs in the existence of the tensile deformation although the threaded portion carries bending moment at the elastic region.
- When the deformation mechanism at the threads described previously occurs, the shank portion of the bolt continues to carry a bending moment because this portion is not completely deformed plastically.

For future studies, the bending deformation characteristics can be investigated for the screwed connections which do not contain nut part. The bolt bending moment diagrams for this type of joint may differ due to the stiffness variation between the nut and a stiff foundation. Moreover, the effect of the damage accumulation on the bolt bending deformation can be evaluated by performing finite element analyses with an explicit solver. Furthermore, a numerical study using XFEM can be performed for the bolt involving a crack at the shank portion to demonstrate the bending deformation mechanism and whether the flexural response of the bolt differs.



## REFERENCES

- [1] ESDU, An introduction to some methods to calculate loads and stiffnesses in bolted assemblies, ESDU Series, **2010**.
- [2] E. S. Skavhaug and S. I. Østhus, Tension-loaded bolted connections in steel structures, Master of Science Thesis, Norwegian University of Science and Technology, Department of Structural Engineering, Trondheim, **2015**.
- [3] VDI, Systematic calculation of high duty bolted joints: Joints with one cylindrical bolt, VDI Standards, **2003**.
- [4] J. Apeland, Application of FE-analysis in Design and Verification of Bolted Joints According to VDI 2230 at CERN, Master of Science Thesis, Norwegian University of Science and Technology, Department of Mechanical and Industrial Engineering, Genève, **2018**.
- [5] S. E. Yılmaz, Comparison of Experimental Study and Finite Element Analysis of Bolted Flange Connections, Master of Science Thesis, Middle East Technical University, Department of Aerospace Engineering, Ankara, **2015**.
- [6] A. Yıldırım, Development of Bolted Flange Design Tool Based on Finite Element Analysis and Artificial Neural Network, Master of Science Thesis, Middle East Technical University, Department of Aerospace Engineering, Ankara, **2015**.
- [7] N. Kumar, P. V. G. Brahamanandam and B. V. Papa Rao, MIT International Journal of Mechanical Engineering, 1 (**2011**) 35-40.
- [8] E. S. Mistakidis, C. C. Baniotopoulos, C. D. Bisbos and P. D. Panagiotopoulos, Journal of Constructional Steel Research, 44 (**1997**) 51-67.
- [9] J. A. Swanson, D. S. Kokan and R. T. Leon, Journal of Constructional Steel Research, 58 (**2002**) 1015-1031.
- [10] A. B. Francavilla, M. Latour, V. Piluso and G. Rizzano, Engineering Structures, 100 (**2015**) 656-664.
- [11] M. W. Simon and J. B. Hengehold, SAE Transactions, 86 (**1977**) 2103-2112.

- [12] M. Couchaux, M. Hjiiaj, I. Ryan and A. Bureau, *Journal of Constructional Steel Research*, 133 (2017) 459-474.
- [13] A. Loureiro, R. Gutiérrez, J. M. Reinoso and A. Moreno, *Journal of Constructional Steel Research*, 66 (2010) 1516-1522.
- [14] A. Abidelah, A. Bouchaïr and D. E. Kerdal, *Journal of Constructional Steel Research*, 76 (2012) 13-27.
- [15] G. Liang, H. Guo, Y. Liu, D. Yang and S. Li, *Thin-Walled Structures*, 137 (2019) 271-283.
- [16] D. Hua, J. Papadopoulos and G. G. Adams, *Journal of Constructional Steel Research*, 169 (2020) 106027.
- [17] M. Atasoy, *Determination of Prying Load on Bolted Connections*, Master of Science Thesis, Middle East Technical University, Department of Aerospace Engineering, Ankara, 2012.
- [18] Abaqus 6.14 Online Documentation, Dassault Systèmes, 2014.
- [19] R. Verwaerde, P. A. Guidault and P. A. Boucard, *Computational Mechanics*, 65 (2020) 1531-1548.
- [20] R. Askri, C. Bois, H. Wagnier and J. Lecomte, *Finite Elements in Analysis and Design*, 110 (2016) 32-42.
- [21] H. Razavi, A. Abolmaali and M. Ghassemieh, *Journal of Constructional Steel Research*, 63 (2007) 647-657.
- [22] B. Blachowski and W. Gutkowski, *Engineering Structures*, 111 (2016) 93-103.
- [23] J. Kim, J. C. Yoon and B. S. Kang, *Applied Mathematical Modelling*, 31 (2007) 895-911.
- [24] A. Haddar, L. Augustins, A. Daidie, E. Rodriguez and J. F. Diebold, *Advanced Joining Processes*, 125 (2020) 13-28.
- [25] Z. Wu, S. Zhang and S. F. Jiang, *International Journal of Steel Structures*, 12 (2012) 339-350.

- [26] M. D’Aniello, D. Cassiano and R. Landolfo, *Steel and Composite Structures*, 24 (2017) 643-658.
- [27] A. Mudrov, G. Šaučiuvėnas, A. Sapalas and Ivar Talvik, *Engineering Structures and Technologies*, 8 (2016) 85-93.
- [28] Y. Amir, S. Govindarajan, S. Iyyanar, *Bolted Joints Modelling Techniques, Analytical, Stochastic and FEA Comparison*, Proceedings of the ASME 2012 International Mechanical Engineering Congress & Exposition, 9-15 November, Houston, Texas, USA, 2012.
- [29] A. Söderlund, *Influence of Surface Flatness on Bolted Flanges Bolt Section Method and Fatigue Strength Limit*, Master of Science Thesis, Karlstad University, Faculty of Health, Science and Technology, Division of Mechanical Engineering, 2017.
- [30] L. Molnár, K. Váradi and B. Liktör, *Modern Mechanical Engineering*, 4 (2014) 35-45.
- [31] K. Bommisetty, K. Narayanan, *Three-Dimensional Finite Element Analysis of Bolted Joint with Helical Thread Connection*, Proceedings of the ASME 2014 Gas Turbine India Conference, 15-17 December, New Delhi, India, 2014.
- [32] Y. Hu, L. Shen, S. Nie, B. Yang and W. Sha, *Journal of Constructional Steel Research*, 126 (2016) 174-186.
- [33] Q. M. Yu and H. L. Zhou, *Procedia Engineering*, 130 (2015) 1385-1396.
- [34] S. Ganeshmurthy and S. A. Nassar, *Journal of Manufacturing Science and Technology*, 136 (2014) 012018.
- [35] D. Chen, Y. Ma, B. Hou, R. Liu and W. Zhang, *International Journal of Mechanical Sciences*, 153-154 (2019) 240-253.
- [36] M. Pavlović, Z. Marković, M. Veljković and D. Buđevac, *Journal of Constructional Steel Research*, 88 (2013) 134-149.
- [37] H. Z. Deng, C. Li, X. Q. Song, F. Li and P. C. Fu, *Journal of Constructional Steel Research*, 161 (2019) 309-327.
- [38] M. Abid, *NED University Journal of Research*, 11 (2014) 39-47.



- [39] M. Abid, D. H. Nash, Bolt Bending Behaviour in a Bolted Flanged Pipe Joint: A Comparative Study, ASME 2006 Pressure Vessels and Piping/ICPVT-11 Conference, 23-27 July, Vancouver, BC, Canada, **2006**.
- [40] F. Dinu, D. Dubina, I. Marginean, C. Neagu, I. Petran, Axial Strength and Deformation Demands for T-Stub Connection Components at Catenary Stage in the Beams, 8<sup>th</sup> International Conference on Behavior of Steel Structures in Seismic Areas, 1-3 July, Shanghai, China, **2015**.
- [41] X. C. Liu, X. N. He, H. X. Wang, Z. W. Yang, S. H. Pu and Z. Ailin, Journal of Constructional Steel Research, 145 (**2018**) 28-48.
- [42] J. W. Hu, R. T. Leon and E. Choi, International Journal of Steel Structures, 11 (**2011**) 1-11.
- [43] R. Bai, S. L. Chan and J. P. Hao, Journal of Constructional Steel Research, 113 (**2015**) 13-27.
- [44] A. C. Faralli, Large deformation of T-stub connection in bolted steel joints, PhD Thesis, University College London, Department of Mechanical Engineering, **2019**.
- [45] J. C. Schilling and J. E. Gutknecht, Bolting Arrangement Including a Two-Piece Washer for Minimizing Bolt Bending, United States Patents, **2006**.
- [46] T. B. Hyatt and C. B. Klinetob, Moment Relief Barrel Washer, United States Patents, **2017**.
- [47] S. A. Nassar, Y. P. Zuo, Effect of Non-Parallel Underhead Contact of a Tightened Fastener on Clamp Load and Optically Measured Deformation Field, ASME 2005 Pressure Vessels and Piping Conference, 17-21 July, Denver, Colorado, USA, **2005**.
- [48] Anonymous, Joint Face Angularity, The Effect of Joint Face Angularity on the Fatigue Life of Bolts, <https://www.boltscience.com/pages/nutfaceangularity.htm> (Date of Access: **3 August 2021**).
- [49] X. Yang, S. A. Nassar, Effect of Non-Parallel Wedged Surface Contact on Loosening Performance of Preloaded Bolts Under Transverse Excitation, ASME 2011 Pressure Vessels and Piping Conference, 17-21 July, Baltimore, Maryland, USA, **2011**.
- [50] E. Radzimovsky and R. Kasuba, Experimental Mechanics, 2 (**1962**) 264-270.

- [51] T. Sawa and H. Maruyama, *Bulletin of JSME*, 27 (**1984**) 1085-1092.
- [52] T. Sawa, T. Morohoshi and K. Yamamoto, *Bulletin of JSME*, 30 (**1987**) 2018-2026.
- [53] T. Sawa, H. Shiraishi, Y. Minakuchi, S. Makino and M. Fuji, *Bulletin of JSME*, 25 (**1982**) 444-451.
- [54] T. Sawa, H. Miyazawa and K. Rikukawa, *Bulletin of JSME*, 26 (**1983**) 619-626.
- [55] M. Tanaka, T. Sasaki, S. Hoshino and H. Inoue, *Stress Analysis of T-Flange Bolted Joint with a Simplified Spring and Beam Model*, Annual Report of the Faculty of Education of Iwate University, Vol. 51, Morioka, **1992**.
- [56] E. Bakhiet, M. Khalil, A. Khattab, J. Guillot, *New analytical model of bolted connections subjected to eccentric loading: The case of T-flange connection*, Computational Methods and Experimental Measurements, WIT Transactions on Modelling and Simulation, Vol. 9, **1999**.
- [57] G. N. Stamatopoulos and J. C. Ermopoulos, *International Journal of Steel Structures*, 10 (**2010**) 73-79.
- [58] N. L. Pedersen, *Wind Energy*, 20 (**2017**) 1069-1082.
- [59] M. Couchaux, M. Hjiij, I. Ryan and A. Bureau, *Engineering Structures*, 171 (**2018**) 817-841.
- [60] N. B. Khan, M. Abid, M. Jameel and H. A. Wajid, *Proceedings of the Institution of Mechanical Engineers, Part E: Journal of Process Mechanical Engineering*, 231 (**2015**) 555-564.
- [61] A. Abidelah, A. Bouchaïr and D. E. Kerdal, *Engineering Structures*, 81 (**2014**) 181-194.
- [62] W. Bao, J. Jiang, Z. Yu and X. Zhou, *Engineering Structures*, 196 (**2019**) 109334.
- [63] R. Tartaglia, M. D’Aniello and M. Zimbru, *Structures*, 27 (**2020**) 2137-2155.
- [64] A. B. Camara, F. Pennec, S. Durif, J. L. Robert, A. Bouchaïr, *Fatigue life assessment of bolted connections*, 12<sup>th</sup> International Fatigue Congress, 25 May, Online, **2018**.
- [65] M. Hagiwara, R. Suzuki and Y. Inagaki, *Journal of Advanced Mechanical Design, Systems, and Manufacturing*, 14 (**2020**) JAMDSM0031.

- [66] B. B. Ajaei and S. Soyoz, *Journal of Constructional Steel Research*, 166 (2020) 105933.
- [67] Z. Wu, S. A. Nassar, Effect of Underhead Design Configuration on Bolt Behavior Under Shear Loads, ASME 2015 Pressure Vessels and Piping Conference, 19-23 July, Boston, Massachusetts, USA, 2015.
- [68] L. M. Bezerra, J. Bonilla, W. A. Silva and W. T. Matias, *Engineering Structures*, 218 (2020) 110770.
- [69] A. Ahmed, N. Kishi, K. Matsuoka and M. Komuro, *Journal of Applied Mechanics*, 4 (2001) 227-236.
- [70] M. Komuro, N. Kishi and A. Ahmed, *Advances in Engineering Structures, Mechanics & Construction*, 140 (2006) 289-301.
- [71] S. N. El Kalash and E. G. Hantouche, *Journal of Constructional Steel Research*, 145 (2018) 518-528.
- [72] F. Huang, D. Zhang, W. Hong and B. Li, *Journal of Constructional Steel Research*, 132 (2017) 97-107.
- [73] E. Piraprez, *Journal of Constructional Steel Research*, 27 (1993) 55-68.
- [74] G. Srinivasan and T. F. Lehnhoff, *ASME J. Pressure Vessel Technol.*, 123 (2001) 381-386.
- [75] J. P. Jaspart, R. Maquoi, Effect of bolt preloading on joint behaviour, Proceedings of the First European Conference on Steel Structures, 18-20 May, Athens, 1995.
- [76] A. M. G. Coelho, L. S. da Silva and F. S. K. Bijlaard, *Journal of Structural Engineering*, 132 (2006) 918-928.
- [77] H. Guo, G. Liang, Y. L. Li and Y. Liu, *Journal of Constructional Steel Research*, 139 (2017) 473-483.
- [78] R. Soltani and D. E. Kerdal, *Turkish J. Eng. Env. Sci.*, 35 (2011) 1-20.
- [79] G. Liang, H. C. Guo, Y. Liu and Y. L. Lia, *Thin-Walled Structures*, 122 (2018) 554-571.

- [80] T. Wulan, P. Wang, Y. Li, Y. You and F. Tang, *Engineering Structures*, 169 (2018) 15-36.
- [81] H. X. Yuan, S. Hua, X. X. Dua, L. Yang, X. Y. Cheng and M. Theofanous, *Journal of Constructional Steel Research*, 152 (2019) 213-224.
- [82] G. A. Anwar, F. Dinu and M. Ahmed, *International Journal of Steel Structures*, 19 (2019) 970-977.
- [83] M. S. Zhao, C. K. Lee and S. P. Chiewc, *Journal of Constructional Steel Research*, 122 (2016) 316-325.
- [84] K. S. Elias, *Thin-Walled Structures*, 145 (2019) 106398.
- [85] R. G. Budynas and J. K. Nisbett, “Shigley’s Mechanical Engineering Design”, 10<sup>th</sup> Edition, McGraw Hill Education, 2015.
- [86] EN 1993-1-8: 2005, Eurocode 3: Design of steel structures. Part 1.8: Design of joints, European Standard, Brussels, 2005.
- [87] Z. Y. Wang, W. Tizani and Q. Y. Wang, *Engineering Structures*, 32 (2010) 2505-2517.
- [88] Y. Q. Wang, L. Zong and Y. J. Shi, *Journal of Constructional Steel Research*, 84 (2013) 1-16.
- [89] A. M. Ibrahim, T. H. Radwan, S. A. Ibrahim and A. K. Dessouki, *Journal of Constructional Steel Research*, 174 (2020) 106273.
- [90] ISO 898-1:2009, Mechanical properties of fasteners made of carbon steel and alloy steel, Part 1: Bolts, screws and studs with specified property classes — Coarse thread and fine pitch thread, International Standard, 2009.
- [91] ASTM A370, Standard Test Methods and Definitions for Mechanical Testing of Steel Products, ASTM International, 2003.
- [92] J. Fernandez-Ceniceros, A. Sanz-Garcia, F. Antoñanzas-Torres and F. J. Martinez-de-Pison, *Engineering Structures*, 82 (2015) 236-248.
- [93] K. Ydstebø, Capacity of Bolted T-stub Connections Between Different Materials Subjected to Tension and Thermal Load, Master of Science Thesis, University of Stavanger, Faculty of Science and Technology, 2017.

- [94] V. Piluso, C. Faella and G. Rizzano, *Journal of Structural Engineering*, 127 (2001) 694-704.
- [95] S. E. Yılmaz, A. Kayran, E. Gürses, D. Çöker, *Parametric Study for the Study of the Effect of Contact Parameters for Plastic Analysis of Bolted Flange Connections*, 8<sup>th</sup> Ankara International Aerospace Conference, 10-12 September, Ankara, Turkey, **2015**.
- [96] J. M. Reinoso, A. Loureiro, R. Gutierrez and M. Lopez, *Journal of Constructional Steel Research*, 90 (2013) 156-163.
- [97] M. Akkurt, *Makine Elemanları: Birinci Cilt, 2. Baskı*, Birsen Yayınevi, İstanbul, **2012**.
- [98] F. Trebuňa, F. Šimčák and J. Bocko, *American Journal of Mechanical Engineering*, 1 (2013) 403-406.
- [99] *Technical Information*, Bossard AG, **2005**.

## APPENDICES

### APPENDIX 1 - The technical drawing of the dogbone specimens

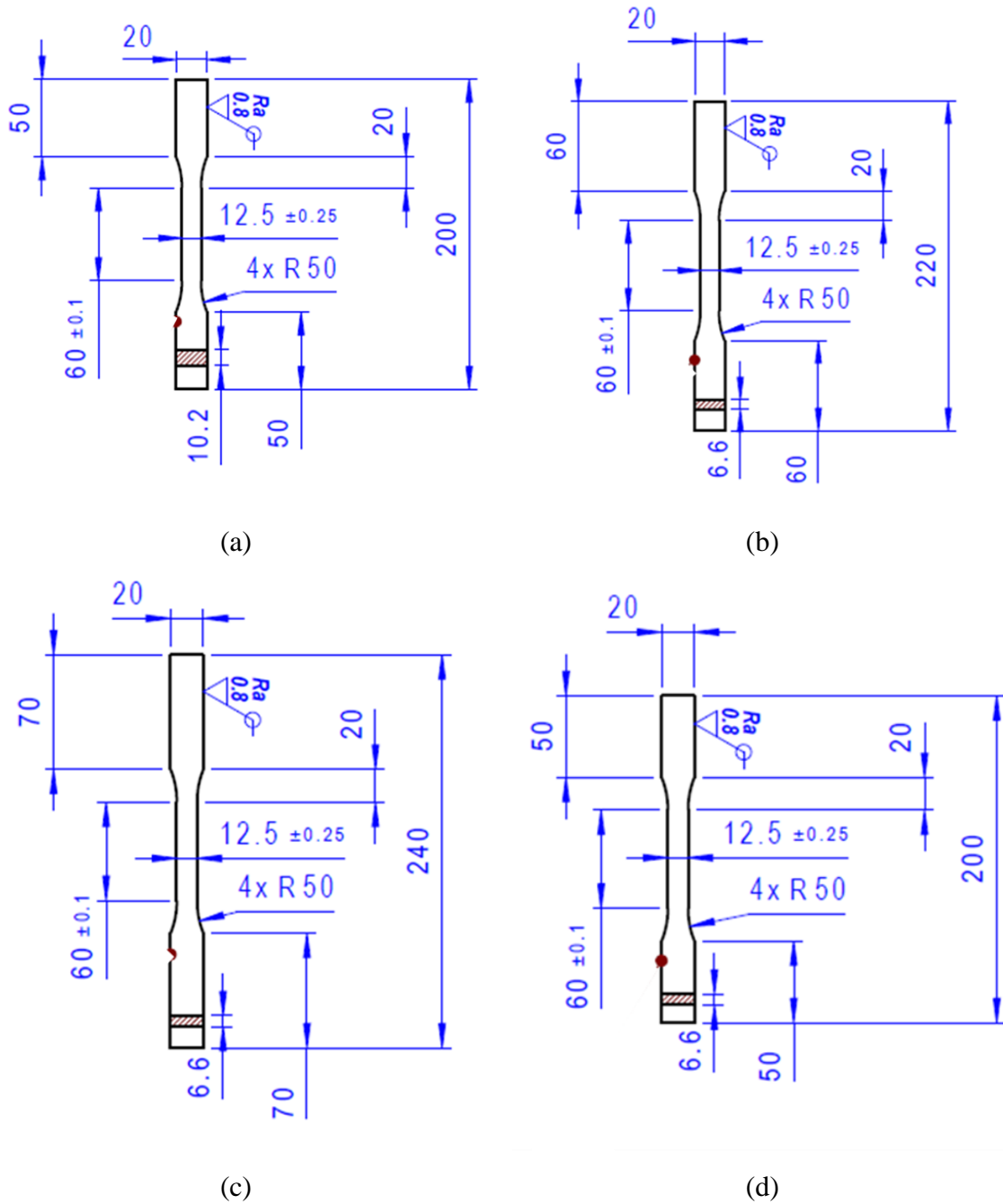


Figure A.1. The technical drawing of the dogbone specimens of (a) 0-W, (b) 45-W, (c) 90-W, (d) 0-F.

**APPENDIX 2 - The technical drawing of the setup parts.**

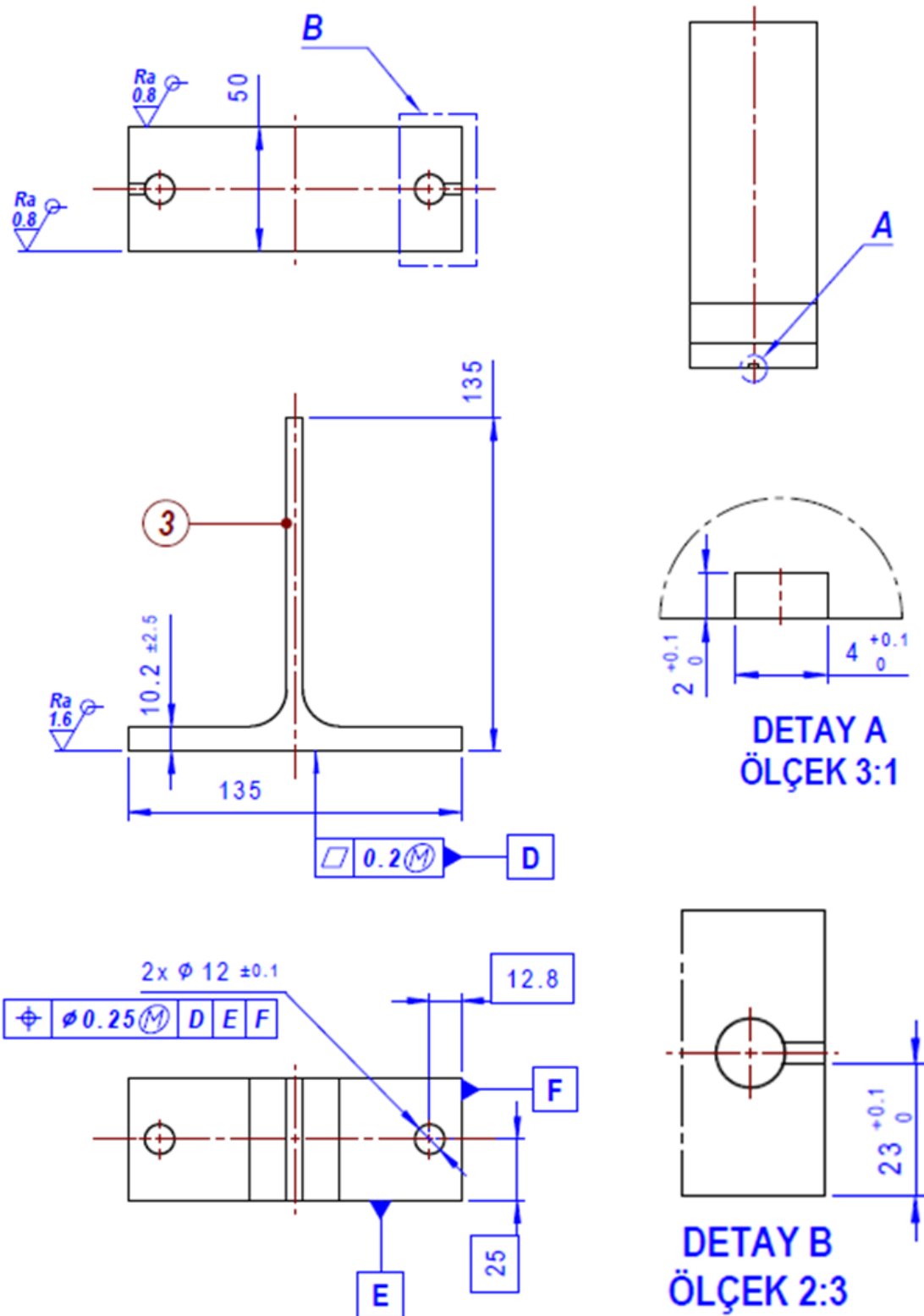


Figure A.2. The technical drawing of the setup part with higher eccentricity.

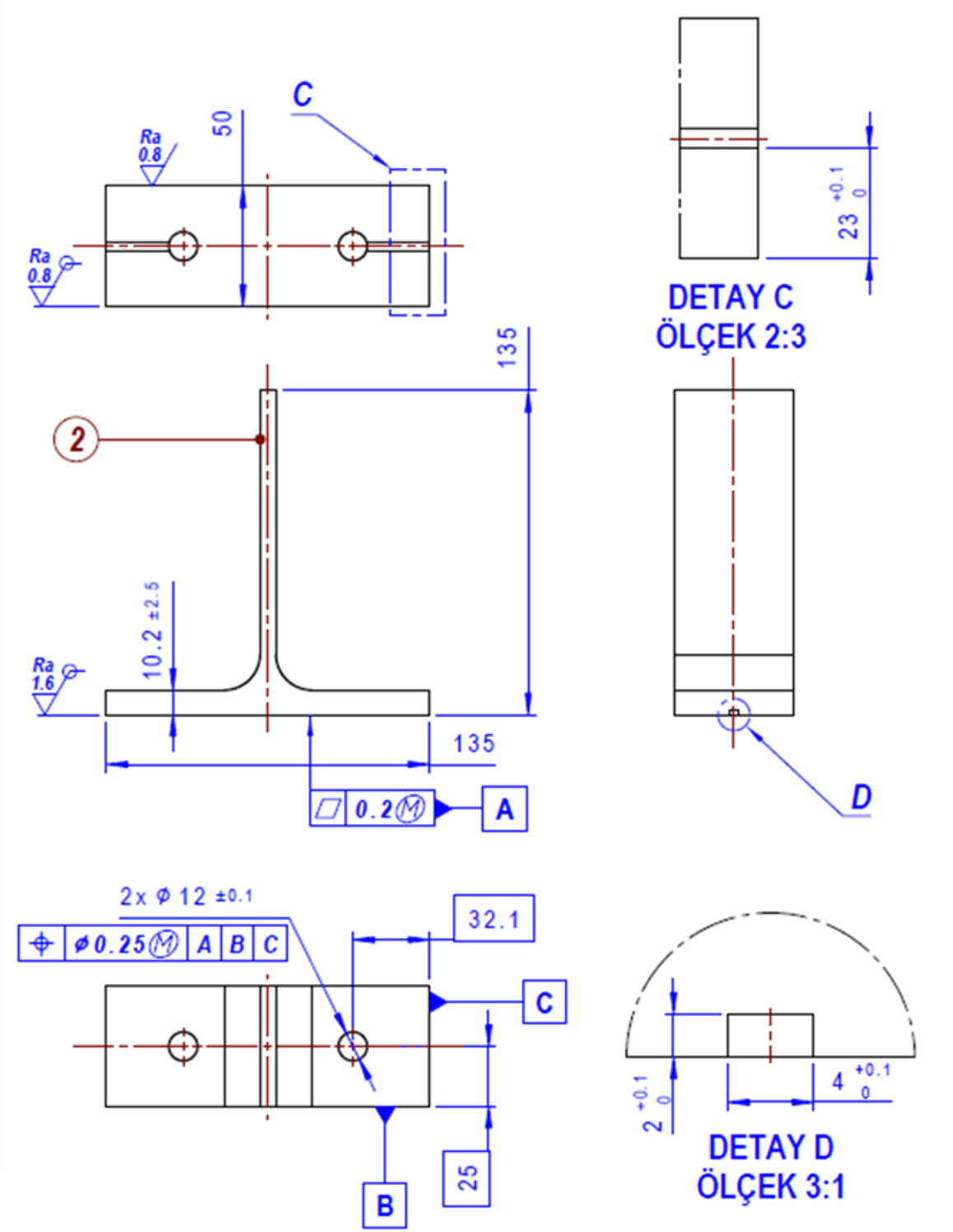


Figure A.3. The technical drawing of the setup part with lower eccentricity.